2009

Synthesis and Evaluation of Anibamine and Its Analogs as Novel Anti-Prostate Cancer Agents

Kendra Haney
Virginia Commonwealth University

SYNTHESIS AND BIOLOGICAL EVALUATION OF ANIBAMINE AND ITS ANALOGS AS NOVEL ANTI-PROSTATE CANCER AGENTS

A Thesis submitted in partial fulfillment of the requirements for the degree of Master of Science at Virginia Commonwealth University

by

By Kendra May Haney
BS in Biochemistry at Washington and Lee University, 2006

Major Director: YAN ZHANG, Ph.D.
ASSISTANT PROFESSOR, DEPARTMENT OF MEDICINAL CHEMISTRY

Virginia Commonwealth University
Richmond, Virginia
December, 2009

Acknowledgements

I would like to take this opportunity to thank my advisor, Dr. Yan Zhang, for his guidance and teaching from the first day I was accepted in to the Department of Medicinal Chemistry until now. I would also like to thank him for providing me with generous financial support. My day to day experiences in the lab could not have been successful without the help from Dr. Guo Li whose patience is endless. I would also like to thank Dr. Joy Ware in the Department of Pathology for the opportunity to work in her lab and gain valuable experience outside an organic chemistry lab and Amanda Richardson for her infinite help with cell culture as well as for always letting me talk about my mutts. I would like to thank the other members of Dr. Yan Zhang's lab, past and present, for helping me learn more about organic chemistry and teamwork. To my friends, I would like to extend my gratitude for giving me friendship, support, and laughter. Thank you Genevieve, for always being willing to take a break. I am especially grateful to Nolan, for sitting through practices of seminars and listening to every detail about my day, and loving me anyway. I would like to thank my family for tolerating my extended stay in Virginia, for buying many plane tickets, and all their love and support. I would especially like to thank my parents for their constant love and support throughout my life, especially in my higher education years. I would never have come this far in science without the interest and knowledge instilled in me by my high school chemistry teacher, Mr. Bill Cunningham, and my undergraduate chemistry professor, Dr. Erich Uffelman. And love and thanks to my father and grandfather, without whom I might not have found myself with such a passion for anti-cancer research.

Table of Contents

List of Tables

page

List of Figures

List of Schemes

List of Abbreviations

Å	Angstroms
°C	degrees Celsius
δ	chemical shift
%	percent
AAH	atypical adenomatous hyperplasia
10-CSA	10-camphorsulfonic acid
AcOH	acetic acid
AR	androgen receptor
br	broad peak
bFGF	basic fibroblast growth factor
CCL2	CC chemokine ligand 2
CCL3	CC chemokine ligand 3
CCL4	CC chemokine ligand 4
CCL5	CC chemokine ligand 5
CCL7	CC chemokine ligand 7
CCL8	CC chemokine ligand 8
CCL19	CC chemokine ligand 19
CCL20	CC chemokine ligand 20
CCL21	CC chemokine ligand 21
CCR2	CC chemokine receptor 2
CCR5	CC chemokine receptor 5
CCR7	CC chemokine receptor 7
CDCl3	deuterated chloroform
CH_2Cl_2	dichloromethane
$CHCl_3$	chloroform
CI	chronic inflammation
CO_2	carbon dioxide
CXCL8	CXC chemokine ligand 8
CXCL12	CXC chemokine ligand 12
CXCL16	CXC chemokine ligand 16
CXCR4	CXC chemokine receptor 4
d	doublet
DC	dendritic cells

DHT	dihydroxytestosterone
DIBAL-H	di-isobutyl aluminum hydride
DMF	dimethylformamide
DMSO	dimethylsulfoxide
DU-145	dura mater derived prostate cancer cell line
ECM	extracellular matrix
EGF	epidermal growth factor
EGF-F	epidermal growth factor receptor
EL2	extracellular loop 2
EtOAc	ethyl acetate
Et_2O	diethyl ether
FBS	fetal bovine serum
FGF-R	fibroblast growth factor receptor
fs	femtoseconds
g	grams
G-CSF	granulocyte-colony stimulating factor
GOLD	genetic optimization for ligand binding
GPCR	G protein coupled receptor
HIV	human immunodeficiency disorder
HPV	human papillomavirus
Ic_{50}	half maximal inhibitory concentration
IFN	interferon
IGF	insulin-like growth factor
IGFB	insulin-like growth factor binding protein
IGF-I	insulin-like growth factor type 1
IGFR	insulin-like growth factor receptor
IL	interleukin
IP_3	inositol-1,4,5-triphosphate
IR	infrared
ITS	insulin, transferrin, selenium
kDa	kilodalton
K_{ow}	octanol-water partition coefficient
LC_{50}	half maximal lethal concentration
LHMDS	lithium hexamethyldisalizide
LNCaP	lymph node derived prostate cancer cell line
μM	micromolar
m	multiplet
M12	metastatic prostate cancer cell line
MeOH	methanol

MHz	megahertz
mL	milliliters
mmol	millimolar
MMP	matric metalloproteinase
mRNA	messenger ribonucleotidic acid
MsCl	methane sulfonyl chloride
NAD:	oxidized nicotinamide adenine dinucleotide
NADH	reduced nicotinamide adenine dinucleotide
NH_4OH	ammonium hydroxide
nm	nanometers
nM	nanomolar
NMR	nuclear magnetic resonance
P69	non-neoplastic prostate epithelial cell line P
PBS	phosphate buffer solution
PC-3	bone derived prostate cancer cell line
PCa	prostate cancer
PIA	proliferative inflammatory atrophy
PIN	prostate intraepithelial neoplasia
PLCβ	phospholipase Cβ
PSA	prostatic specific antigen
RANTES	regulated upon activation normal T cell expressed
SV40	Simian vacuolating virus 40
T	triplet
TADC	tumor-associated dendritic cells
TAM	tumor-associated macrophages
TBAB	tetrabutylammonium bromide
TEA	triethylamine
TFA	trifluoroacetic acid
THF	tetrahydrofuran
TIL	tumor-infiltrating cells
TGF-α	transforming growth factor alpha
TGF-β	transforming growth factor beta
TGF-β-R	transforming growth factor beta receptor
TLC	thin layer chromatography
TNF	tumor necrosis factor

Abstract

SYNTHESIS AND BIOLOGICAL EVALUATION OF ANIBAMINE AND ITS ANALOGS AS NOVEL ANTI-PROSTATE CANCER AGENTS

By Kendra May Haney

A Thesis submitted in partial fulfillment of the requirements for the degree of Master of Science at Virginia Commonwealth University

Virginia Commonwealth University, 2009

Major Director: Yan Zhang, Assistant Professor, Department of Medicinal Chemistry

The chemokine receptor CCR5 has been implicated in the pathogenesis of prostate cancer. A novel natural product, anibamine, was isolated and found to be a micromolar inhibitor of the receptor. Anibamine was used as a new anti-prostate cancer lead compound. To discover the pharmacophore, analogs of anibamine were designed using the "deconstruction-reconstruction-elaboration" approach and synthesized. The establishment of a stereoselective route to only one isomer was explored, to increase yield and eliminate elaborate purification procedures. Analogs were found to have anti-prostate cancer activity at levels higher than the parent compound. The molecular modeling studies of the deconstructed analogs indicate that due

to the psuedo-symmetry of the parent compound, the binding conformation of the deconstructed analogs may not be very different from each other. All this information together may help identify a next generation lead compound for anti-prostate cancer treatment.

I. Introduction

Prostate cancer (PCa) is the most common cancer in men after lung cancer.[1] The American Cancer Society estimates that nearly 200,000 new cases of PCa will be diagnosed in 2009, with 27,000 deaths attributable to PCa in the United States alone.[2] Better detection rates have helped those in the early stages of cancer but there is no cure for the metastatic disease. Age is the greatest risk factor[3] and with an ever increasing population of men over the age of 50, establishment of successful treatment of PCa proliferation, angiogenesis, and metastasis is in high demand. Though the cause of prostate cancer is unknown, chronic inflammation (CI) has been implicated as playing a role in the pathogenesis of PCa.[4] Nearly one and half centuries ago, Rudolf Virchow noticed that cancers often occurred at sites of chronic inflammation.[5] Since then several cancers have been attributed to CI, including cancers of the liver, colorectum, ovary and cervix.[5]

Suspicion of the influence of inflammation on PCa development led to the discovery that the chemokine receptor, CCR5, is overexpressed in PCa tissues when compared to the non-cancerous condition, benign prostate hyperplasia (BPH).[6] Chemokine receptor CCR5 is part of the chemokine network which plays an important role in the immune system by attracting leukocytes to sites of inflammation. CCR5 and another chemokine receptor, CXCR4, were found to be essential co-receptors for the invasion of the human immunodeficiency virus, HIV, into cells.[7] This discovery sparked an urgent search for CCR5 antagonists by high-throughput screening of small molecule libraries. The existence of phenotypically normal people with a mutated, inactive CCR5 gene that essentially renders them immune to human immunodeficiency virus (HIV) infection lends some substance to the suitability of blocking this particular receptor.[8]

To date only one of several CCR5 antagonist drug candidates has passed the FDA's rigorous screening process to become an approved drug as an HIV-1 entry inhibitor.[9] Maraviroc is the only chemokine receptor antagonist to gain approval for any therapeutic use. Another CCR5 antagonist, TAK-779, was found to inhibit the proliferation of PCa cell lines in vitro.[10]

Screening of a natural product extract led to the discovery that anibamine, a charged alkaloid from the species *Aniba panurensis*, was a CCR5 antagonist at the micromolar level.[11] Anibamine was also tested against the National Cancer Institute's panel of 60 cancer cell lines.[12] Anibamine was hemolytic and had a high $\log K_{o/w}$ value making it initially unsuitable as drug candidate. Preliminary studies have shown that anibamine also inhibits proliferation of prostate cancer cell lines.[13] In order to enhance the anti-cancer properties and reduce undesirable toxicity, further refinement of the lead structure was necessary.

The total synthesis of anibamine was accomplished recently in our lab.[14] Using anibamine as a new lead compound, multiple analogs were designed following the "deconstruction-reconstruction-elaboration" approach for discovering the pharmacophore and ideally a next generation lead compound. The synthetic route accommodates the synthesis of multiple analogs along diverted synthesis schemes. The purpose of this project was to synthesize anibamine and deconstructed analogs. Following the synthesis a number of analogs were tested for anti-proliferative effect in multiple metastatic prostate cancer cell lines. Binding modes of synthesized ligands were also analyzed using computer generated models of CCR5 based on the crystal structures of fellow G-protein coupled receptors (GPCR), bovine rhodopsin and human beta-2 adrenergic receptor. All this information together may help identify a next generation lead compound for anti-prostate cancer treatment.

II. Background

A. Prostate cancer

Prostate cancer is one of the leading causes of cancer death for American men. The primary cause of prostate cancer remains unclear, though chronic inflammation is believed to play a role in its development. With increasing life expectancies as well as a surge in male population over 50 years old, PCa is likely to become even more prevalent. Current therapies have little effect on preventing or treating metastases though they may benefit early stages.[15] Though PCa is generally a slow progressing adenocarcinoma, development of bone metastases is ultimately fatal.[16,17]

1. The prostate and prostatic disorders

The prostate is a secretory gland in the male reproductive system surrounding the prostatic urethra. The anatomy of the prostate is classified into four different zones; the peripheral zone , the central zone, the transition zone , and the anterior fibromuscular zone. Most prostate carcinomas arise from the peripheral zone and about one-third arise from the transitional zone.[18] The cells of the prostate are of three distinct cell types; secretory luminal, basal, and endocrine-paracrine (EP) cells.[19] Secretory luminal cells produce prostate specific antigen (PSA) and express androgen receptor (AR). PSA is a glycoprotein that is used in early detection of PCa.[20] AR is a nuclear receptor that upon binding to the hormones testosterone or dihydroxytestosterone (DHT) increases the transcription of genes involved in cell growth and differentiation.[15,21] Basal cells are androgen independent but a small amount are androgen

responsive.[19] The androgen responsive basal cells are believed to be the progenitor cells of the secretory luminal cells and endocrine-paracrine cells.[18] Maitland and Collins suggest that there is a spectrum of differentiation between the basal cells and secretory luminal cells.[19] The primary function of the prostate is to secrete proteins necessary for sperm function. In normal prostate tissue, growth and differentiation are regulated by circulating hormones and growth factors from the surrounding stroma.[19] The biggest surge in development of the prostate is during puberty.[18] Later in life, the prostate can be the source of many complications.

There are several medical problems associated with the prostate. In the transitional zone, benign prostatic hyperplasia (BPH) and atypical adenomatous hyperplasia (AAH) are common maladies. Proliferative inflammatory atrophy (PIA) and prostate intraepithelial neoplasia (PIN) are lesions commonly found in the peripheral zone. PCa occurs most commonly in both transitional and peripheral zones. Studies and comparisons of several different prostatic tissues can benefit the understanding the causes of PCa and how to prevent and treat PCa development and metastasis.[6,17]

The maladies of the transitional zone are benign prostate hyperplasia and AAH. BPH is a non-cancerous enlarged prostate, the symptoms of which are often confused with PCa. With progressing age, the balance between androgens and estrogens acting on prostatic cells changes. An age-related reduction in DHT circulation may be involved in development of BPH. The number of androgen responsive basal cells proliferating increases in BPH compared to the normal tissue which results in abnormal secretory luminal cell counts. This is considered a differentiation issue rather than a regulatory abnormality[19] which makes BPH non-cancerous. Also there is a significant amount of inflammatory cells in the stroma surrounding BPH tissues.[4]

In AAH, the proliferation compartment resembles normal and BPH tissue, meaning the basal cells are the predominant type of cells proliferating.[19] Proliferation rates for AAH range between the relative rates of BPH and PCa.[22] It has been suggested that AAH is an intermediary in differentiation from BPH to transitional zone PCa[22] as AAH resembles low grade PCa.[19] Bonkhoff and Remberger state that neoplasms that might originate from AAH generally are not be lethal.[19] Comparing BPH, AAH and PCa can identify factors that lead to PCa in the transitional zone.

Two common lesions appear in the peripheral zone that may lead to PCa. PIA, as described by De Marzo et. al, is characterized by focal atrophy interspersed between normal tissue and inflammatory cells. PIA lesions increase with age and are commonly found with areas of PCa.[4,23] Many instances of PIA are highly proliferative and have decreased apoptosis due to irregularities in Bcl-2, an apoptosis regulating protein.[4] Mutation of the p53 oncogene is also seen in PIA.[4] In PIN, the secretory luminal cells proliferate, when normally secretory luminal cells do not proliferate.[19] Like PCa, expression of Bcl-2 is increased, resulting in increased lifespan of the secretory luminal cells. It has been hypothesized that PIA may either lead directly to PCa or develop into PIN which may also develop into PCa.[23]

Comparison of the phenotypes of the different prostatic conditions have helped to unearth mechanisms of prostate cancer development. The differentiation of the proliferating cells as well as the rate of proliferation are the most distinguishable characteristics among the different prostatic conditions. In the long term progression from normal prostatic epithelial cells to prostate adenocarcinoma a number of mutations and alterations have been documented including the common oncogene p53. Somatic changes in AR occur in most PCa tissues. Receptor

overexpression coupled with signal amplification can make the remaining receptors very sensitive to decreased hormone levels during androgen withdrawal therapy.[15] Change in ligand-specificity has also been noted, allowing the AR receptors to be activated by other hormones as well as AR activation through other growth factor networks.[15] Initial success with androgen ablation is usually curtailed by the development of androgen independent malignancies. After this point, there is little hope for remission.

2. Prostate cancer cell lines

Standardized in vitro models of PCa can help pinpoint effects of different factors while the use of immortalized normal prostatic epithelial cells can serve as controls for these experiments. Human cell models can help address unknowns regarding regulation and differentiation. Also using immortalized normal cells and malignant cells are useful in finding methods to block angiogenesis, invasion, and metastasis.[21]

The PC-3 prostate cancer cell line was originally removed from the lumbar vertebra of a 62 year old caucasian man. It was described as “poorly differentiated prostatic adenocarcinoma.” Hormone therapy was used to treat the patient.[24] PC-3 is androgen independent, which could be related to the use of hormone therapy to select for AR unresponsive malignant cells. PC-3 also does not express PSA. Bone marrow transferrin stimulates growth of this cell line. PC-3 expresses high levels of the growth factors transforming growth factor-β (TGF-β) and insulin-like growth factor-1(IGF-1); fibroblast growth factor receptor (FGF-R), TGF-β-R, and IGF-1-R are also seen in PC-3, possibly resulting in an autocrine growth loop.[24]

DU-145 was derived from a central nervous system PCa metastasis. The patient was also a Caucasian man in his 60s treated with androgen withdrawal therapy. Consequently, DU-145 is also mostly androgen independent. High expression of endothelial growth factor (EGF), EGF-R, IGF-1 and IGF-1-R and TGF-α are observed in this cell line, also resulting in possible autocrine growth loops.[24] DU-145 has mutations in the common oncogene p53.[20]

The M12 cell line is derived from the immortalized prostatic epithelial cell line, P69SV40T.[25,26] P69SV40T was injected into athymic mice subcutaneously and tumors formed in two of eighteen mice after nine months. After selecting for invasiveness after successive injections, the cell line M12 was found to invasive and have a shorter latency time of two weeks when compared to the parent cell line. Subsequent intraperitoneal injections of the M12 cell line into nude mice developed into metastases in the lungs and diaphragm consistently.[25,26] Chromosomal investigations showed that the M12 subline lost 16q and gained 8q which are both frequently observed chromosomal abnormalities in PCa tissue.[26]

3. Inflammation and Prostate Cancer

As previously mentioned, chronic inflammation has been accused of playing a role in the development of prostate cancer. Both BPH and PIA are associated with inflammatory cells in prostatic tissue. Of note is that prostatitis, inflammation of the prostate, is the most commonly diagnosed prostatic condition.[18] Chronic inflammation is a persistent inflammatory response, lasting months to years. The immediate stimulus for an inflammatory response in prostatic tissue is unknown. Men with a reported history of sexually transmitted infections, like gonorrhea and syphilis, have increased risk of PCa.[27] One virus, human papillomavirus (HPV) is known to

cause cervical cancer. At least two viruses, human papovavirus BK and Xenotrophic MuLV-related virus, have been detected in abnormal prostatic tissue.[18] These infections may trigger an inflammatory response in the prostatic tissue. There is also evidence that carcinogens reach the prostatic tissue and may result in chemical damage that induces an immune response.[18] The influx of inflammatory cells can damage the prostatic tissue by production of reactive nitrogen and oxygen species, thereby inducing increased proliferation of cells to replace those lost and which can lead to development of somatic mutations.[18] Another possible consequence of an inflammatory response and cause of cancer is the selection of mutated progenitor cells that may thrive in the inflammatory environment.[18] After the immune response wanes, these selected cells may undergo apoptosis, lay dormant until further stimulation or they might have developed an autocrine growth pattern, leading to cancer.[18] Because of the possible role inflammation plays in prostate cancer development, several genes and proteins of the inflammatory network have been studied in PCa and other prostatic tissues.

Chronic inflammation may lead to either BPH or PCa. Konig et al. studied the presence of inflammatory proteins in both BPH and certain PCa cell lines, PC-3 and LnCAP. They found that IL-8 and CCL5 were expressed more frequently in PCa than in BPH. CCR5 and MMP-9 also had higher expression in PCa. BPH had a higher expression of CCR3, CXCR-4, and cox-II when compared to PCa.[6]

4. CCR5 and CCL5/RANTES in PCa

Konig et al. reported the increased expression of both CCR5 and RANTES (Regulated upon Activation Normal T cell Expressed) in PCa compared to BPH. Further study into the role

of these members of the chemokine/chemokine receptor family has been undertaken. Vaday et al. reported that PCa cell lines, LNCaP, DU-145 and PC-3, express mRNA for RANTES to different degrees. LNCaP and DU145 secrete higher levels of RANTES than PC-3.[10] These cell lines also express CCR5 mRNA and surface CCR5. This led the authors to the idea that this ligand-receptor pair has developed into an autocrine feedback loop to promote growth of PCa cells. The authors also used RANTES and a CCR5 small molecule antagonist, TAK-779, to determine whether RANTES can induce invasion in PCa cells as it has been shown to do in breast cancer cell lines.[10] The CCR5 antagonist inhibited both proliferation and invasion of PCa cell lines in the presence of RANTES. The ligand-receptor pair RANTES/CCR5 may play a role in the growth and invasiveness of PCa.

Polymorphisms in both RANTES and CCR5 are present in human populations. A few studies have looked at allelic frequency of normal and abnormal RANTES and CCR5. Sáenz-López et al. found a statistically significant increase in Allele A vs Allele G in RANTES. Higher transcription is reported with Allele A.[28] An Italian group studied the CCR5Δ32 genetic mutation in Sicilian patients with PCa compared to men over 100 years old without PCa. The CCR5Δ32 mutation results in a non-functioning receptor that is not expressed on the cell surface. Balistreri et al. found that the centenarian population had more CCR5Δ32 mutations than the PCa population, which suggest that in this European population, the CCR5 mutation may have a protective effect in the development of PCa.[29] However, another study in Australia indicated that there was no difference in PCa risk between CCR5 or RANTES alleles.[30] They did observe that men with the CCR5Δ32 gene had a moderately higher incidence of PCa if there were two or more immediate family members that also had PCa but it was unclear whether other family

members were carriers of the same alleles.[30] More study is needed in larger populations to ascertain whether these genetic polymorphisms do indeed produce an increased susceptibility or protective effect in development of PCa.

5. Prevention and Treatment

While the exact cause of PCa remains elusive, so does effective preventive measures. Use of NSAIDs has been shown to decrease prostate cancer development[4,18] but these studies have been retrospective in nature, relying on the recollective abilities of the subjects. Age is still the primary risk factor for developing PCa, followed by heredity and ethnicity.[3] Dietary habits have come under scrutiny as a possible risk factor, especially since geography appears to play more of a role in defining susceptibility than ethnicity[3] as in Asian migrants to areas of high incidence also experience an increased incidence over a generation.[31] After diagnosis of PCa, surgery, radiation therapy or hormonal treatment with diethylstilbestrol or luteinizing hormone-releasing hormone is intended to slow growth by stopping the growth factor function of AR. However this may lead to selection of androgen unresponsive tumors.[20] Some chemotherapeutic approaches include 5-fluoruracil, taxol and cisplatin, but these can lead to drug resistance. The DU145 cell line is particularly resistant to cisplatin.[20] More treatments for the metastasis of PCa are needed because of the morbidity associated with metastatic spread.

B. Chemokines and Chemokine Receptors

The chemokine/chemokine receptor system is a critical mediator of cell motility in routine immune surveillance, inflammation, and development. The immune system depends on

the chemokine system to guide needed lymphocytes to sites of tissue damage or antigen presentation. Irregularities in these proteins can contribute to HIV infection, inflammatory diseases and cancer. Due to this disease involvement, chemokines and their receptors have been scrutinized as a means to both better understand and treat these conditions. The chemokine receptor CCR5 has been shown to be an HIV invasion coreceptor and involved in proliferation of neoplastic cells in various types of cancers, including prostate cancer.

1. Chemokine and Chemokine Receptor Structure and Signaling

Chemokines are so named because they are *chemo*tactic cyto*kines*. The class is composed of nearly 50 soluble proteins ranging from 70 to 130 amino acids with the exception of CX_3CL1 (fractalkine) and CXCL16 which are much larger and can be tethered to the cell surface by a mucin-like stalk. The chemokines are split into 4 families, based on the relative positions of two conserved cysteine residues that form disulfide bonds with other cysteines. In the CC chemokine family, the cysteines are adjacent. In the CXC and CX_3C chemokine families, the X represents the number of non-cysteine residues that separate the conserved pair. In the C family of chemokines, there exists only one N-terminus cysteine residue.[32] Though chemokines share from a low 20% to a high 90% homology among each other,[33] the soluble chemokines retain a characteristic fold with an unstructured N-terminus critical for binding to their receptors, a 3 stranded β-sheet connected by loops and turns with an α helical C-terminus.[32] Chemokines function to create a chemical gradient, helped by binding to glysoamino glycans (GAGs) on epithelial cell surfaces, in order to attract various immune cells to sites of infection. Immune cells express chemokine receptors on their cell surface and move toward the source of the

gradient which can be various cells involved in the immune response. Chemokines bind to chemokine receptors.

Chemokine receptors are also grouped into 4 families, according to which chemokine they bind. Hence, CC receptors bind CC chemokines, etc. There are 20 known signaling chemokine receptors and 3 "scavenger" receptors that do not induce a signaling cascade.[33] Chemokines and their receptors exhibit a multitude of promiscuity, with many chemokines binding different receptors and vice versa, though members of each family of ligands only bind members of the same family of receptors. This redundancy may allow for fine tuning of immune response; oligomerization of ligands and/or receptors, temporal and spatial compartmentalizations also attenuate this complex system.[33] Chemokine receptors are G-protein coupled receptors (GPCRs) having 7 transmembrane helices, 3 extra-cellular loops, 3 intra-cellular loops, an extra-cellular N-terminus and an intracellular C-terminus with a molecular weight around 350 kDa. Most chemokine receptors have a highly conserved DRYLA amino acid sequence in the second intracellular loop.[34] Chemokine receptors are mostly coupled to $G\alpha_i$ proteins and are inhibited by pertussis toxin, though there is evidence for coupling to other G-proteins.[32,34] It has been suggested that receptor/G protein pairings may be cell type specific[34] or depend on the chemokine ligand.[35] There is ample evidence for receptor hetero- and homo-dimerization, as well as higher order oligomers.[36] Dimers can activate pathways distinct from monomeric proteins.[34] Any cell type can express chemokines or their receptors[37] though leukocytes including monocytes, dendritic cells, eosinophils, lymphocytes, and natural killer cells but not neutrophils express CC chemokines and receptors.[5] Receptor expression is

determined by cell lineage and stage of differentiation but microenvironmental conditions like growth factors, cytokines, hormones and hypoxia can modulate receptor expression.[5,34]

2. Chemokines and the Tumor Microenvironment

In 1863 Rudolf Virchow observed that cancers often occured at sites of chronic inflammation, connecting luekocyte infiltration with neoplastic tissues.[5] Nearly one and a half centuries later, 15% of the cancers worldwide are related to infectious agents, involving chronic inflammation.[5] The influx of leukocytes into the area surrounding and in between tumor cells has prompted the study of the tumor microenvironment as a whole, instead of focusing only on cancer cells.[19]

Tumor associated chemokines play several roles in the tumor microenvironment, including directing the infiltration of leukocytes to the tumor microenvironment, acting as growth factors, encouraging angiogenesis, directing migration and evading the host immune response. The tumor microenvironment and tissue at the peak of an inflammatory response resemble one another.[32]In the tumor microenvironment, host luekocytes termed “tumor infiltrating leukocytes” (TIL) are found in both the surrounding stroma and tumor areas. Chemokines recruit and control the TIL.[38] TIL may contribute to the growth, spread, and immunosuppression of tumors. Chemokines can also act as growth factors, either through autocrine or paracrine pathways. In many cancers that express the chemokine receptor, CXCR4, there is evidence that the CXCR4 ligand, CXCL12, stimulates growth and proliferation of cancer cells.[38] In addition, other growth factor expression levels are associated with expression of chemokine receptors on cancer cells.[7] The other roles of chemokines in the tumor

microenvironment, direction of migration and manipulating the host immune response, will be discussed in more detail.

a) Chemokines and Immunotolerance

Although immune cells are present in the tumor microenvironment, their anti-tumorigenic properties are inadequate. This phenomenon is not fully understood and there are two prevailing (but not mutually exclusive) hypotheses to explain how the tumor cells escape immune surveillance; the macrophage balance hypothesis and immune tolerance through commandeering of the chemokine system.[39] Tumor associated macrophages are capable, with appropriate stimulation, to either kill the tumor cells or induce damage to the vascular endothelium.[5] They also have the capacity to encourage tumor cell proliferation and tumor ability to generate new vasculature, migrate and metastasize through the production of growth and angiogenic factors.[5] Secreted CCL2 recruits tumor associated macrophages to the tumor microenvironment.[5] Chemokines, macrophages and disease outcome are related to each other but the relationship varies between cancers and is termed the "macrophage balance hypothesis."[32,40]

Another leukocyte component of the tumor microenvironment are tumor associated dendritic cells (TADC). Dendritic cells are antigen presenting cells that provide a link between adaptive and innate immunity by both participating in the triggering of antigen specific immunity and the establishment of immunotolerance.[5] Tumors secrete chemokine that are active on immature dendritic cells (iDC) including CCL2, CCL7, CCL8 and the CCR5 ligands, CCL3, CCL4 and CCL5 which can lead them to the tumor microenvironment.[41] Generally the TADC are immature in development and incapable of eliciting appropriate effector responses; immature

dendritic cells can take up antigen but are dysfunctional in presenting antigen.[7] Like TAM, tumor associated dendritic cells also have the capability of being either pro-tumorigenic (through angiogenic factors and tolerance inducing factors) or anti-tumorigenic (by T-cell activation).[32] It has been suggested that the quantity and quality of signals to immature dendritic cells determine whether they will activate T-cell populations to fight cancer, remain inside the tumor microenvironment and not elicit any immune response, or migrate to lymph nodes and induce tolerance to the tumor.[41] A key factor in immature dendritic cell maturation is expression of the chemokine receptor CCR7 which can direct them to lymph nodes by lymphatic vessel release of chemokine ligand CCL21, a CCR7 ligand.[41] The complete role of chemokines and dendritic cells in cancer cell proliferation, tolerance or destruction is not yet fully understood.

The balance of signals provided to cells and the tumor microenvironment can tip the scale toward immunosuppression or induction of an immune response.

b) Chemokines and Metastasis

Nine out of ten cancer deaths are attributable to cancer metastases.[19,42] Little is known about the specific mechanisms of cancer metastasis. Because of its relationship to cancer morbidity it represents an urgent need for more research. If cancer metastasis can be slowed or halted, survival rates will greatly increase. It is known that cancer cell migration and metastasis is not a random process, but a highly organized, complex and selective process.[43] There are three major hypotheses to explain the mechanism of metastases.[44] The first implies that cancer cells have little to no direction in migration, but can only survive in certain tissues that provide the proper growth factors. This idea was first introduced by British surgeon Stephen Paget in the 19th

century. Paget compared cancer cells and sites of metastasis to seeds and fertile soil.[44] The seeds will not grow in nutrient deficient soil but require nourishment from the soil. The second theory is that the adhesion to distant endothelial luminal surface is selective only at the specific organ site. Finally, the third proposed mechanism suggests that receptors on the neoplasms direct the migrating cancer cells to follow a gradient of soluble factors (chemokines) to the tissue producing these attractants.[44] Evidence exists to support each hypothesis. It seems that at least the first and third hypothesis need not be mutually exclusive, if it can be imagined that the seed is directed to the fertile soil (by chemokines).

There are several interdependent steps in the metastatic process, beginning with the successful growth of the primary tumor. It is unknown what causes a primary tumor to undergo metastasis, though it is thought hypoxia might play a role in some cancers.[44] Next neoplastic cells must detach and invade either blood vessels or lymphatic vessels which requires degradation of the extracellular matrix (ECM) and a change in morphology of the cell.[32] Neoplasts then follow a pattern that closely resemble leukocytes trafficking by exiting the vasculature and homing to distant organs.[32] Finally, development of a pro-tumor microenvironment in the new site forms a deadly metastasis. The same factors critical for growth at the primary site also influence secondary site success but even more so as the cells are in a foreign tissue and must be provided with stimulatory signals from the tumor microenvironment. To get from one tissue to another involves a host of signals, some of which are provided by the chemokine system.

In order for a neoplastic cell to leave the primary tumor site, the extracellular matrix must be degraded by secreted proteases such as matrix metalloproteinases (MMP). In the “counter-

current invasion" hypothesis, Opdenakker et al. proposed that the invading leukocytes, attracted by tumor-secreted chemokines, degrade the ECM on their way to the tumor microenvironment in a way that clears a path for the tumor cells to then reach the blood or lymph vessels.[45] Overexpression of CXCL8 in PCa resulted in expression of MMP-9, which in nude mice, increased PCa invasiveness and metastatic potential.[46] In breast cancer, increased CCL5/ RANTES expression also upregulates MMP-9, furthering disease progression.[32] Degradation of the basement membrane is an early step in the metastatic process.

Cancer cells have a proclivity to metastasize to particular secondary sites. That chemokines play a role in this predilection was first noted in breast cancer in 2001.[47] Homey et al. reported that the chemokine receptors CCR7 and CXCR4 were highly expressed by breast cancer cells, both in the primary site and metastatic sites and showed that the ligands for the overexpressed receptors, CXCL12 and CCL21, had highest expression in the tissues where the most common breast cancer metastases are found, such as the lung and liver. Blocking the CXCL12 binding site on CXCR4 with a receptor antibody led to a decrease in metastasis in a murine model showing a relationship between this receptor on the tumor cells and their directed metastasis.[47] Since this discovery, several other chemokine ligand/receptor pairs have been implicated in metastatic homing. Whether these chemokines direct migration over very long distances has yet to be determined but it remains that the overexpression of chemokine receptors is characteristic of many cancers.[48,42]

In summary, chemokines and their receptors have been extensively studied and play many diverse and sometimes opposing roles in the progression of cancer. The manipulation of the chemokine/chemokine receptor system may be useful in treating cancer.

2.3 The Chemokine/Chemokine Receptor System in Cancer Therapy

The chemokine system is clearly involved in many steps of neoplastic growth, spread, and evasion of the immune system. There are different points in the timeline of a neoplastic growth where exploitation of the chemokine/chemokine receptor network may lead to suppression of growth, activation of immune response, and inhibition of metastatic spread. The introduction of chemokines to recruit effector immune cells and the antagonism of chemokine receptors to block tumorigenic properties of chemokines are both possible ways to manipulate the chemokine system.

There are instances when chemoattractive chemokines can recruit effector T-cells to the cancer cells or induce anti-tumoral immune responses through dendritic cells. Injecting intratumoral chemokines can disrupt the balance between immune suppression and activation mediated by chemokines and TILs. For example, CCL5/RANTES was shown to direct effector T-cell recruitment after injection into tumors.[46] In fact, many chemokines can delay or halt tumor progression in experimental models when injected into tumors.[43] Some of these chemokines act by recruiting dendritic cells (DC), like CCL19, CCL20, and CCL21.[38,43] Properly activated DCs can present tumor antigens and activate immune responses against the tumor. Changing the balance of CKs can disrupt immunotolerance and activate proper host inflammatory response.

Overexpression of chemokine receptors is seen in many human tumors. Antagonism of these receptors has already shown promise in blocking metastases; CXCR4 antagonism blocked CXCL12 directed breast cancer metastases.[39,47] There are a few different methods of antagonism that have been tried to date, including development of chemokine receptor antibodies,

modification of endogenous chemokines and design and development of small molecule chemokine receptor antagonists. Antagonism of chemokine receptors is currently being investigated for not just cancer therapies, but also for treatment of multiple sclerosis, HIV, rheumatoid arthritis, and chronic obstructive pulmonary disease.[7] As GPCRs, chemokine receptors belong to a highly exploited class of receptors for drug targets; nearly 50% of currently marketed drugs target GPCRs in vivo.[9] The introduction of Met-CCL5, a RANTES derivative with antagonistic effect on CCR5, into a murine model of breast cancer led to a reduction of TIL, especially TAM, and reduced the growth of the tumor models.[38] Monoclonal antibodies of CXCR4 have also been found to inhibit lung metastases of a murine melanoma and prostate cancer metastases to the bone in a murine model[49] in addition to earlier findings that CXCR4 antibodies inhibit incidence of breast cancer lung metastases.[43] High throughput screening of small molecule libraries has produced new leads for the development of chemokine receptor antagonists. Thus far, only one chemokine antagonist, Maraviroc, a CCR5 antagonist, has been approved by the FDA.[7] Maraviroc is used as an HIV-1 entry inhibitor. CCR5 is currently being explored also as a target in PCa progression.

4. CC Chemokine Receptor 5 (CCR5): Structure, Function, and Antagonists

CC Chemokine Receptor 5 (CCR5) is of particular interest because of its involvement in HIV-1 entry[7] and a later discovery that a CCR5 antagonist inhibited proliferation of PCa cells.[10] CCR5 is also implicated in the pathogenesis of many immune and inflammatory conditions, including multiple sclerosis, rheumatoid arthritis (RA), psoriasis, atherosclerosis, and chronic hepatitis.[50] CCR5 is normally expressed on resting effector T-cells, monocytes, macrophages and

immature dendritic cells.[7] The endogenous ligands for CCR5 include CCL3, CCL4, and CCL5[7] though other chemokines have been shown to bind CCR5 at higher than physiological concentrations.[35] Like other CC chemokines, CCR5 has 4 cysteine residues in its exracellular regions, a conserved DRYLA amino acid sequence in the second intracellular loop which is thought to be necessary for G protein binding.[7] (Figure 1) CCR5 shares the highest homology (71%) with CCR2. CCR5 is comprised of 352 amino acids and coded on chromosome 3p21.[7] CCR5-Δ32 is a genetic variant of CCR5 where 32 base pairs are deleted, translating into a truncated protein which is not expressed at the cell surface. Individuals with this gene variant are resistant to M-tropic HIV-1. High-throughput screening yielded several hits which further resulted in new leads from several companies. Development of CCR5 antagonists has led to the marketing of Maraviroc, a selective small molecule antagonist. Maraviroc is the only chemokine receptor antagonist to successfully complete clinical trials.[7] One of these leads, TAK-779, was found to inhibit proliferation of PCa cells.[10]

The activation of CCR5 by endogenous ligands involves many effector proteins inside the cell and can result in increase of intracellular free Ca^{2+} concentration, inhibition of adenylyl cyclase and activation of MAP kinase and Jun-N-terminal kinase (JNK)[51] resulting in transcription of genes that effect T-cell proliferation and activation of cytokines.[7] There is a proposed two step process in chemokine binding, where sulfated tyrosines on the N-terminus attract the core of the chemokine to the extracellular terminus and extracellular loop 2 (EL-2) of the receptor followed by an interaction of the N-terminus of the chemokine with the α-helical transmembrane domains of the receptor.[7] CCR5 is generally believed to be coupled to $G\alpha_i$ but research has shown different chemokine ligands exhibit biphasic response curves which could

indicate a change in G protein coupling.[35] Other experiments have demostrated that in lipid rafts with low cholesterol levels CCR5 can signal through pertussis toxin insensitive pathways.[51]

Figure 1. 2-D structure of CCR5 with palmitoylation sites and two disulfide bonds.

After ligand binding, the Gα subunit dissociates from the Gβγ subunits. $G\alpha_i$ inhibits adenylyl cyclase and slowly hydrolizes GTP to GDP. The activity of the Gβγ is important for chemotaxis of the cell.[36] Gβγ activates phospholipase C β (PLCβ) isoforms. PLCβ activation results in increased levels of diacylglycerol (DAG), inositol(1,4,5)triphosphate, and calcium ion. Gβγ signalling results in cell motility through Pyk-2 and JNK.[34] CCL5 activates RhoA, which is among many small GTPases that affect actin polymerization, cell motility, and polarity. Counter-regulatory mechanisms are initiated through DAG stimulation of protein kinase C (PKC) which facilitates C terminal phosphorylation, increasing affinity for β-arrestin binding.[7]

Signaling of CCR5, like other GPCRs, is terminated by receptor internalization followed by either recycling or degradation. The chemokine ligand is not always released through internalization and recycling back to the cell membrane, resulting in further signaling. Two serine phosphorylation sites are necessary for arrestin binding followed by receptor endocytosis in clathrin coated pits.[7] Dephosphorylation followed by palmitoylation of the conserved cysteine residues can direct the protein back to the cell surface. Phosphorylation-deficient cells can also internalize CCR5 through caveloae. Palmitoylation of the cysteine residues while the protein is expressed on the cell surface may direct the receptor towards cholesterol rich areas of the lipid bilayer.[7] Resensitization brings the ligand binding-receptor signaling cascade full circle.

The involvement of CCR5 in HIV-1 pathology prompted a rapid and extensive search for antagonists. Pharmaceutical companies including Pfizer, Schering, Astrazeneca, Takeda, andGlaxoSmithKline all had a CCR5 antagonist drug candidate undergoing clinical trials as of 2008. All candidates were HIV entry inhibitors expect for Aztrazeneca, which was testing a drug for rheumatoid arthritis.[7] All candidates were optimized leads from high-throughput screening. Maraviroc (Figure 2) was the only approved small molecule chemokine receptor antagonist to complete clinical trials with success. TAK-779 (Figure 2) was a precursor to the Takeda drug candidate in clinical trials. It was found to inhibit prostate cancer cell lines. Screening of natural product extracts has resulted in the discovery of anibamine, a high affinity antagonist of CCR5.[11,12] (Figure 2)

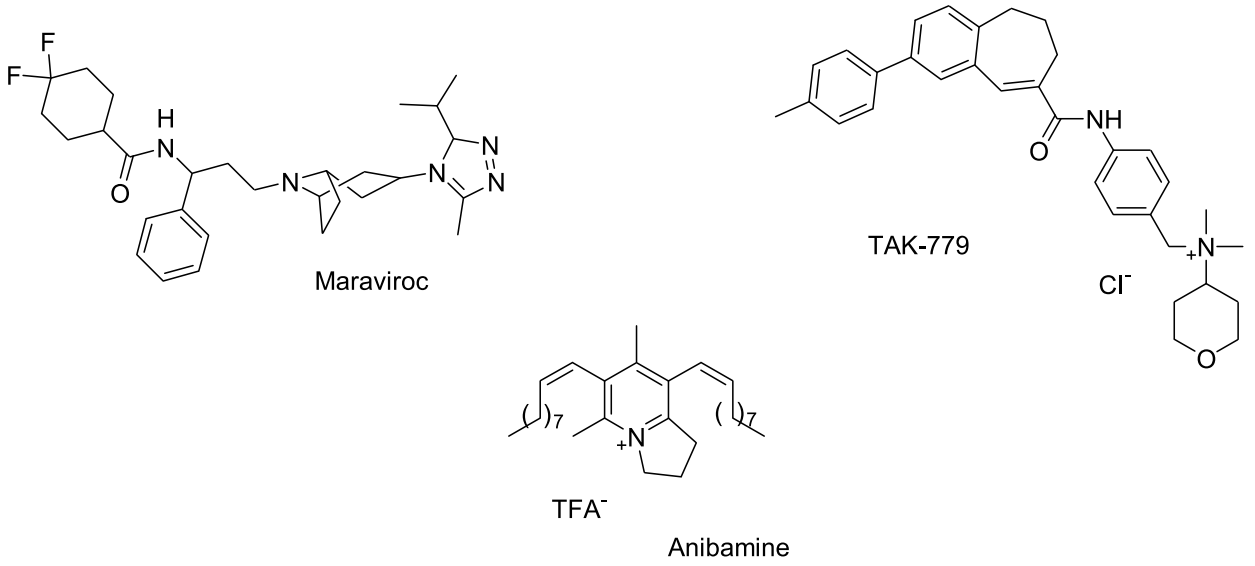

Figure 2. Structures of CCR5 antagonists-Maraviroc, TAK-779 and Anibamine.

C. Natural Products and Drug Discovery

Terrestrial plants, microorganisms and marine life provide an abundance of molecules with the potential for biological activity in the human body. High throughput screening hits of natural products as well as traditional medicine have provided drug candidates for anticancer activity, perhaps most notably taxol and camptothecin.[52] These natural products often have novel mechanisms of action and provide unique chemical structures as new leads for drug development, especially compared to synthetic libraries created by combinatorial chemistry. Though combinatorial chemistry has gained popularity as a source of new leads, it has not produced the results expected while natural product research has been deemphasized by major pharmaceutical companies in recent years.[53] The study of natural products, their structures, biosynthesis, and mechanisms of action, have benefitted medicine, synthetic organic chemistry, biology and will continue to be important in medicinal chemistry and drug development.

1. Natural Products and Their Target Proteins

The majority of the natural products useful as new drug leads are secondary metabolites. Primary metabolites are produced to maintain the normal basic functions of the cell or organism. Secondary metabolites are produced by pathways turned on for alternate functions such as defense from predation, disease, and starvation.[54] Dixon et al. suggested that secondary metabolites are purposed to interact with and manipulate macromolecular targets.[55] For example, many alkaloids are produced by plants to protect them from being eaten by animals. These compounds, including morphine, nicotine, and quinine, (Figure 3) have developed to bind to animal, mainly mammalian, proteins. Snake venom binds mammalian ion channels in nerve cells, rendering paralysis or death. The bacterial and fungal organisms responsible for the production of natural products like cyclosporin, FK506, and rapamycin probably intended to utilize them for protection, instead they are used to sustain immunocompromised patients.[56] These secondary metabolites must be manufactured in the cell by proteins from ostensibly the same building blocks as primary metabolites.

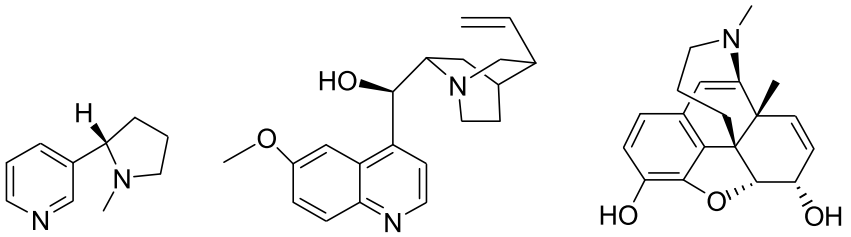

Figure 3. Structures of natural products-nicotine, quinine, and morphine.

A corollary to the idea of the biosynthesis of these natural products is that, to be synthesized by proteins, they must be bound to protein catalysts, which is the second key point in understanding the usefulness of natural products as drug leads. A small molecule may bind one

or more domains on a given protein as a part of a biosynthetic pathway. A domain is defined as a part of the protein that folds independently from other parts, like an α helix or a β sheet. Although the total number of proteins is currently unknown, it is accepted that the number of different domains will be much smaller, estimates range from less than one percent of the number of different proteins to half.[56] With such a relatively low number of possible domains, it is likely that molecules can be promiscuous in their binding, even across species, especially given that among all species there are many protein types that possess the same or similar function.[54] A protein family can no longer be defined by only sequence homology or similar catalytic activity, the arrangement of the domains in the three dimensional structure must be taken into consideration as those domains may bind to the same or similar ligands.[56] In the future, it may be possible to predict ligands based on domain homology even though the function of the protein is unknown. Protein catalysts bind and synthesize the secondary metabolites of lower organisms that can bind to protein domains in other organisms.

2. Structural Attributes of Natural Products

Another virtue of natural products is their structural qualities. Natural products differ from synthetic molecules in their complexity. In general, natural products have more stereogenic centers, more carbon, hydrogen, and oxygen atoms and less nitrogen, sulfur and halogen containing groups than synthetic molecules.[57] Also, in violation of Lipinski's "rule of five" for an ideal drug candidate, often natural products have a molecular weight of greater than 500 daltons. Structural constraint is built into natural products through extensive conjugation, fused ring systems, and macrocyclizations; only 20% of natural product ring systems are accounted for in

current drugs. Entropic loss upon binding to target macromolecule is minimized by these constraints which allows for higher binding affinity allowing them to function as potent ligands.[57] Functional groups on natural products often are beyond the scope of an average chemist's imagination like the enediyne of calicheamicin and the carbolamine group in ecteinascidin[57] The enediyne functional group, (Figure 4) when triggered by redox reactions in other parts of the molecule, forms a diradical intermediate that can damage DNA and produce cytotoxicity at a concentration of one molecule per cell. In ecteinaschidin, the carbolamine group (Figure 4) is dehydrogenated to an iminium ion and forms a covalent bond with DNA. Other natural products produce non-covalent interactions by mimicry of shape or polarity of endogenous ligands. Tetraguanine fragments on telomeres are imitated by telomestatin which has eight heterocycles combined into a macrocycle, inhibiting the function of telomerases.[57] Often natural compounds have excellent pharmacokinetics because they were engineered to locate and bind target compounds in other organisms.[56] Non-intuitive compositional features make natural products excellent sources of novel structures.

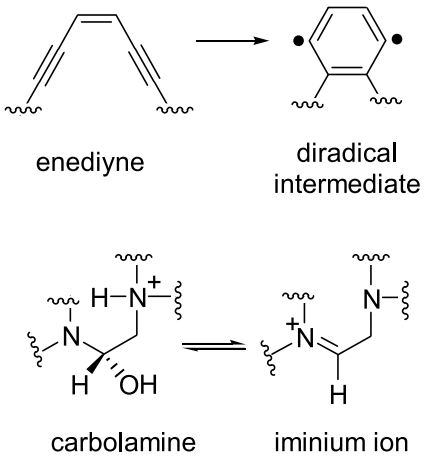

Figure 4. Examples of reactive functional groups in natural products.

3. “Privileged Structures”

Taking these points together, the concept of a privileged structure becomes relevant. The term privileged structure was first used by B.E. Evans and his group in describing the ability of benzodiazepine analogues to bind many different receptor types with high affinity.[58] Natural products can be viewed as privileged structures when they both bind their biosynthetic proteins and one or more target proteins as well. Privileged structures make an excellent starting point for combinatorial synthesis of natural product-like libraries.

Natural product research was neglected in favor of combinatorial chemistry in recent years. However, combinatorial chemistry has been a slight disappointment in the drug development world. Newman et al. reported that from 1981 to 2002, there were 79 new chemical entities for anti cancer therapies. Fourteen were peptide in nature and 48 were small molecule natural products, analogs or mimetics. Only 17 were synthetic with no basis in natural products.[53] The problem with combinatorial chemistry is that the underlying structures for the libraries are not biologically relevant. As Mann observed, “nature has already carried out the combinatorial chemistry,” natural products can serve as leads for building biologically relevant libraries.[59] Libraries based on privileged structures have already proven to be fruitful, such as the nakijiquinones by Waldmann and group and the sarcodictyins by Nicolau and group. By using biologically functional scaffolding, both combinatorial chemistry and natural product chemistry can benefit each other, while increasing the production of active compounds.[59]

4. From Traditional Medicine to the NCI Cancer Panel

Traditional medicine has relied upon various natural products to treat illness and injury for millennia. In the area of anti-cancer research alone, nine natural product based compounds

have been approved for cancer chemotherapy in the US as of 2008.[60] These include vinblastine, vincristine, etoposide, teniposide, taxol, navelbine, taxotere, topetecan, and irinotecan.

Two currently approved chemotherapeutics were developed from a natural product used medicinally by Native American populations. Etoposide and teniposide are derived from podophyllotoxin (Pd), which is an extract from the plant mayapple, *Podophyllum peltatum*. Skin cancers and venereal diseases were treated with extracts from the mayapple by Native Americans,[59] but Podophyllotoxin failed the FDA's Phase I clinical trials in the 1970s. Due to the poor bioavailability and drug resistance of podophylotoxin,analogs etoposide and teniposidewere synthesized. Etoposide is a Topoisomerase II inhibitor, while podophyllotoxin binds tubulin reversibly, resulting in inhibition of microtubule assembly.[61] From the traditionally used podophyllotoxin came two anticancer agents with different mechanisms of action.

Another class of anticancer compounds are known as vinca alkaloids from the genus *Caranthus.* Native populations of the West Indies and Madagascar used *Caranthus rosea* medicinally for various ailments.[61] Vinblastine and vincristine treat Hodgkin's lymphoma and acute childhood lymphoblastic leukemia respectively but with many side effects including peripheral neuropathy, constipation and hair loss. Structural modification has led to analogs that can treat non-small cell lung carcinoma and advanced breast cancer.[61] Pharmacological improvements of another traditionally used natural product has led to new therapies for a variety of cancers.

The discovery that these folk medicines had anticancer affects inspired the National Cancer Institute to begin screening natural product extracts for cytotoxicity. From 1960 to 1982 nearly 35,000 plant samples were tested against mouse leukemia cell lines.[59] These screenings

led to the discovery of taxol, which is currently estimated at producing two billion dollars annually for Bristol-Myers-Squibb. In 1985 the NCI instituted a panel of 60 human cancer cell lines including solid tumors and leukemias for a more thorough testing of natural products.[59]

5. From extract to drug candidate

After a hit is identified on the NCI screening panel, or a similar discovery of cytotoxic activity, there are many steps to produce an FDA approved chemotherapeutic agent or even a compound available for evaluation by medicinal chemists. There are three major obstacles in finding a new lead: identification of duplicates, characterization, and supply. The "supply problem" in natural product drug discovery is frequently due to natural source limitations. For example, four thousand Pacific Yew trees were sacrificed for a mere 360 g of taxol to perform early tests.[59] Potier and colleagues overcame this his problem by using the European Yew tree needle's 10-deacectylbaccatin III as a starting point for the semi-synthesis of taxol in 80% yield. Further technological improvements have ensured the continued production of taxol without use of the Pacific yew tree. In the process of using 10-deacetylbaccatin III in the synthesis of taxol, an analog with even better properties, taxotere, was discovered.[59,62] (Figure 5) Advances in microbial genomics as well as using the chemoenzymatic approach can help produce specific natural products as well. The total synthesis of the natural product from simple precursors is also an option to alleviate the supply problem.

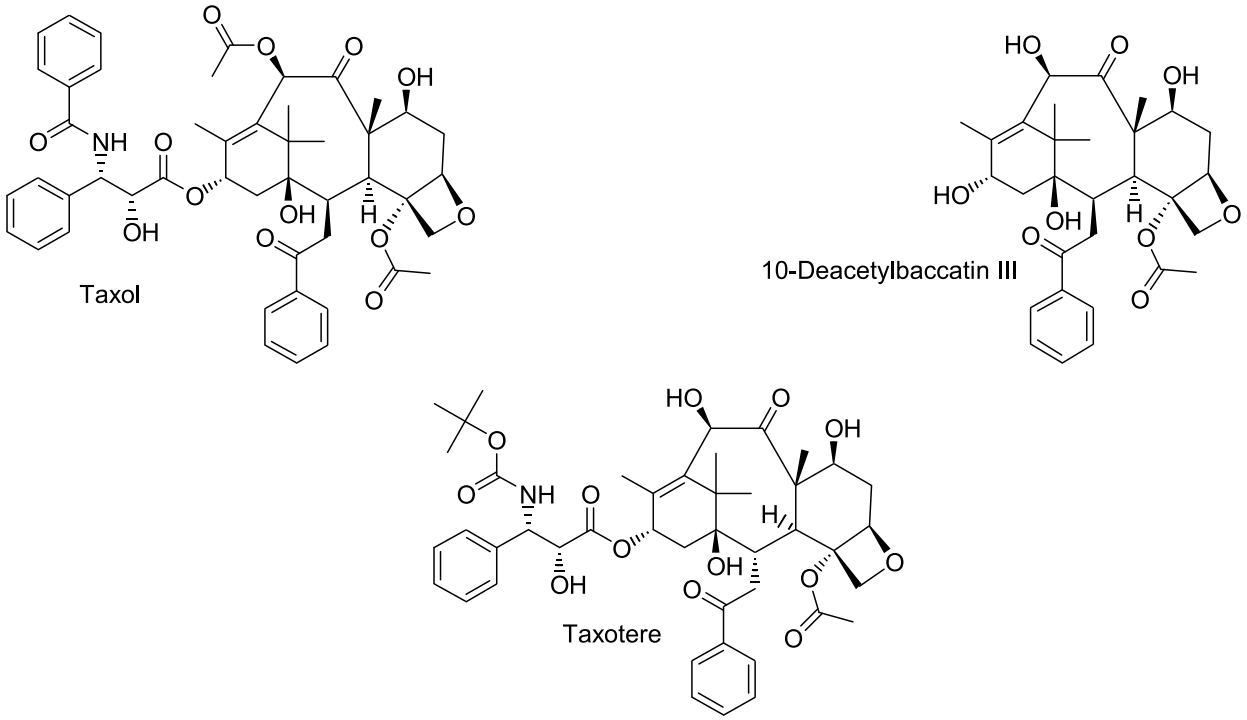

Figure 5. Structures of taxanes-taxol, 10-deacetylbaccatin III, and taxotere.

Total synthesis of natural products has its roots in early synthetic chemistry. Once used to confirm hypothesized structures, now total synthesis is useful in preparing products and analogs for refining of the active component, lowering costs as well as a means for discovering new chemical reactions. The first total synthesis was accomplished by F. Wohler in 1828.[63] He synthesized urea from ammonium cyanate. Later in the nineteenth century, H.E. Fischer synthesized (+)-glucose, the first total synthesis of a chiral molecule. Throughout the twentieth century, total synthesis schemes introduced new routes to natural product synthesis, developing a new understanding of chemistry as well as concocting novel reactions that are now endemic in organic synthesis. Examples include the use of protecting groups, the Wittig reaction, palladium catalyzed C-C bond forming reactions, asymmetric catalysis and the use of "one-pot" synthetic cascades.[63] R.B. Woodward used mechanistic rationale to synthesize complex natural products and pioneered stereocontrol in his syntheses. E.J Corey introduced the idea of retrosynthetic

analysis that is now is indispensable to total synthesis.[63] Clearly total synthesis is a vital part of natural product drug discovery.

Drug development also benefits from a carefully planned total synthesis approach which can accommodate fundamental structural changes to prepare analogs via a diverted total synthesis scheme. It is rare that the natural product produced by a given organism is the best possible drug candidate. More often, a natural product lead provides a scaffold to build on where drug properties can be enhanced and side effects reduced, sometimes with the added benefit of simplifying the lead compound. Biosynthesis cannot always give these altered analogs and building from the natural product scaffold itself (semi-synthesis) is not feasible. A diverted total synthesis scheme can take an intermediate and build in changes in a route parallel to the original total synthesis scheme resulting in an anolog with either more or less complexity than the parent compound.[64] A worthy example of this is the anticancer drug candidate E7389. The total synthesis of cytotoxic Halichondrin B led to the realization that E7389, an analog missing a large portion of the lead molecule, retained antimitotic properties and was more stable in vivo due to a ketone functional group in place of the macrolactone of the lead compound.[65] Preparation of analogous molecules is crucial to refining the active components, which may include molecular modeling, metabolism and mechanism of action investigations as well as structure-activity relationship studies. With the refinement of the pharmacophore, drug development can then address toxological, production, and formulation concerns.

6. Camptothecin and Taxol as Models for Natural Product Drug Discovery

Two important examples of natural product drug discovery and development are taxol and camptothecin, work which was accomplished in the labs of M. E. Wall and M. C. Wani.[52]

Prompted by NCI cytotoxic screenings, they purified and characterized both compounds for their cytotoxicity. A closer examination of the efforts made by these scientists and their colleagues can emphasize many important aspects of using natural products as anticancer drug leads. Wall and Wani developed the use of the bioactivity of a crude extract to guide the purification of the most potent compound. Camptothecin, isolated from the Chinese tree, *Camptotheca acuminate*, led to two first generation analogs, irinotecan and topetecan, (Figure 6) which are used for the treatment of colon and ovarian cancers. Camptothecin itself had poor solubility and early attempts to form it into a salt disturbed a lactone ring moiety that turned out to be necessary for activity. Camptothecin binds Topoisomerase I, which at the time was an unknown target for cancer therapy. Since this discovery, several other topoisomerase "poisons" have been discovered, including etoposide and doxorubicin. Recently it was observed that camptothecins might also target hypoxia-inducible factor 1, a protein involved in maintaining a cancer cell's ability to survive in hypoxic conditions and which may also be involved in metastasis. Taxol, as mentioned previously, was discovered from the Pacific Yew tree. It has been useful in the treatment of ovarian, breast, and lung cancers. Both taxol and its derivative taxotere have the same mechanism of action, microtubule stabilization, another previously unknown cellular target for anticancer drug development. Taxol and camptothecin have launched two new classes of drugs with previously unknown targets. Both were painstakingly purified and characterized from crude extracts of bioactive natural products and are excellent examples of the power of natural products in drug discovery and development.

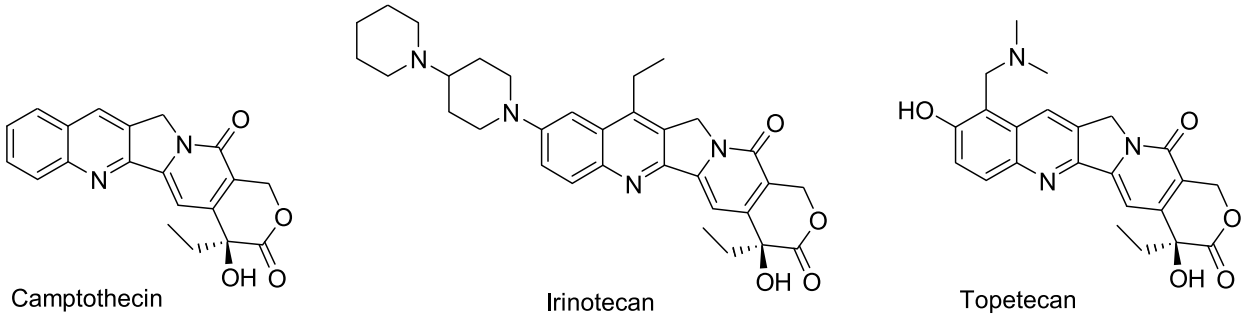

Figure 6. Structures of camptothecin and analogs irinotecan and topetecan.

7. Influence of Natural Products on Cancer Biology

Natural product research has also had an impact on our understanding of biology. Novel mechanisms of actions and consequently the discovery of novel targets have also been benefits of natural product drug discovery. The discovery of taxol led to the study of tubulin stabilization as an anti-cancer mechanism. Topoisomerase I was discovered as an anti-cancer target because of Camptothecin.[52] Frequently, cancer chemotherapeutics are used in combination with another therapy in order to combat cancer cells that have accrued many growth and regulation abnormalities. Also, when first line therapies fail, second line therapy is usually aimed at another cellular target, to combat drug resistance. It is notable that many daughter compounds are used to treat different forms of cancer from the lead natural product, multiplying the therapeutic impact of the parent compound. In fact, some screening has changed from strictly cell based to mechanism of action based.[59] The discovery of more cellular targets is a major help in curbing cancer.

8. Anibamine, a Natural Product Chemokine Receptor CCR5 Antagonist

In 2004, anibamine was isolated from a crude extract fron *Aniba panurensis* by activity guided fractionation for its antimicrobial activity against an azole-resistant strain of *Candida*

albicans,[12] much like the method Wall and Wani pioneered.[52] The novel indolizinium alkaloid was tested against the DTP 60 human cancer cell lines with an LC_{50} of 10^{-5} M with no selectivity. Anibamine was found to have a logP value of 9.1, much higher than that the maximum of five suggested by Lipinski.[12] The same compound was also concurrently isolated from an assay involving human CCR5 receptor, ^{125}I-gp120, and soluble CD4 to test for CCR5 antagonism.[11] The total synthesis of anibamine was established in 2005 in our lab. A ten step synthesis from acetyl acetone and cyanoacetic acid yield anibamine and 3 isomers.[14] Due to its hemolytic activity and high logP, modification is necessary to optimize its activity and lower its toxicity.

9. Summary of Impact of Natural Products on Drug Discovery

The collective decision to slight natural product research was clearly a poor one. The use of natural products has come a long way from primitive man. Bioinformatics and structural biology demonstrate the possibility for promiscuity between small molecules and protein domains; privileged structures bind different kinds of proteins with high affinities. Traditional medicine has led to currently used and refined compounds such as the Vinca alkaloids and campothecins. The success of folk medicines inspired the National Cancer Institute to begin screening of natural product extracts against cancer cell lines which has produced more drug candidates. The hurdle of producing mass quantities of biologically active compounds have been largely overcome by pioneering of synthetic chemistry methodologies. The study of natural products has also benefitted the field of biology by contributing to the elucidation of novel mechanisms of action that has led to new insights in understanding disease targets. The currently undiscovered natural products of the world will certainly yield even more insight in many fields.

III. Project Design and Objectives

The chemokine receptor CCR5 has been implicated in a number of disease states, including HIV-1 and prostate cancer. Because of the wide variety of applications, antagonists of CCR5 are highly sought after. High throughput screening of synthetic libraries have resulted in several drug leads, but only one successful drug has emerged thus far. The realm of natural products should not be overlooked when looking for biologically active lead compounds as antagonists for this receptor.

Anibamine was discovered as a novel natural product with a high binding affinity for chemokine receptor CCR5. However, its pharmacological properties were not ideal. The lipophilicity of the molecule exceeded the guidelines envisioned by Lipinksi. Anibamine also possessed considerable toxicity. In order to refine the active structure and increase the therapeutic index, the structure activity relationship of anibamine needed to be established. This was to be accomplished by synthesizing analogs using the "Deconstruction-Reconstruction-Elaboration" approach. This method was applied by "deconstructing" functional groups and atoms of the lead compound sequentially. Following this, "reconstruction" of the molecule rebuilt the parts of the molecule in a different order. Ideally this would give the pharmacophore, the core of the molecule necessary for its biological activity. To the defined pharmacophore, "elaborations" can be made by the addition of atoms or groups of atoms or altering of stereochemistry. As a natural product, anibamine offered a unique scaffold for modification.

There are several points in the structure of anibamine that can be deconstructed and/or elaborated upon. The proposed structural modification of anibamine are shown in Figure 7. At point (a) the sidechains can be deconstructed. The sidechain double bond configuration can be

elaborated upon at point (b). Elaboration of the ring at part (d) has been accomplished in our lab and deconstruction of the ring at point (c) is ongoing. These modifications were each intended to further refine the pharmacophore of this series of coumpounds.

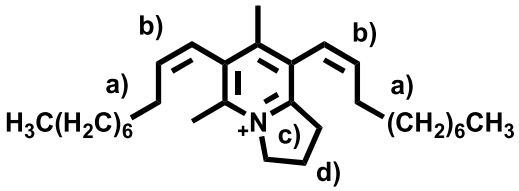

Figure 7. Proposed structural modifications of anibamine

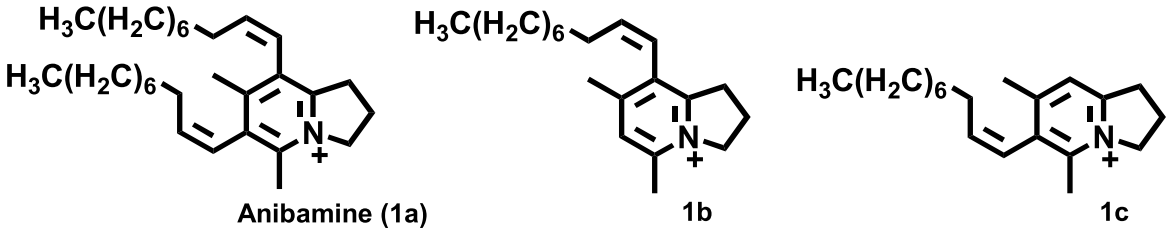

Figure 8. Structure of anibamine, **1a**, and proposed deconstructed analogs **1b** and **1c**.

The purpose of this project was to synthesize and characterize anibamine (**1a**) and two deconstructed analogs (**1b** and **1c**). (Figure 8) The analogs were to retain the indolizinium core structure of anibamine but retain only one of the aliphatic side chains at C-8 or C-6. Synthesis of deconstructed analogs paralleled the total synthesis of anibamine (Scheme 1) with different starting substrates. Synthesis and evaluation of deconstructed analogs would answer the question of which sidechains were important for activity, or whether of not both were critical for activity. The synthetic route yielded two isomers and upon hydrogenation, a third analog. The synthesis and evaluation of analogs with different bonds at point (b) would give elucidate what configuration is ideal and if a saturated bond is best, this would facilitate more efficient synthesis.

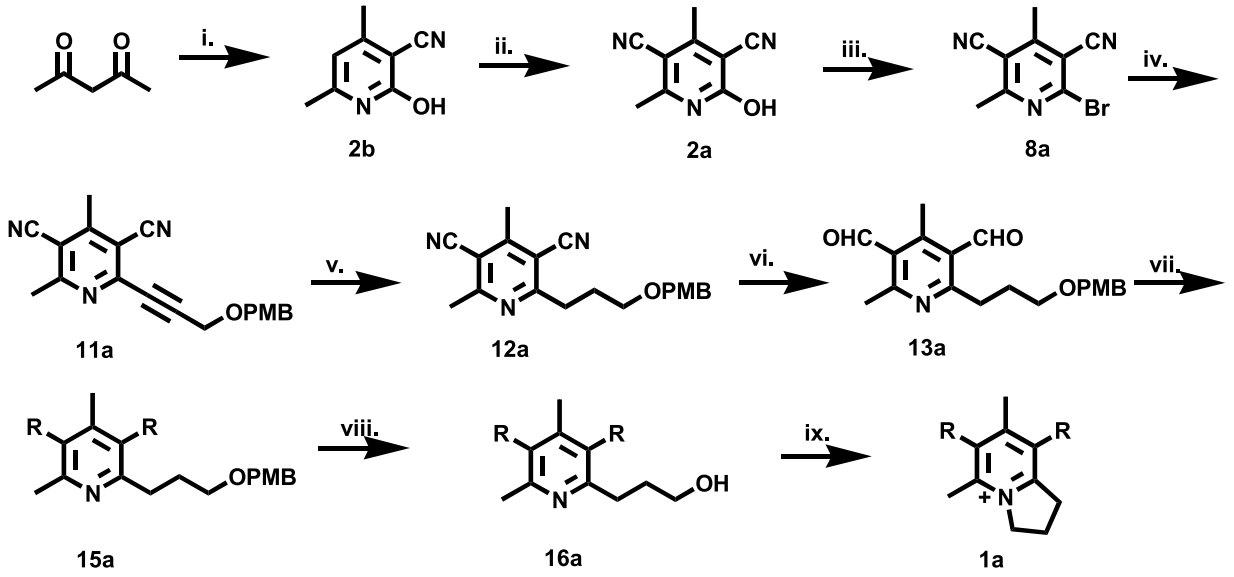

Scheme 1. Total synthesis of anibamine (**1a**) from acetylacetone. Reagents and conditions: i. cyanoacetic acid, K_2CO_3, H_2O, overnight; ii. 1)NBS, H_2SO_4, TFA, 0˚C 2 hours; 2) CuCN, DMF, N_2, reflux 48 hours; iii. TBAB, P_2O_5, toluene 90˚C, 2 hours; iv. CuI, $PdCl_2(PPh_3)_2$, **10**, Et_2O; v. 55 psi H_2, Pd/C, MeOH, 7 hours; vi. 1) DIBAL-H, toluene -78 ˚C, 2 hours; 2) H_2SO_4 (aq); vii. 1) **14**, LHMDS, toluene -78 ˚C, 2 hours; 2) NH_4Cl (aq) (R=-CH=CH$(CH_2)_7CH_3$); viii. 1N HCl, EtOH, reflux 5 hours; ix. MsCl, TEA, CH_2Cl_2 0˚C to rt, 1 hour

In addition to the preparation of analogs, sidechain coupling reactions were explored in order to discover if there was a way to more efficiently synthesize geometric isomers of interest. The original total synthesis scheme used the Wittig reaction to attach the aliphatic sidechains to the aldehyde intermediate. This reaction results in primarily *cis* double bonds in the product. While this was desired to produce anibamine, it also made separation of pure product tedious and expensive by HPLC. To continue to investigate analogs of anibamine, a stereoselective synthesis of only one isomer was desired. Different methods were attempted to yield only the *trans* isomer with varying results.

After the synthesis of the analogs, biological assays were performed to develop structure activity relationships. Previously prepared analogs and deconstructed analogs were evaluated to answers questions of sidechain, ring size, and double bond configuration importance. Three

metastatic prostate cancer cell lines, DU-145, PC-3, and M12, were used in anti-proliferative assays with each drug. The colorimetric agent, WST-1, was used in each screening. The goal of the assays was to determine the next generation lead compound for anti-prostate cancer activity.

Ligand docking experiments were performed using two homology models of CCR5 based on two different crystal structures of other GPCRs. Can these homology model differentiate between the very similar deconstructed analogs? These were performed to analyze possible binding modes of the deconstructed ligands within the binding pocket of CCR5 and to continue to scrutinize the validity of the different models.

IV. Results and Discussion

A. Chemical synthesis of Anibamine and Analogs as CCR5 Antagonists

The total synthesis of anibamine was accomplished in our lab previously.[13] To prepare anibamine and the deconstructed analogs, three key intermediates, **2a, 2b,** and **2c** were synthesized. (Figure 9) From preparation of these intermediates, parallel synthetic routes produced anibamine and analogs **1b** and **1c** along with their *trans* isomers.

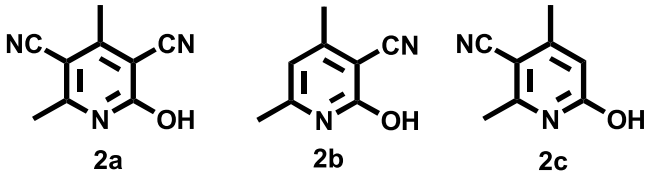

Figure 9. Key intermediates in each synthetic pathway, 2-hydroxy-4,6-dimethylpyridine-3,5-dicarbonitrile (**2a**), 2-hydroxyl-4,6-dimethylnicotinonitrile (**2b**), and 6-hydroxyl-2,4-dimethylpyridine-3-carbaldehyde (**2c**),

1. Synthesis of key intermediates in each route

Two synthetic routes to **2a** in the total synthesis of anibamine were previously reported. Route 1 (Scheme 2) began with the condensation of acetyl acetone and N,N-dimethylformamide dimethyl acetal in neat refluxing conditions.[66] Product **3** was purified by recrystallization in EtOAc with 71% yield. In an acid catalyzed reaction, **4** was prepared using hydroxyl amine hydrochloride in MeOH at reflux.[67] The isoxazole product was purified under reduced pressure distillation affording **4** in 51% yield. Compound **4** was then refluxed neat with 3 equivalents of aniline, followed by an acidic workup.[68] Recrystallization in EtOH afforded **5** in 54% yield. The β−enaminonitrile (**5**) was then dissolved in MeOH with KOH and malononitrile at reflux. The

basic conditions cleaved the aniline group ultimately resulting in the first intermediate, **2a**, in 74% yield.[69]

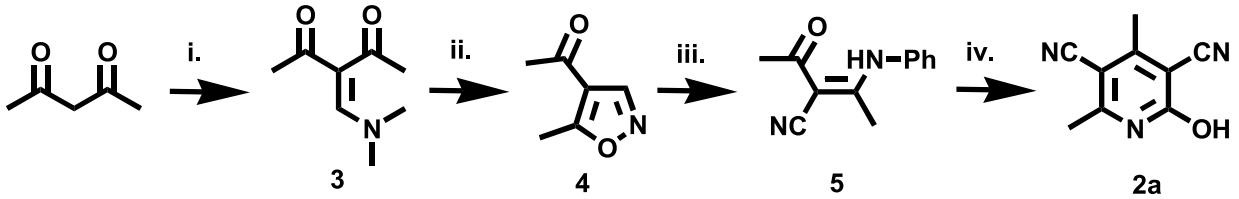

Scheme 2. Route 1 to the first intermediate in anibamine synthesis. Reagents and conditions: i. N,N-dimethylformamide dimethyl acetal, reflux; ii. $HONH_2HCl$, MeOH, reflux; iii. $PhNH_2$, reflux iv. Malononitrile, KOH, MeOH, reflux.

In route 2, the first step (Scheme 3) was condensation of cyanoacetamide and acetyl acetone in a potassium carbonate solution of approximately pH = 9 at room temperature overnight.[70] The product **2b** forms a precipitate in 91% yield. Compound **2b** is also the first key intermediate in the synthesis of anibamine analog **1b.** Bromination at the 5-postion of the pyridine ring with NBS in acidic conditions yielded 5-bromo-2-hydroxy-4,6-dimethylnicotinonitrile in 71% yield.[71]

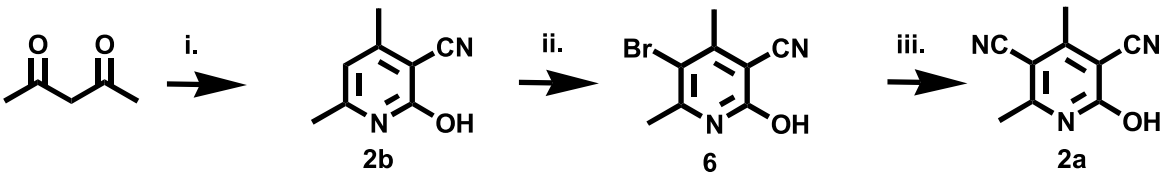

Scheme 3. Route 2 to the first intermediate in anibamine synthesis. Reagents and conditions: i. Cyanoacetamide, K_2CO_3, H_2O, rt; ii. NBS, TFA, H_2SO_4; iii. CuCN, DMF, N_2, reflux.

The next step proved to be the most difficult step in the synthesis of **2a** mostly due to its workup. In the Rosenmond-von Braun reaction, CuCN supplied the nucleophile for nucleophilic aromatic substitution of the bromide at the 5 position on the pyridine ring. CuCN is used in 20% excess with DMF as solvent at reflux.[72] The reaction turned to dark brown over 48 hours at

reflux under N_2 protection. At this point no starting material would show on a TLC plate. The mechanism of the reaction involves a copper^{III} complex being formed in an oxidative addition step. (Scheme 4) To reduce this complex, aqueous ferric chloride ($FeCl_3$ in H_2O and HCl) was used. Attempts to neutralize this acidic solution before extraction created large amounts of precipitate which generally trapped the product. The best method of purification was to rinse the precipitate with EtOAc multiple times to extract as much product from the inorganic salts as possible. Also, extracting the acidic solution with EtOAc yielded some product. The crude product was purified by recrystallization in AcOH to yield a white powder at 50% yield or less. The mother liquor of the recrystallizations was collected to purify more product after combining with subsequent trials.

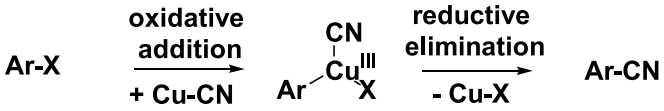

Scheme 4. Mechanism of Rosenmund-von Braun reaction.

Due to the difficulties encountered in the traditional Rosemund-von Braun reaction an another attempt at cyanation of aryl bromides was made. Literature search revealed a seemingly promising domino reaction using 20% KI, 10% CuI, and 120% NaCN with a diamine ligand in toluene.[73] (Scheme 5) The rationale behind this reactions is that the aryl bromide is converted into the more reactive aryl iodide by copper catalysis, then the aryl iodide is converted to the aryl cyanide. Toluene was the solvent suggested in the paper by Zanon et al. because it retained the delicate balance between aryl bromide, aryl iodide, and sodium cyanide in solution. Unfortunately, **5** was barely soluble in toluene. Nearly 40 times the recommended amount of toluene was necessary to dissolve the aryl bromide, which disrupted the concentration of soluble sodium cyanide, resulting in little progress over 24 hours.

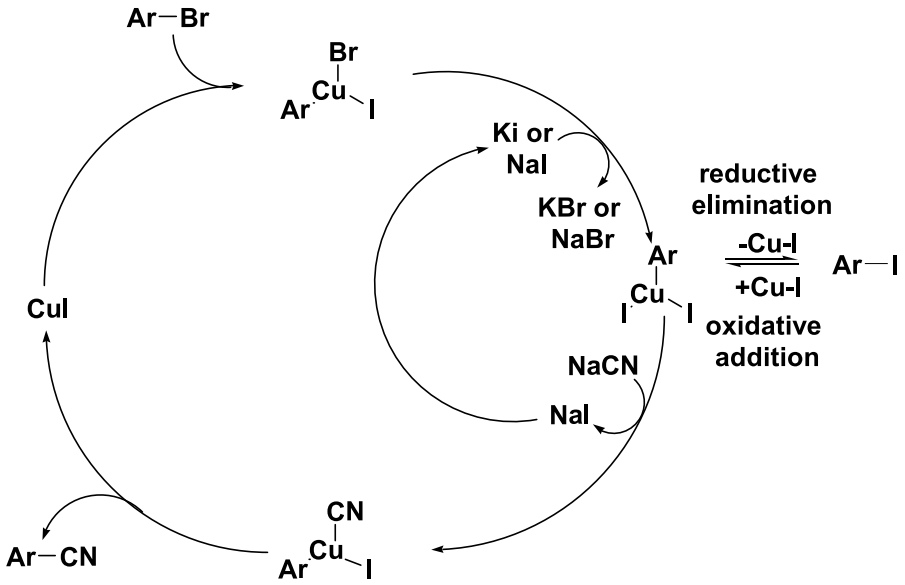

Scheme 5. Mechanism for copper-catalyzed domino halide exchange-cyanation of aryl bromides

Compound **2c** is the first key intermediate in the synthesis of deconstructed analog **1c**. The synthesis of **2c** is accomplished in two steps from cyanoacetic acid. Stoichiometric amounts of morpholine, triethyl orthoacetate, and cyanoacetic acid were condensed in a neat reflux to form 3-morpholinobut-2-enenitrile (**7**).[74] (Scheme 6) This three component reaction turned out to be rather messy and the beta-cyanoenamine was difficult to purify. In literature, it was suggested to conduct recrystallization to purify the product but it was hardly feasible given that the melting point for the product was around 40°C. Column chromatography was the best means of purification though reduced pressure distillation may prove even more efficient. Yields for this reaction remained low, less than the literature value of 54%. Condensation of two molecules of **7** formed the pyridine ring intermediate **2c** through an imino acid intermediate. The production of **2c** was reported as an undesired product of a reaction between **7** and 4,4,4-trifluoroacetoacetate in acetic acid to prepare a trifluromethyl substituted heteraromatic compound. Because this by-product was described as being a self-condensation reaction of **7**, 4,4,4-trifluoroacetoacetate was not used as a reagent for our purposes to achieve a yield of **2c** as the main product.[75]

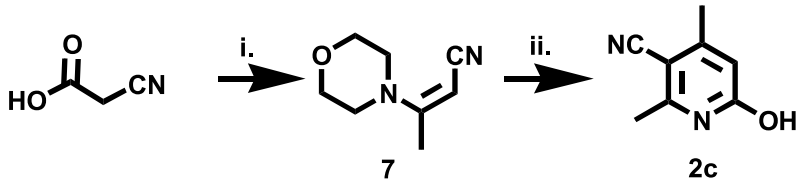

Scheme 6. Synthetic route to the first intermediate in the synthesis of **1c.** Reagents and conditions: i. Morpholine, triethyl orthoacetate, reflux; ii. AcOH, reflux.

2. Bromination of key intermediates

After synthesis of the key intermediates **2a**, **2b**, and **2c**, each series of compounds paralleled the synthetic route of anibamine. Bromination of **2a**, **2b**, and **2c** took place in a heated toluene solution with tetrabutylammonium bromide as the bromine ion supplier and phosphorous pentoxide becoming a phosphate ion leaving group.[76] (Scheme 7) Phosphorous pentoxide is highly hygroscopic and in this reaction sometimes produced a sticky layer at the bottom of the flask presumably where starting material was trapped and unable to react. TLC analysis of the toluene layer showed no remaining starting material but yields remained low when this sticky film was present. Lowering the reaction temperature to 85-90°C from the literature suggested value of 100°C and increasing the amount of solvent improved yields. After the reaction was completed, ice was added to the reaction. Neutralization of the water did not have much effect on increasing yields during extraction. Recrystallization in EtOAc or column chromatography on Al_2O_3 produced the pure products 2-hydroxy-4,6-dimethylpyridine-3,5-dicarbonitrile (**8a**), 2-bromo-4,6-dimethylnicotinonitrilepyridine (**8b**), or 6-bromo-2,4-dimethyl nicotinonitrile (**8c**).

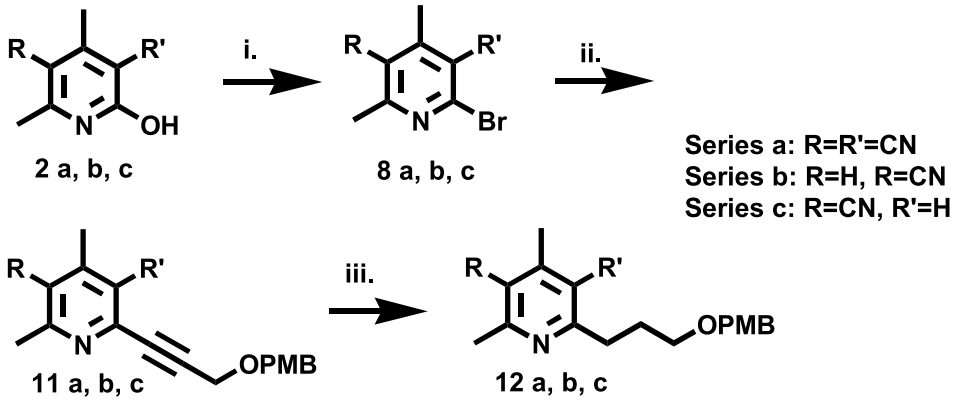

Scheme 7. Synthetic route from key intermediate to the hydrogenation products. Reagents and conditions: a. TBAB, P_2O_5, toluene 90˚C, 2 hours; b. CuI, $PdCl_2(PPh_3)_2$, **10**, Et_2O; c. 55 psi H_2, Pd/C, MeOH

3. Sonogashira coupling

Sonogashira coupling of the bromopyridines with PMB protected propargyl alcohol was rather straightforward. The preparation of the PMB protected propargyl alcohol involved a two step reaction.[77] (Scheme 8) Under N_2 protection a catalytic amount of sodium hydride deprotonated 4-methoxy benzyl alcohol in Et_2O which then reacted with trichloroacetonitrile at 0°C forming 4-methoxybenzyl trichloroacetimidate (**9**). The dried crude imidate was dissolved in a solution of hexane: CH_2Cl_2 (2:1, v/v) and propargyl alcohol was added. The solution was cooled to 0°C under N_2 protection and a catalytic amount of 10-camphorsulfonic acid was added. The reaction was allowed to warm to room temperature overnight. Protected propargyl alcohol (**10**) was purified by column chromatography for use in the coupling reaction.

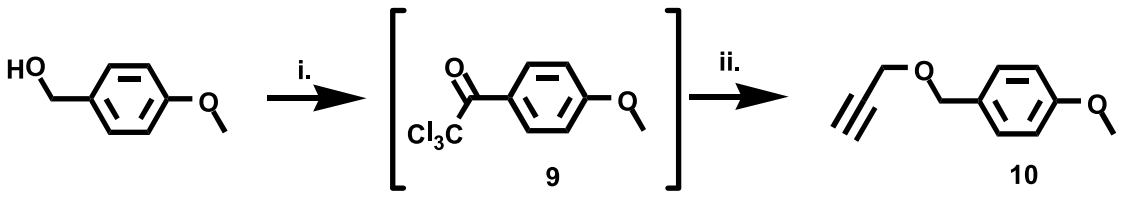

Scheme 8. Synthesis of **10**. Reagents and conditions: i) NaH, trichloroacetonitrile 0°C to RT, N_2, 4 hours; ii. Propargyl alcohol, hexane:CH_2Cl_2, 10-CSA 0°C to RT, overnight

Compound **10** was dissolved in Et_2O before slow addition to a solution of CuI, $Pd(P\varphi_3)_2Cl_2$, TEA, and bromopyridine in Et_2O at room temperature under N_2 protection.[78] (Scheme 7) In Series a, the product, **11a** formed a precipitate in the Et_2O layer. The precipitate could be filtered and then recrystallized in EtOH to form the pure product in 66% yield. In Series b, the purification of **8b** proved very difficult. Both chromatography and recystallization were attempted to get a product suitable for hydrogenation. Original literature by Kenkichi Sonogashira suggests passing the organic extract through Al_2O_3 followed by recrystallization in EtOH results in complete removal of catalyst to yield pure product.[79] Following this workup procedure, **11b** was purified to move on to the hydrogenation. The series c product, **11c**, was prepared without difficulty.

4. Hydrogenation of alkyne intermediates

Hydrogenation of alkynes was without complication except in the case of **11b** as menioned above. Each alkyne was dissolved in MeOH with a catalytic amount of Pd/C.[13] (Scheme 7) Hydrogenation took place between 45-55 psi H_2 over an average of 7 hours in yields of 85% or higher. Alkynes **11a** and **11c** were hydrogenated directly to their alkane counterparts **12a** and **12c**. Many attempts at hydrogenation of **11b** failed. At times, the alkene product was isolated, indicating that the catalyst was poisoned. Also loss of starting material was observed. The purity of the starting material was confirmed by TLC, melting point and ^1H NMR. Finally, when the alkyne was purified by the original Sonogashira methodology described above, hydrogenation to **12b** occurred quickly in quantitative yield.

5. DIBAL-H reduction

After hydrogenation, each nitrile group was reduced to an aldehyde. This was accomplished by di-isobutyl aluminum hydride (DIBAL-H) in toluene.[80,81] An excess amount DIBAL-H is capable of reducing the nitrile to its amine equivalent, which was not desired. To avoid this, reactions were maintained at low temperatures and a minimal amount of DIBAL-H was used. Just over two equivalents were used to reduce the dicarbonitrile to **13a** at -78°C. (Scheme 9) Slightly more than one equivalent was used for the substrates **12b** and **12c**. (Scheme 10) The mono-nitrile substrates did not react at the low temperature of -78°C so the reaction temperature was raised to 0°C to afford the reduction products **13b** or **13c**. In this reaction, the lone pair of electrons on the nitrile nitrogen reacts with the aluminum atom of DIBAL-H and the hyride ion then transfers to the nitrile carbon. Dilute sulfuric acid was used to hydrolize the nitrogen-aluminum complex, forming the aldehyde. The reaction yields were mild, from 60% to 70%.

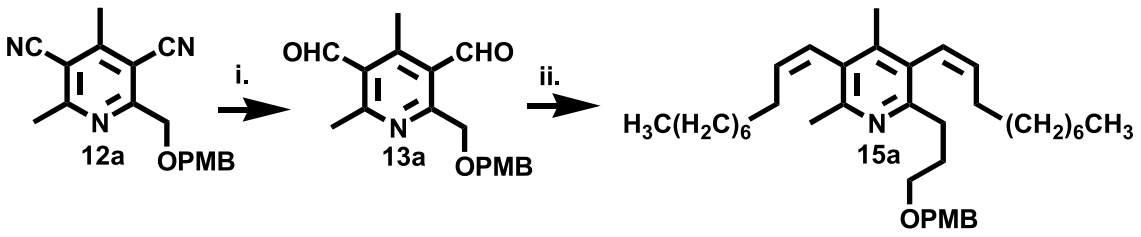

Scheme 9. Synthetic route from first hydrogenation product to Wittig product in synthesis of Anibamine. Reagents and conditions: i. 1) 2.1 eq DIBAL-H, toluene, -78˚C, N_2, 2 hours, 2) H_2SO_4 (aq); ii. 1) 2.2 eq **14**, LHMDS, toluene -78˚C, N_2, 2 hours 2) NH_4Cl (aq).

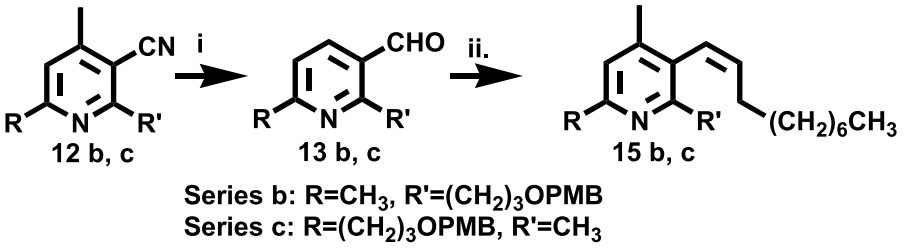

Scheme 10. Synthetic route from first hydrogenation product to Wittig product in synthesis of **1b** and **1c**. Reagents and conditions: i. 1) 1.3 eq DIBAL-H, toluene -78˚C, N_2, 2 hours, 2) H_2SO_4 (aq); ii. 1) 1.2 eq **14**, LHMDS, toluene -78˚C, N_2, 2 hours 2) NH_4Cl (aq).

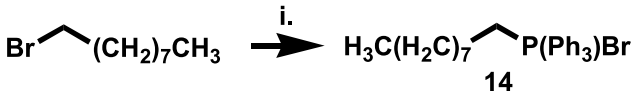

Scheme 11. Synthesis of non-1-yl triphenyl phosphonium bromide (**14**). Reagents and conditions: i. 1-bromononane and triphenylphosphine, toluene, N_2, Δ, 60 hours

6. Exploration of sidechain coupling reactions

The transient nature of the aldehyde called for immediate reaction with a Wittig reagent often without purification of the aldehyde. A phosphonium bromide salt was synthesized by refluxing 1-bromononane and triphenylphosphine in toluene for several days.[13] (Scheme 11) After evaporation of toluene, the crude product was washed with Et_2O and extensively dried before reacting in toluene with lithium hexamethyldisalizide (LHMDS) under N_2 protection forming the Wittig reagent. After formation of the bright red phosphonium ylide, the reaction mixture was cooled to -78°C and the aldehyde in toluene was added slowly over several minutes. Upon addition of the aldehyde, the deep red color of the reaction was reduced to yellow or orange indicating the reaction was proceeding. After about 15 minutes at -78°C, the reaction mixture was allowed to warm to room temperature and stirred for an hour. When the reaction was complete, addition of saturated aqueous ammonium chloride resulted in a clear solution.[13]

The reaction yielded mainly the *Z* isomer, with some *trans* product at about 70% total conversion rate.

The Wittig reaction produced both *cis* and *trans* isomers but a more direct route to the *trans* isomer was desired. Several attempts at increasing *trans* isomer yields were made. (Table 1) Literature searched revealed a promising and seemingly uncomplicated variation of the Wittig reaction, the Schlosser modification, that yielded predominantly *trans* alkenes. (Scheme 12) The principle behind this method is that the addition of soluble lithium salts stabilize the betaine ylide intermediate in a form that results in *trans* stereochemistry in the product after elimination.[83] In the first step of this reaction, phenyl lithium and lithium bromide are added to a phosphonium bromide salt. The phenyl lithium deprotonates the α carbon next to the phosphorous atom resulting in ylide formation. Addition of the aldehyde causes the nucleophlic attack of the ylide carbanion at the carbonyl carbon. The positively charged lithium ion stabilizes the betaine. A second addition of phenyl lithium and lithium bromide deprotonates the α carbon and a lithium atom replaces the proton thus removing the stereochemistry at this site. At this point the betaine undergoes a spontaneous pyramidal interconversion inverting the stereochemistry at the α carbon resulting in a predominantly *threo* conformation. From here, the addition of acid reprotonates the α carbon removing the lithium. A tert-butoxide ion delithiates the oxygen, resulting in *trans* alkene and phosphine oxide formation.[84]

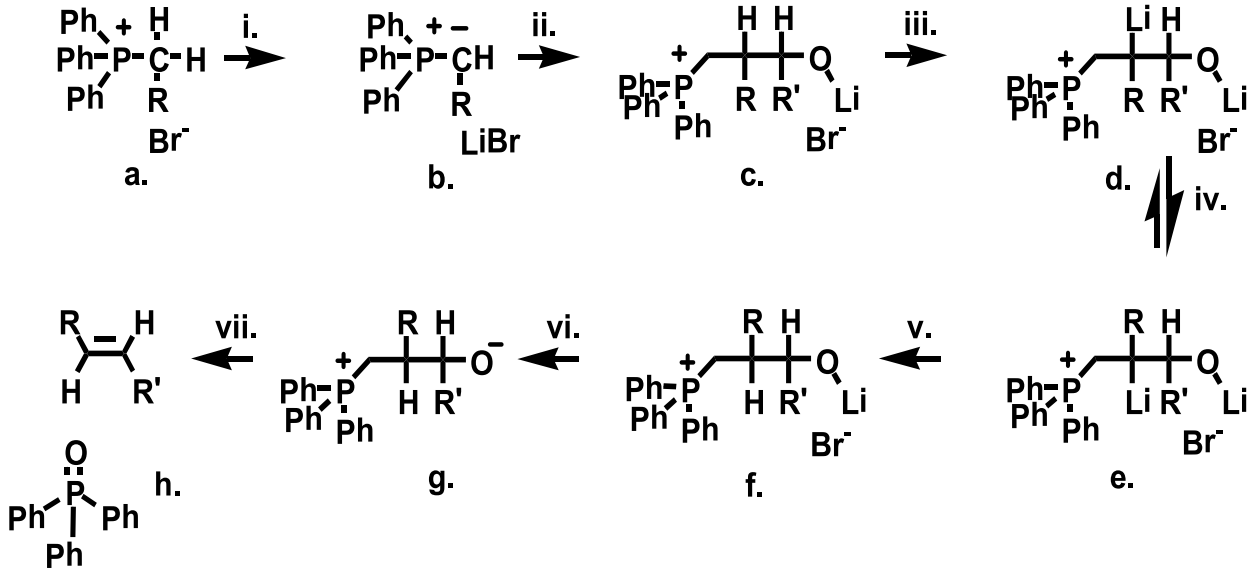

Scheme 12. Proposed mechanism for Schlosser modification of the Wittig reaction

The problem with this reaction is a matter of solubility. In the literature, diethyl ether is the recommended solvent, with THF as a second choice. In our case the Wittig reagent, **14,** is not soluble in either solvent so a toluene/THF solution had to be used which was not ideal for the solubility of the lithium salt. Soluble lithium salts are critical for the formation of mainly *trans* alkenes. Literature suggested using "homemade" phenyl lithium as a product of bromobenzene and lithium which results in a stoichiometric amount of lithium bromide as a sideproduct. As a second choice, the literature recommended adding two equivalents of LiBr to the phosphonium bromide at the beginning of the reaction before adding the commercially available PhLi in di-n-butyl ether solution which was the procedure adopted.[84] Still, it seemed the lithium salt solubility and 1-nonyl phosphonium bromide solubility were inversely proportional and more than one equivalent of PhLi was needed to reach the deep red color of the prepared Wittig reagent. After addition of the aldehyde another equivalent of PhLi in solution was added. However, a majority of trans product was not observed. Percent conversion and isomeric excess seemed to be

inversely proportional; it seemed that the longer the reaction ran, the more *cis* alkene and conversion of starting material was observed. An earlier attempt was made using LiCl with **13b** as the substrate with similarly low percentage of *trans* isomer and percent conversion. Different variations in conditions afforded no significant changes in *cis*:*trans* ratios.

Another method tried was to prepare the traditional Wittig reaction but heat it to reflux in toluene for 24 hours; during the course of the reaction the *cis* product would be isomerized to the more thermodynamically stable *trans* isomer. This method was tried with **13b** as starting material. Proton NMR revealed nearly a 1:1 ratio of products, but only 55% conversion. Subsequently, a traditional Wittig at low temperature also resulted in an equal ratio of isomers but with 79% converstion.

The Grignard reaction was tried also to prepare trans alkene.[80,81] Both **13a** and **13b** were used as starting material for different attempts. Again it appears solubility played a major role in the progress of this reaction. 1-bromononane was added to magnesium and iodine in THF slowly and allowed to gently reflux. (The reaction had been tried also with diethyl ether as solvent to no avail.) In THF at reflux, It seemed that the Grignard reagent, 1-nonylmagnesium bromide, had been formed. However when the reaction was cooled to -70°C in preparation for addition of the aldehyde, some precipitate formed. After addition of the aldehyde, no reaction took place. The reaction temperature was raised first to 0 °C, then room temperature and finally reflux, but there was no change. One equivalent of benzaldehyde was added in attempt to determine the problem. No reaction took place with benzaldehyde either. It was concluded that the Grignard reagent was not formed or not soluble at low temperature.

Table 1. Reaction conditions, yields and stereoselectivity of the various coupling reactions. The letters a, b, and c correspond to the series of the compounds used as substrate.

Reaction Conditions	% *trans*	% *cis*	% conversion
Wittig (a)	35%	65%	73%
Wittig (b)	50%	50%	80%
Wittig (c)	38%	63%	67%
Wittig reflux (b)	50%	50%	55%
LiBr (a)	50%	50%	50%
LiBr (b-1)	25%	75%	25%
LiBr (b-2)	34%	66%	30%
LiBr (c)	16%	66%	77%
LiCl (b)	21%	71%	40%
Grignard (a)	n/a	n/a	NR
Grignard (b)	n/a	n/a	NR

7. Deprotection and Cyclization Reactions

After the aliphatic sidechains were coupled, the para methoxy benzyl protecting group was removed to expose the alcohol for cyclization to the final product. (Scheme13) Deprotection was carried out in a solution of ethanol and 1 M hydrochloric acid at reflux.[85] Cyclization to the final 1*H*-indolizinium ion took place in dichloromethane with TEA and MsCl from 0°C to room temperature.[86] The isomeric mixtures were purified first on a silica gel column with CH_2Cl_2:MeOH as eluent.

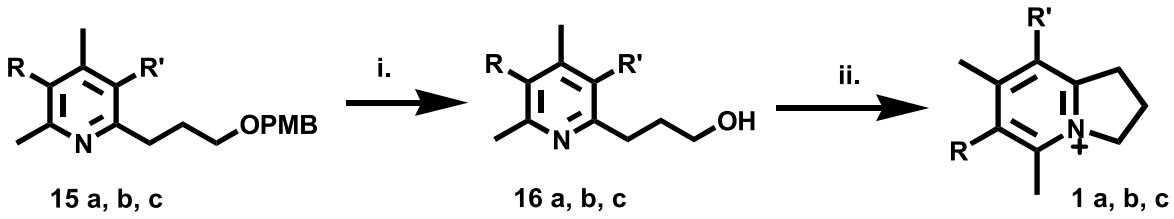

Scheme 13. Synthetic route from Wittig product to final product for all routes. Reagents and conditions: a. 1N HCl, EtOH, reflux 5 hours; b. MsCl, TEA, CH_2Cl_2 0˚C to rt, 1 hour.

8. Separation of isomers

As a result of the various Wittig reactions, each reaction center resulted in *cis* and *trans* isomers. Three geometric isomers of anibamine (**17a**, **18**, and **19**) were synthesized in addition to anibamine. (Figure 10) *Trans* isomers (**17b** and **17c**) of each deconstructed target compound were also synthesized. (Figure 11) Separation of geometric isomers was first attempted on HPLC. Anibamine and its isomers had been previously separated on HPLC and the same conditions were successfully repeated. For series c, HPLC separation of **1c** and its *trans* isomer was attempted using the conditions for anibamine as a starting point. All the peaks appeared to come out in under 15 minutes, so the percentage of water was increased by 5% from 47.5% to

72.5% before separation of peaks became visible after about two hours. In order to distinguish separate peaks, the injection sample was extremely dilute. Continued separation at this concentration was not feasible and higher concentrations were not separable so alternate methods of separation were explored.

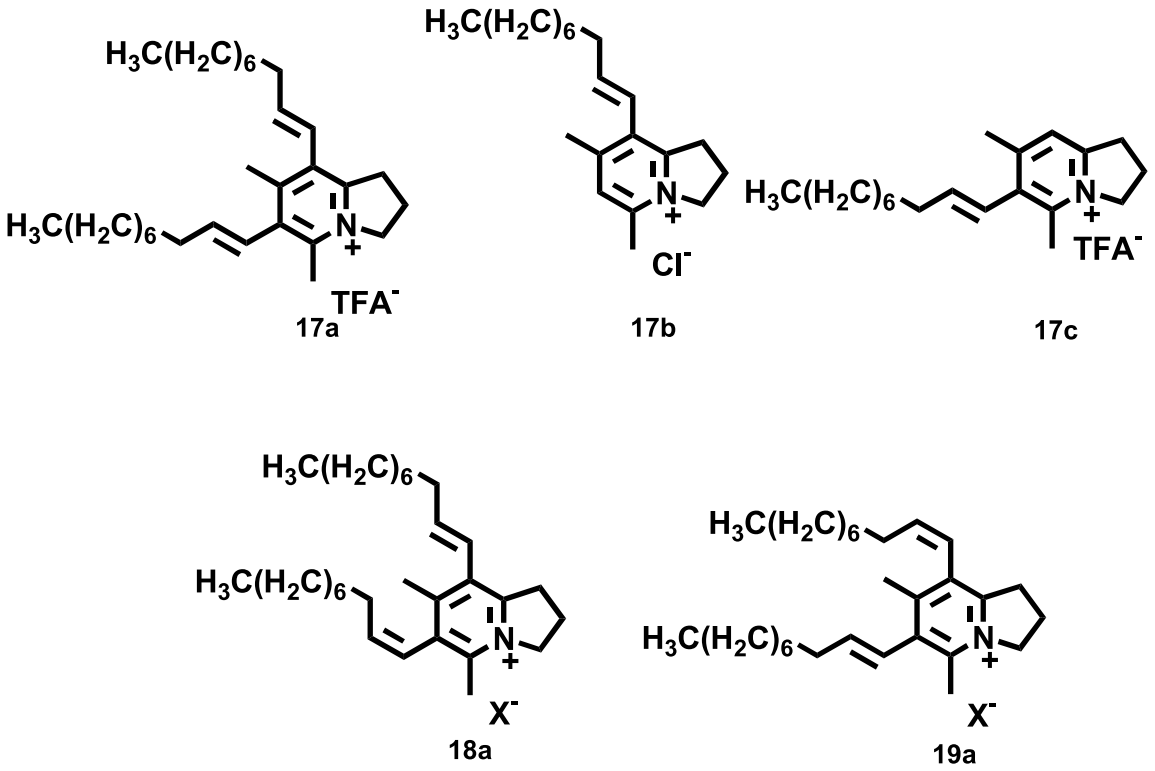

Figure 10. Geometric isomers of target compounds. (X^- = TFA^- or Cl^-)

Since silver nitrate has been reported to separate isomeric fatty acids on prep TLC plates, a brief investigation of $AgNO_3$ prep TLC was carried out. The *cis* and *trans* double bonds are supposed to form different strength bonds with the silver ions embedded on the silica gel resulting in greater separation of isomers. Different ways of preparing the plates exist in literature, for this the plates were developed in a solution of $AgNO_3$ dissolved in MeCN. In fatty acid separation, Rhodamine 6G, a fluorescent indicator, is used to visualize the bands but this

would not work for the compounds in this research. Due to poor visualization and inconsistencies between plates, this option was ruled out. Separation was attempted on prep TLC plates without $AgNO_3$ with poor results. A mixture of **1c** and its *trans* isomer, **17c**, was developed up to 7 times in CH_2Cl_2:MeOH (25:2, v/v). Three bands were collected and characterized by ^{1}HNMR but no desired pure isomers were observed. It was concluded that the acidity of the prep TLC plates was causing some degradation of the sample. For series b, the separation of the deprotected products, **16b** and its *trans isomer*, was attempted on prep TLC. Two bands were present after 3 developments in hexane/ethyl acetate (2:1, v/v) solvent system. The top band was pure *cis* isomer but the lower band contained a mixture of both isomers, with trans present in the majority. After cyclization, separation of the mixed product was attempted but with the same poor results as in the series b. For the mono sidechain analogs only 6-dec-1*Z*-enyl-5,7-dimethyl-2,3-dihydro-1H-indolizinium chloride (**1b**) was purified from its isomer. Hydrogenation of the mixtures yielded a saturated analog for each series. (**20a, 20b and 20c**) (Scheme 14) All of the final compounds were characterized by proton and carbon nuclear magnetic resonance spectroscopy (NMR) and mass spectrometry (MS).

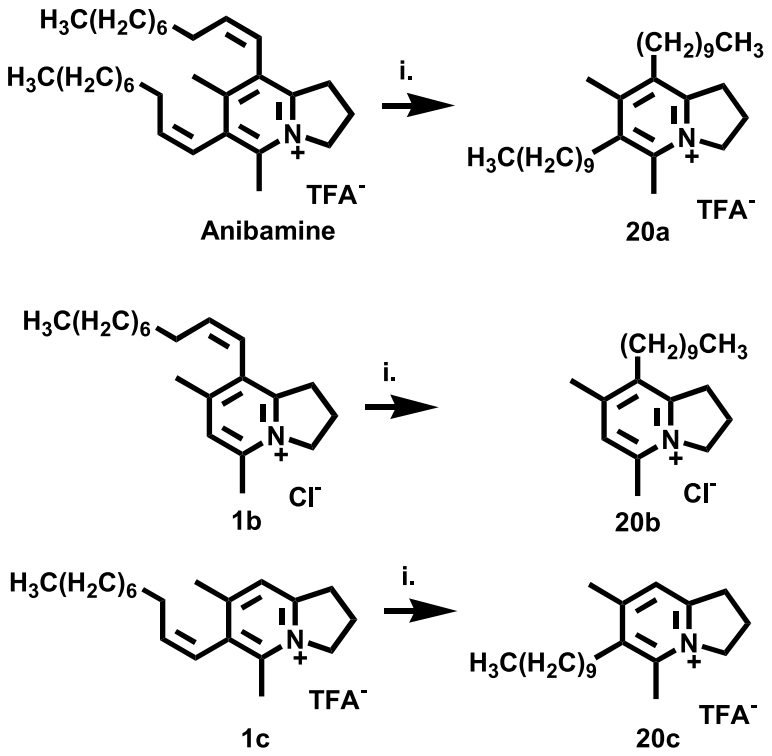

Scheme 14. Synthesis of hydrogenated final products. Reagents and conditions: i) 55 psi H2, Pd/C, MeOH, 8 hours.

In conclusion, six new analogs of anibamine were synthesized following the diverted total synthesis scheme. Efforts to stereoselectively synthesize of *trans* isomer were not very successful though in some instances the percentage of *trans* in the final product was increased. All the attempts to synthesize *trans* analogs were based on an aldehyde starting material. This starting material was used because the rest of the synthetic scheme had been previously worked out as had the separation of anibamine and its geometric isomers. Other synthetic routes are currently being explored in our lab to improve stereoselectivity. If selectivity is increased, then the separation issue becomes less important. For now, prep TLC separation of the deprotected analogs seems most promising. Separation of the anibamine isomers was possible because of a combination of higher molecular weight and greater differences between isomers because of the two double bonds. The compounds

with only one sidechain were less different from each other and not easily separable. Any reactions that lead to only one isomer will negate the need for an isomeric separation process.

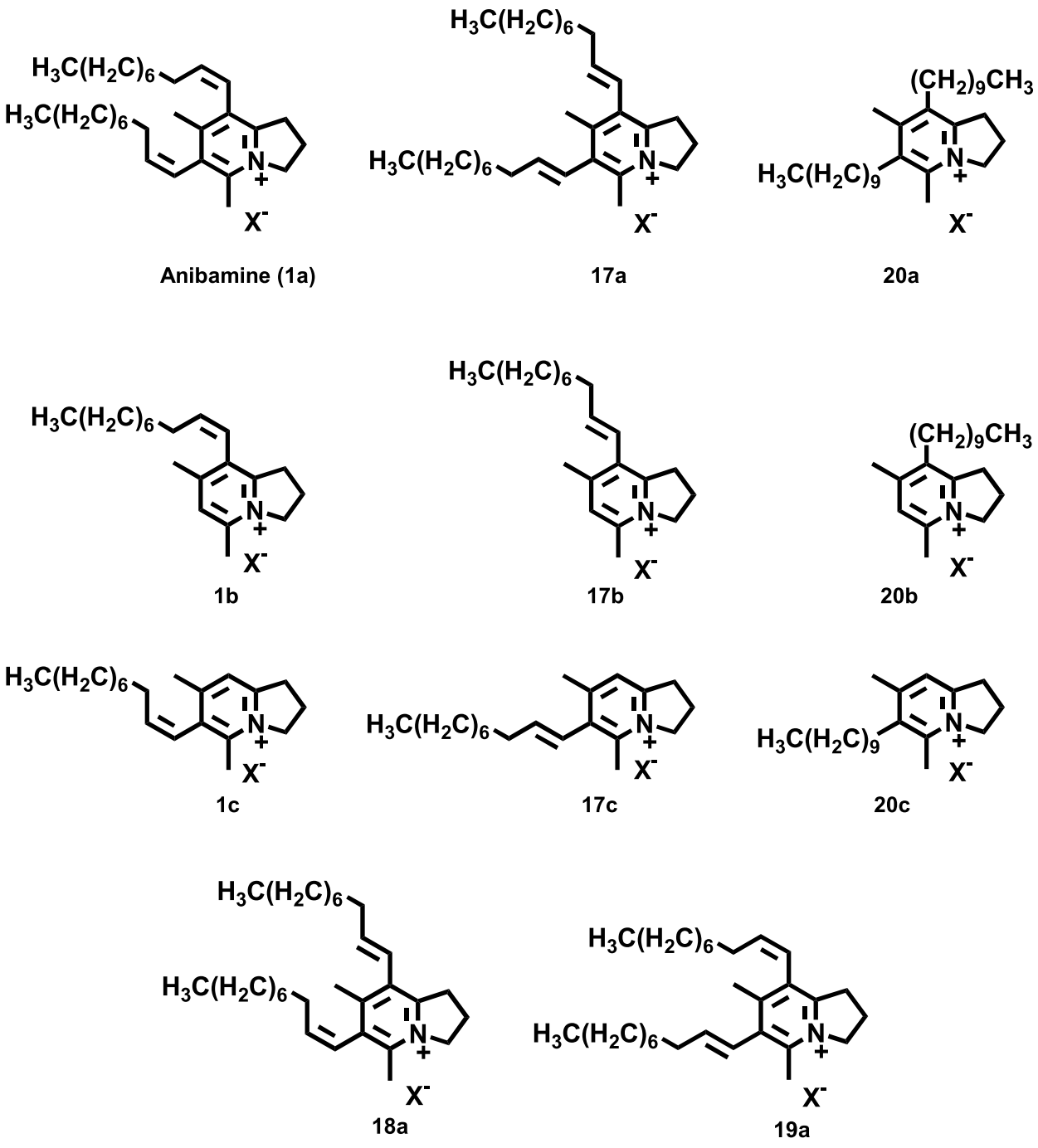

Figure 11. Strucutres of all synthesized compounds. (X^- = TFA^- or Cl^-)

B. Anti-proliferative assays of Anibamine and analogs

Anti-proliferative assays of anibamine and its analogs were performed against various aggressive prostate cancer cell lines to determine structure-activity relationships and to help define a next generation lead compound. Three cell lines, PC-3, M12, and DU-145, were in this assay. Previous data suggested that a 72 hour drug incubation time resulted in the best dose dependent effect (data not shown). Some deconstructed analogs of anibamine were also tested at 24 and 48 hours. Cells were plated 10^3 cells per well on 96 well plates with a volume of 100 µL media containing 1% L-glutamine, 0.1 % ITS (insulin, 5µg/mL; transferrin, 5µg/mL; and selenium, 5 µg/mL) and 0.1 % gentamicin. The media for M12 cells contained 5% fetal bovine serum (FBS); media for DU-145 and PC-3 contained 10% FBS. Twenty-four hours after plating, different concentrations of drug were added to a total well volume of 150 µL and the cells were incubated for a further 24, 48 or 72 hours. After the allotted time interval the media was unceremoniously removed and serum free media was added to each well to a volume of 100 µL. Ten µL of the anti-proliferative reagent WST-1 was added and the cells incubated a further 3 hours before the absorbance of each well was read by an ELISA at 450 nm. WST-1 is a tetrazolium salt that is cleaved by mitochondrial dehydrogenases into a water

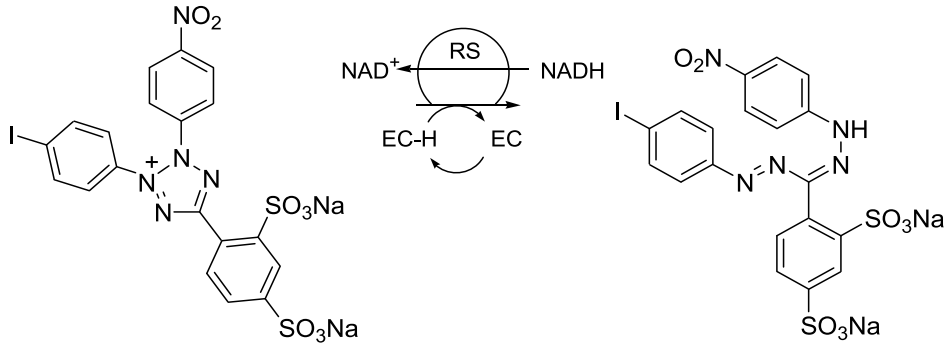

Figure 12. Metabolic cleavage of WST-1 into soluble formazan dye. RS:mitochondrial reductase, EC: electron coupling reagent[87]

soluble formazan dye that is dark red in color. (Figure 12) The viable cells contain active mitochondrial dehydrogenases which increase production of the formazan dye thus increasing absorbance of each well with viable cells. [87]

The drugs used for this assay were anibamine and analogs containing 5-, 6-, or 7-membered rings fused to the pyridine ring synthesized in our lab. (Figure 13) Compounds 21, 22, and 23 have a 6-membered fused ring. Compounds 24, 25, and 26 have a 7-membered fused ring. For each group of compounds with a common ring size, there is also a *trans, trans, cis, cis,* and saturated analog. Also compounds **1b**, **20b**, and **20c** were tested from series b and c and mixtures of *cis* and *trans* isomers of each set of deconstructed analogs. The IC_{50} values for the twelve purified compounds are presented in table 2. Comparisons can be made by ring size and double bond configuration for the first nine compounds. Among deconstructed analogs, further scrutiny will determine which sidechain might be more important for anti-proliferative activity and if the double bond plays a role. Variations among activity in each cell line is indicative of CCR5 expression differences. Vaday, et al. reported that DU-145 expressed more cell surface CCR5 than PC-3.[10] J. Adams showed that M12 expressed significantly more CCR5 than either other cell line.[13] Because of differences among each cell line, structure-activity relationships are discussed for each cell line.

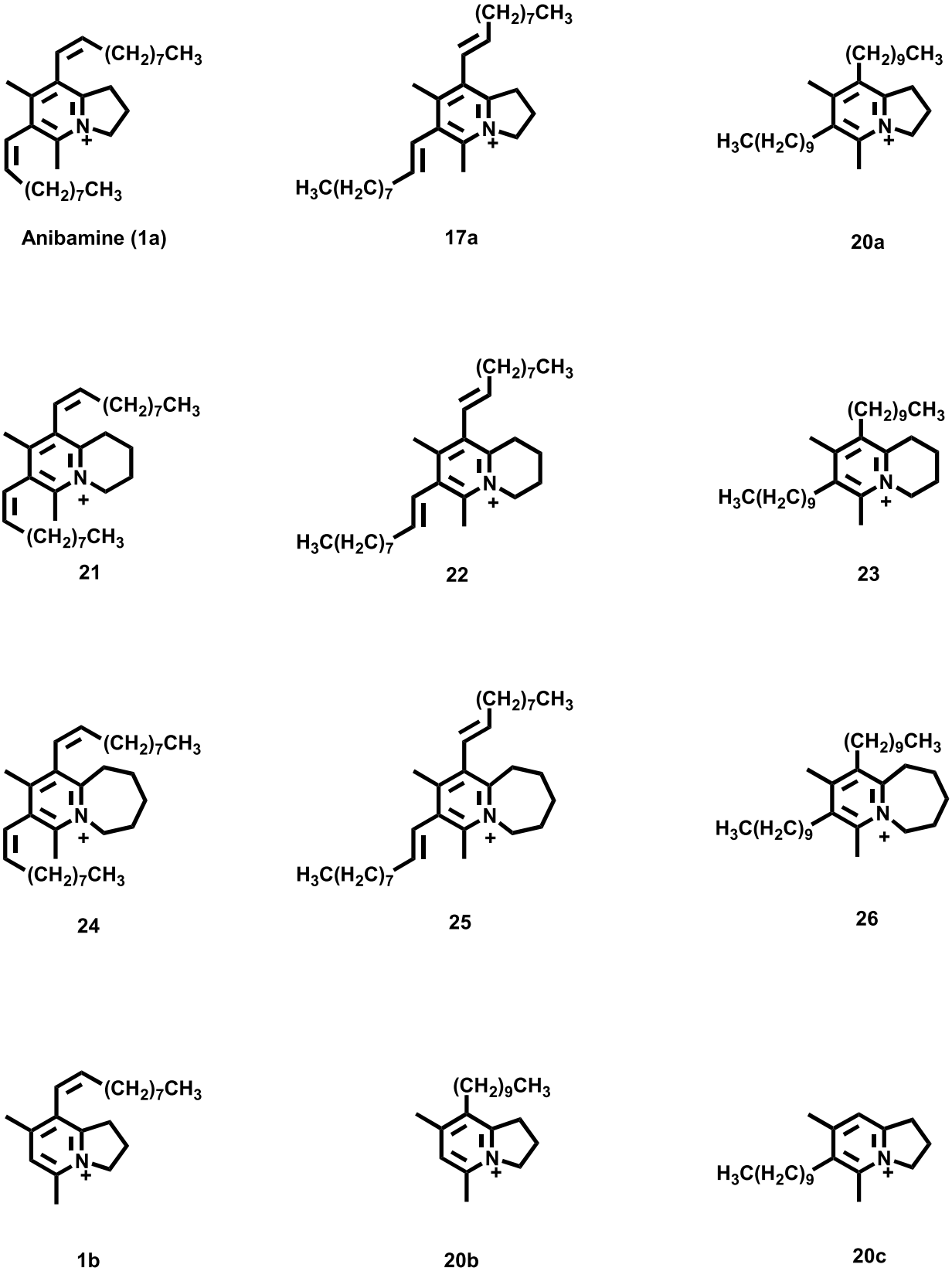

Figure 13. Structures of Anibamine and eleven analogs tested for anti-proliferative activity.

Table 2. Half maximal inhibitory concentration (IC_{50}) of 12 compounds in three cell lines at 72 hours.

Compound	IC_{50} (nM) M12	IC_{50} (nM) DU-145	IC_{50} (nM) PC-3
Anibamine	1.8 ± 1.7	172.5 ± 41.0	898.3 ± 75.1
17a	5.9 ± 1.5	**63.0 ± 14.9**	409.1 ± 48.4
20a	9.0 ± 6.3	155.1 ± 103.4	364.2 ± 22.8
21	5.9 ± 3.7	212.5 ± 30.5	187.1 ± 35.0
22	> 1,000	> 5,000	> 2,000
23	21.1 ± 15.4	371.0 ± 38.7	271 ± 61.6
24	8.1 ± 6.8	336.2 ± 82.1	158.7 ± 62.9
25	2.4 ± 2.2	256.4 ± 61.5	170.8 ± 89.6
26	**1.2 ± 1.1**	156.1 ± 47.5	317.6 ± 30.4
1b	5.9 ± 1.9	422.9 ± 63.0	22.7 ± 19.7
20b	142.7 ± 83.6	189.1 ± 60.4	618.0 ± 92.26
20c	2.6 ± 2.1	159.9 ± 36.3	**9.55 ± 7.2**

1. Anti-proliferative activity of Elaboration products on PC-3 cell line

The PC-3 cell line had the least response to the drugs, but was still inhibited to an extent. This is consistent with its lower expression of CCR5 compared to the other cell lines. Compounds **24**, **25,** and **26** all have 7 membered rings fused to the pyridine. **24** had the highest activity of the nine compounds with two sidechains (Figure 14 and) **25** had the highest activity of all compounds with two *trans* double bonds and **26** had, within standard error, the highest activity of the saturated analogs with two sidechains. Figure 15 depicts the structures of all *cis, cis* compounds and their IC_{50}. For this cell line, the 7-membered ring compounds had the highest activity of all compounds with two sidechains. The double bond configuration seems to be less important than ring size in the PC-3 cell line.

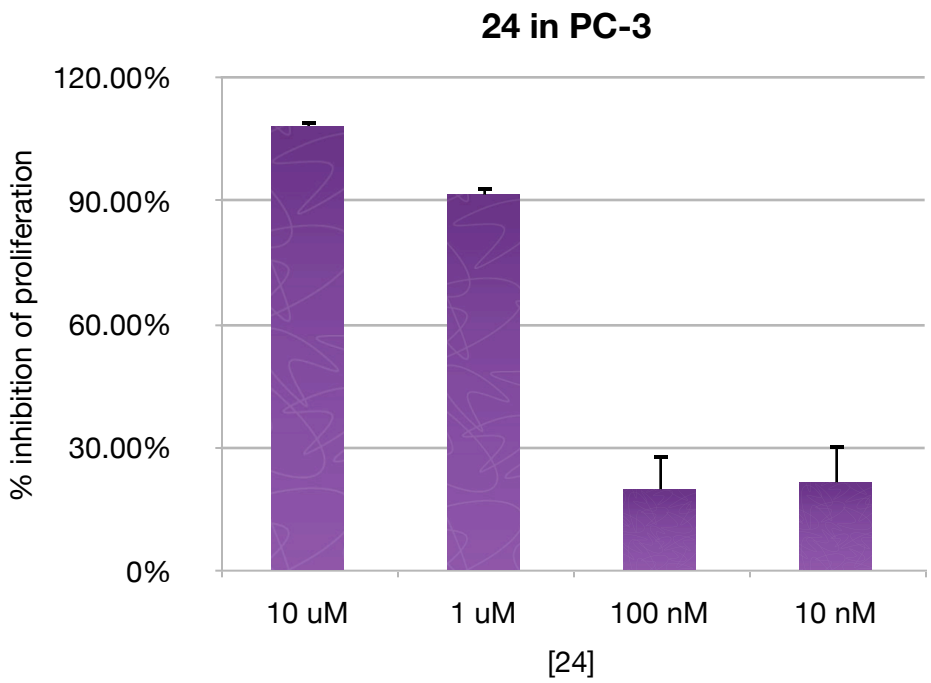

Figure 14. Percent inhibition of PC-3 cell line by **24** at four concentrations.

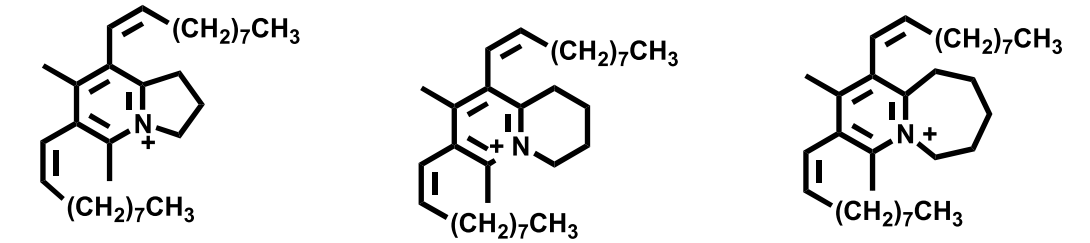

Figure 15. Structures and IC_{50} of **24**, **21**, and **1a**.

2. Anti-proliferative activity on DU-145 cell line

The DU-145 cell line was the fastest growing cell line. The *E,E*-geometric isomer of anibamine, **17a**, had the lowest IC_{50} value in this cell line, the only IC_{50} value under 100 nM. (Figure 16) Anibamine (**1a**) had the highest activity of all compounds with *cis* double bonds. Compound **20a** had, within standard error, the highest activity of the saturated analogs with two sidechains. For DU-145 the 5-membered ring compounds had the highest activity. Figure 17 depicts the structures of all *trans, trans* compounds and their IC_{50}. Comparing double bond configuration for each group of compounds gives no indication of activity. Ring size seems to be the most important structural feature in this cell line.

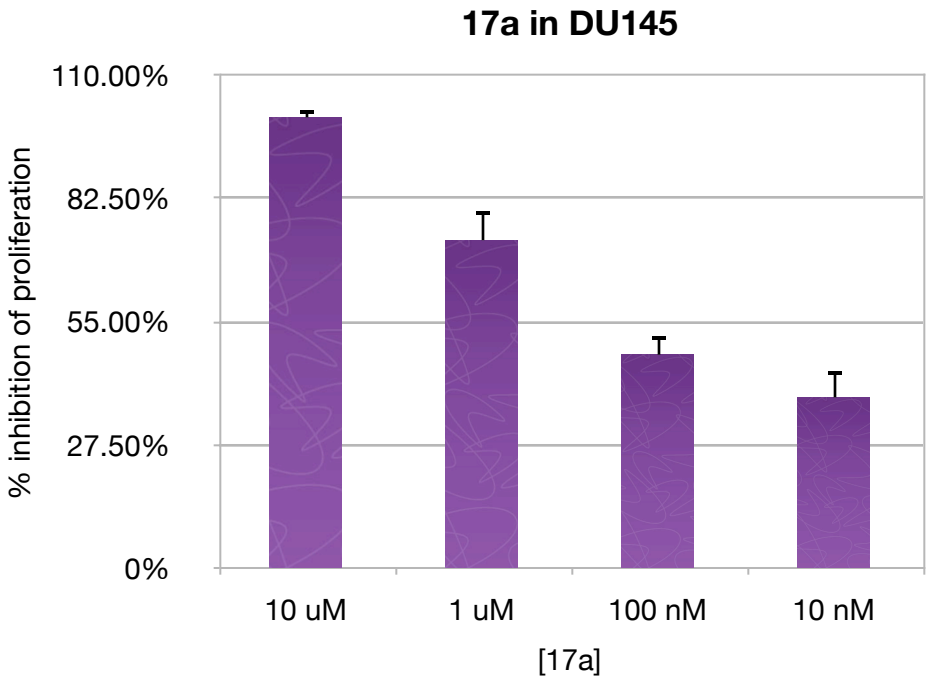

Figure 16 Percent inhibition of DU-145 cell line by **17a** at four concentrations.

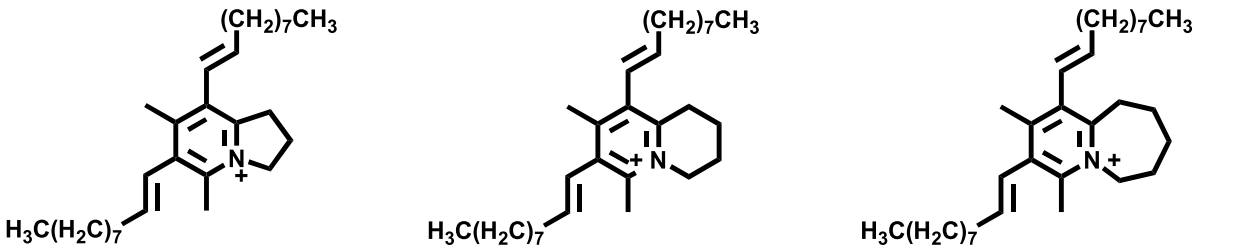

17a
DU145 EC_{50}= 63.0 +/- 14.9

22
DU145 EC_{50}= > 5,000

25
DU145 EC_{50}= 256.4 +/- 61.5

Figure 17. Structures of **17a**, **22**, and **25**.

3. Anti-proliferative activity on M12 cell line

M12 cells were the most affected by the drugs. The majority of the compounds had IC_{50} values under 10 nM, which was the lowest concentration of drug tested. **26**, a saturated analog in the 7 membered ring series, had the most activity. (Figure 18) With many of the IC_{50} values being lower than the lowest concentration tested, the standard error places the IC_{50} values of these compounds very close to each other, making it difficult to analyze which structural features are most important. For the M12 cell line, the therapeutic index (not calculated) of the compounds will be more important to determine a new lead.

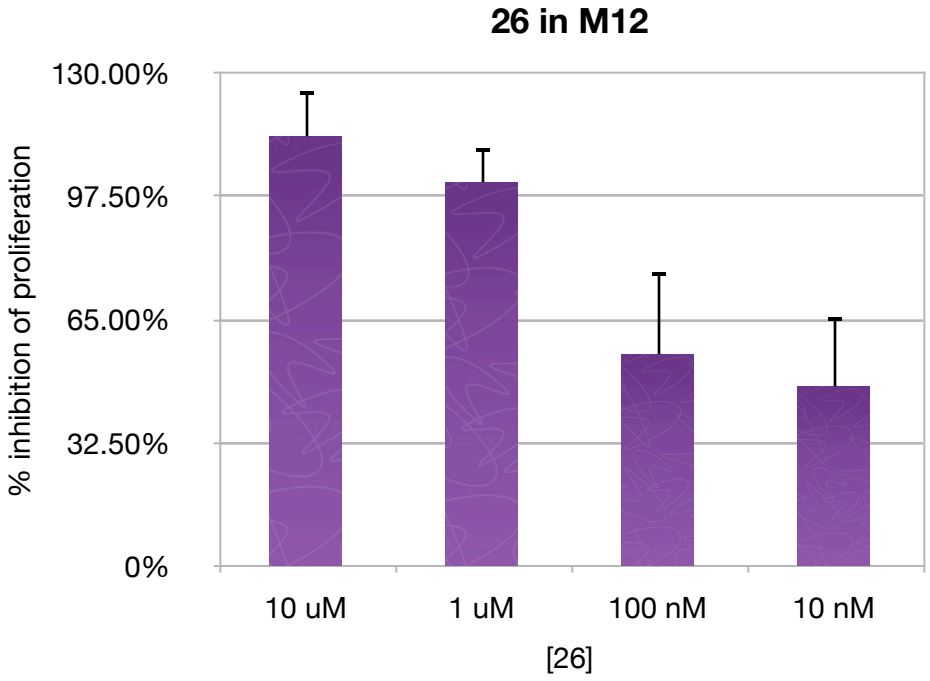

Figure 18 Percent inhibition of M12 cell line by **26** at four concentrations.

4. Anti-proliferative activity of deconstructed analogs

The deconstructed analogs, **1b**, **20b**, and **20c**, along with the isomeric mixtures of **1b** and **1c** were analyzed in each cell line after incubation at 24, 48, and 72 hours. Tables 3, 4, and 5 show the percent inhibition of each compound tested at 72 hours in the three cell lines. Structure-Activity comparisons can be made directly between **20b** and **20c** to determine which sidechain is more critical for activity. Comparing **1b** and **20b** can elucidate whether a *cis* double bond is more favorable than a saturated bond. Care must be taken when using the data from either mixture to draw any conclusions about structure-activity relationships. Because they are isomeric mixtures the individual contribution to activity of each component cannot be measured. For series 2, the *cis* isomer was tested individually so some insight can be gained by comparing it to the isomeric mixture, which contains 80% *trans* isomer.

Compounds **20b** and **20c** are constitutional isomers; they both have one saturated sidechain but the sidechain is in a different position on the imidazolinium core. In the PC-3 cell lines, **20c** had the highest activity of all compounds tested. **20b** had significantly less activity. In the M12 cell line, **20c** again had relatively high activity and **20b** relatively less activity. In these two cell lines there is a clear difference in activity between sidechain positions. The relationship is less clear in the DU-145 cell line, where both compounds have similar IC_{50} values. Looking at a chart of their anti-proliferation activity shows an interesting activity profile. (Figure 19) At higher concentrations, **20c** has very high activity, but at lower concentrations this effect is greatly reduced. At the lowest concentration, it has no effect at all. On the other hand, **20b** does not reach maximal effect but retains relatively high activity at lower concentrations of drug. The

concentration where both produce a half maximal effect is nearly the same, but the overall effect is different.

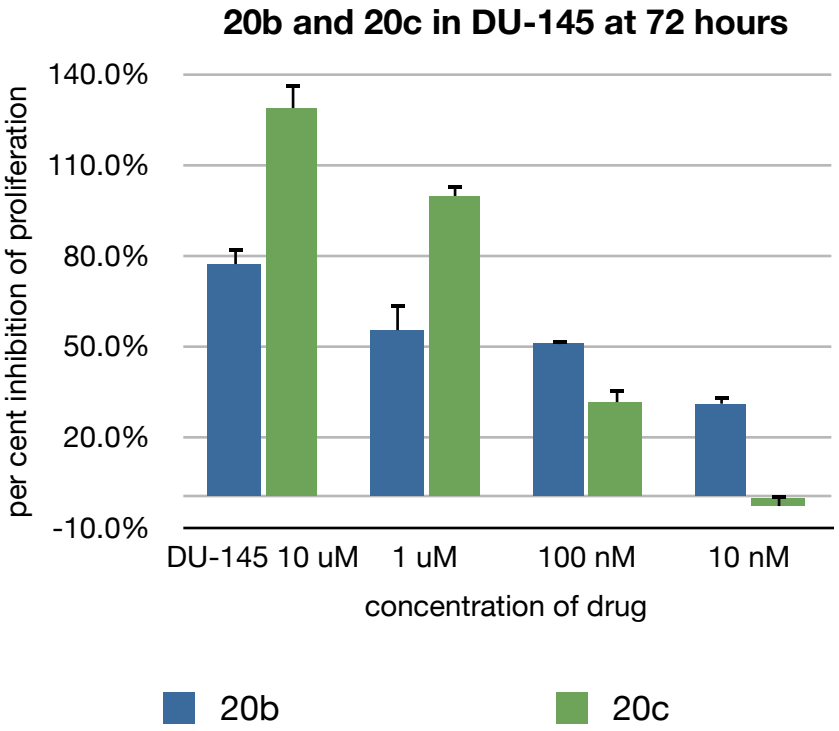

Figure 19. The percent inhibition of both saturated deconstructed analogs in DU145 cell line.

Compounds **1b** and **20b** contain the same sidechain but differ only in the presence or absence of a *cis* double bond. For the first 9 compounds, it seemed that the double bond did not play much of a role in the overall activity of each molecule. Here is seems that in both the M12 and PC-3 cell line, the presence of a *cis* double bond significantly increases activity. In the DU-145 cell line, there is a slight increase in activity of the saturated analog. The mixture of **1b** and its *trans* isomer maintained nearly the same activity as **1b** alone in PC-3 and M12 cell lines, maybe indicating that there is little difference between double bond configuration for this set of compounds.

Table 3. Percent inhibition of **1b**, **20b**, **20c**, and isomeric mixtures **1b** and **1c** in the M12 cell line at 72 hours.

	M12			
	10 uM	**1 uM**	**100 nM**	**10 nM**
20c	111.72% ± 1.19%	113.82% ± 4.09%	90.38% ± 21.08%	59.04% ± 3.51%
1b	113.08% ± 3.35%	109.06% ± 6.67%	83.20% ± 14.75%	48.89% ± 15.54%
20b	94.31% ± 13.23%	77.66% ± 8.68%	53.84% ± 12.69%	35.45% ± 18.34%
Mix of 1b & 17b	110.29% ± 0.81%	101.72% ± 17.06%	84.07% ± 15.99%	56.15% ± 9.39%
Mix of 1c &17c	105.00% ± 6.38%	94.54% ± 2.72%	85.62% ± 9.30%	43.01% ± 11.21%

Table 4. Percent inhibition of **1b**, **20b**, **20c**, and isomeric mixtures **1b** and **1c** in the PC-3 cell line at 72 hours.

	PC-3			
	10 uM	**1 uM**	**100 nM**	**10 nM**
20c	124.83% ± 7.82%	118.92% ± 7.75%	84.87% ± 9.55%	44.14% ± 16.90%
1b	125.77% ± 8.98%	102.26% ± 14.23%	94.44% ± 6.45%	36.26% ± 25.98%
20b	81.14% ± 1.92%	74.35% ± 2.46%	7.66% ± 1.13%	1.76% ± 2.19%
Mix of 1b & 17b	129.42% ± 9.69%	92.00% ± 9.09%	87.60% ± 16.02%	43.20% ± 25.47%
Mix of 1c &17c	123.75% ± 4.94%	91.53% ± 15.21%	89.03% ± 11.34%	30.38% ± 21.23%

Table 5. Percent inhibition of **1b**, **20b**, **20c**, and isomeric mixtures **1b** and **1c** in the DU-145 cell line at 72 hours.

	DU145			
	10 uM	**1 uM**	**100 nM**	**10 nM**
20c	128.68% ± 8.46%	99.58% ± 4.08%	31.38% ± 4.60%	-3.02% ± 4.04%
1b	126.60% ± 4.43%	51.33% ± 5.08%	11.35% ± 5.57%	-11.26% ± 6.21%
20b	77.05% ± 6.12%	55.14% ± 9.44%	51.00% ± 1.58%	30.84% ± 3.27%
Mix of 1b & 17b	128.79% ± 4.13%	53.09% ± 7.60%	18.04% ± 5.59%	5.04% ± 7.70%
Mix of 1c &17c	125.68% ± 5.24%	54.20% ± 8.93%	8.59% ± 14.97%	-6.39% ± 11.00%

5. Anti-proliferative effect over time

Measuring the effect at earlier hours establishes a timeline for inhibitory activity. Because of the large difference in control cells among each day, it is better to analyze the drug effect by looking at the absorbance values rather than percent inhibition calculated values. By following a concentration of drug through the time intervals and comparing them to the control values for each time interval we can see how the drug effects the cell proliferation over a short period of time. **20c** will serve as a representative example to monitor how the drugs effect the cells. (Table 6)

In the DU-145 cell line, the control cells grew to near confluence by the end of the first 24 hours after drug incubation, the control absorbance values increased slightly over the next one and two days. At the highest concentration of **20c**, an anti-proliferative effect is seen immediately and the cells do not recover growth. The absorbance values for 24, 48, and 72 hours remain within standard error of each other. At 1 μM, the absorbance values are slightly less than the control at 24 hours but by 72 hours, the absorbance has significantly decreased. At 100 nM, the absorbance remain about the same over all three days, ultimately at 73% of the control value. The cells incubated with the lowest concentration, 10 nM, grew slowly in the presence of drug, at about the same rate as the control cells. At higher concentrations, the cell proliferation was significantly inhibited and absorbance decreased over time.

Table 6 Absorbance values of **20c** at three time intervals in three cell lines.

drug/cell line	time	control cells	10 µM	1 µM	100 nM	10 nM
20c DU145	24 hours	1.103 ± 0.028	0.523 ± 0.036	0.959 ± 0.027	1.060 ± 0.044	1.085 ± 0.029
	48 hours	1.155 ± 0.007	0.597 ± 0.054	0.961 ± 0.088	1.104 ± 0.051	1.144 ± 0.018
	72 hours	1.181 ± 0.025	0.547 ± 0.029	0.691 ± 0.007	1.027 ± 0.019	1.196 ± 0.030
20c PC-3	24 hours	0.664 ± 0.045	0.536 ± 0.016	0.581 ± 0.030	0.591 ± 0.031	0.628 ± 0.033
	48 hours	0.924 ± 0.054	0.562 ± 0.022	0.740 ± 0.086	0.824 ± 0.106	0.821 ± 0.032
	72 hours	1.084 ± 0.022	0.556 ± 0.016	0.581 ± 0.011	0.724 ± 0.066	0.899 ± 0.071
20c M12	24 hours	0.705 ± 0.010	0.579 ± 0.016	0.592 ± 0.015	0.678 ± 0.019	0.726 ± 0.017
	48 hours	0.959 ± 0.010	0.673 ± 0.060	0.687 ± 0.065	0.773 ± 0.056	0.856 ± 0.042
	72 hours	0.946 ± 0.070	0.547 ± 0.021	0.539 ± 0.035	0.615 ± 0.056	0.735 ± 0.040

In the PC-3 cell line, the pattern of inhibition was different than in DU-145 for the same drug. The control cells proliferated steadily throughout the time interval. Again the highest concentration of drug halted cell proliferation at all time intervals. The absorbance values for 1 µM remained constant for each day. At 100 nM in 24 hours the cells showed no proliferation but had grown slightly by 72 hours, meaning that the compound is not toxic. The absorbance increase daily with 10 nM of drug but the inhibition of proliferation was still greater than 50% after 72 hours.

The proliferation of the M12 cell line was greatly inhibited by **20c**. M12 control cells also had the lowest absorbance values of all cell lines. For all concentrations of drugs, the 48 hour absorbance values were the highest. At 24 hours, the drug absorbance values were much lower than control, then increased slightly and ultimately the absorbance values fell even lower by 72 hours, except for 10 nM which had nearly the same absorbance values on days 1 and 3.

There are many variables to account for the difference in activities of the compounds among cell lines. First is expression of CCR5 which has already been discussed. Downstream signaling pathways of the cells may compensate differently to the antagonism of CCR5 among cell lines. The genetic material effected by the activity of the CCR5 is also influenced by other signaling cascades. Other pathways and second messenger systems among cell lines can delay or negate the effect of our drug. Finally, the rate of growth of the cells compared to concentration of drug is different among cell lines. At plating, there are approximately 1000 cells in each well. After one day of growth, drug is added so that the drug concentration of the *well* is fixed. As time progresses, presuming the cells are still growing, there will be a lower concentration of drug compared to the amount of cells in each well. Drug metabolism is another factor effecting its concentration over time. Coupling that with the difference in receptor expression levels can explain why there are not only differences among cell lines but among each day of growth.

C. Molecular Dynamics Simulations and Docking of Anibamine and Its Analogs

Two homology models of chemokine receptor CCR5 were previously generated in our lab.[88] One was based on the crystal structure of β_2 adrenergic receptor (PDB code 2RH1) with a resolution of 2.4 Å and one was based on the crystal structure of bovine rhodopsin (PDB code 1F88) at 2.8 Å. The crystal structure of bovine rhodopsin contains a bound antagonist, retinal, resulting in a model in the "dark state" while β_2-AR was crystallized with an inverse agonist, carazolol. No mutagenesis data is available for anibamine in the CCR5 receptor while data from studies with other CCR5 ligands suggest Glu283 as a hydrogen bond acceptor to protonated quaternary nitrogen atoms. Therefore this residue was used as a starting point for defining the binding pocket of anibamine and its analogs.

1. Construction of anibamine and its analogs.

The docking conformation of anibamine has been previously studied in the two homology models of CCR5.[88] Molecular models of the anibamine and eight synthesized analogs were developed in Sybyl. (Figure 20) The lowest energy conformation of each ligand was saved for use in GOLD.

2. Dynamics simulation of prepared homology models for docking studies.

The prepared homology models were accessed with anibamine bound in the proposed binding pocket. A dynamics simulation of anibamine docked into each receptor was performed in an attempt to enlarge the binding pocket with defined aggregates and constraints. An averaged structure was saved for ligand docking in GOLD.

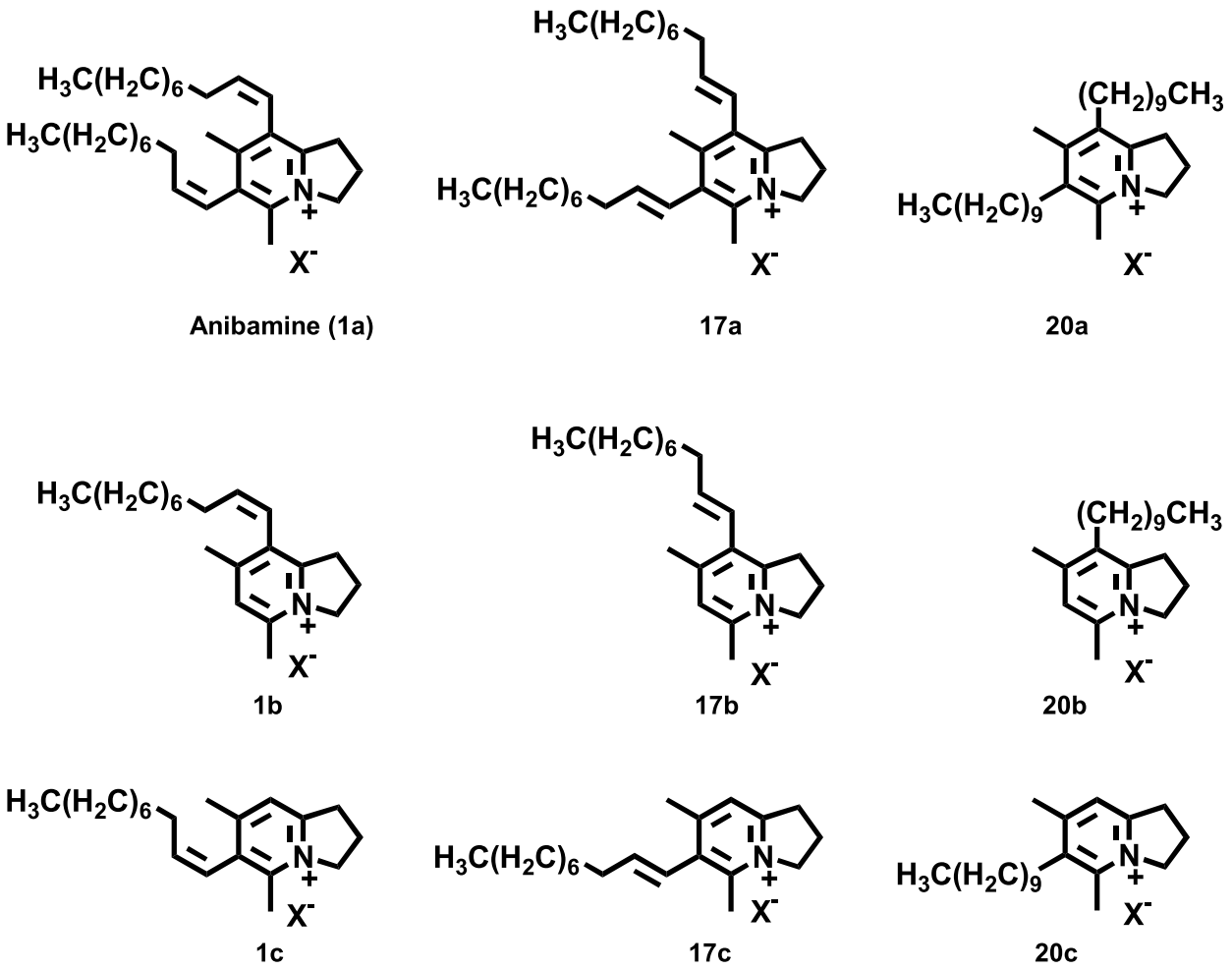

Figure 20. Structure of anibamine and docked ligands.

3. GOLD docking of ligands into CCR5 homology models.

Automated docking of all ligands was performed using GOLD3.1. Two constraints were used to guide the ligands to the proposed binding pocket of the receptor. A distance constraint directed the charged nitrogen atom of the ligand to the carboxylate group on Glu283. A similarity constraint based on the common core (Figure 21) derived from the previously bound anibamine molecule was also used to guide ligands to the proposed binding pocket. The number of operations in each GOLD run was increased to 300,000 to accommodate the flexible sidechains. The top ranked configurations of each ligand was visualized in Sybyl.

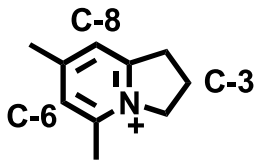

Figure 21. The common indazolinium core of anibamine and all docked ligands with labeled key carbons.

Comparisons of the binding modes of anibamine and other known CCR5 antagonists were made using both models. Based on how the GOLDscore is produced, each of the compounds with two sidechains ultimately resulted in higher GOLDscores than the deconstructed analogs. Because they are larger, they inherently have more interactions to raise the GOLDscore. All the ligands bound to the receptor in roughly the same binding pocket in both models, therefore, the majority of the discussion focuses on the configurations of the ligands themselves.

4. Analysis of ligand binding to CCR5 model based on 1F88 structure

Anibamine and eight analogs were docked into the CCR5 receptor model based on the rhodopsin crystal structure using GOLD3.1. The GOLDscores for each ligand are presented in table 7. The highest ranked ligands were anibamine (**1a**), its saturated analog (**20a**) and its geometric isomer (**17a**). The *trans* analogs of all series **(17a, 17b** and **17c**) had the lowest scores.It seemed that the *trans* configuration at the double bond decreases the GOLDscore.

Table 7. GOLDscores in 1F88 CCR5 model

ligand	Fitness	s(hb_ext)	s(vdw_ext)	S(hb_int)	s(int)	s(con)
Anibamine (1a)	73.06	0.00	61.67	0.00	-21.62	9.88
1b	58.67	0.00	43.29	0.00	-9.34	8.49
1c	58.19	0.00	41.58	0.00	-7.78	8.80
17a	61.71	0.00	56.31	0.00	-23.75	8.03
17b	54.09	0.00	39.78	0.00	-7.92	7.32
17c	54.41	0.00	38.92	0.00	-7.74	8.65
20a	65.96	0.00	62.08	0.00	-28.67	9.27
20b	59.84	0.00	42.02	0.00	-6.70	8.76
20c	57.54	0.00	40.81	0.00	-7.50	8.91

Note: Cmpd. – compound; S – Gold score component; hb – hydrogen bonding; vdw – Van der Waals interactions; ext – external interactions; int – internal interactions. Con-constraint.

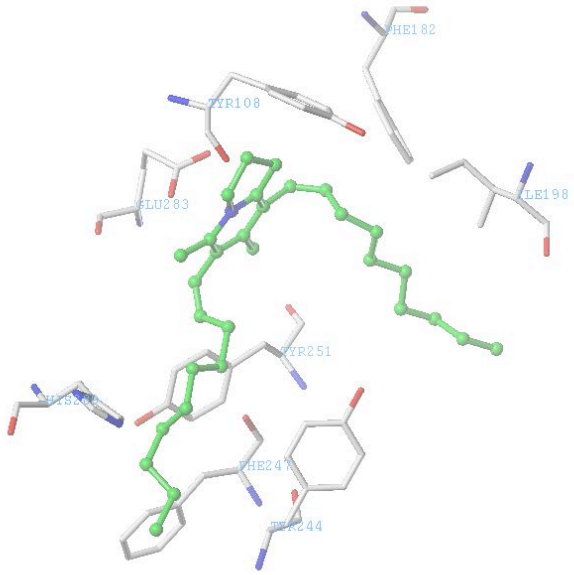

Figure 22. Binding of anibamine (in ball and stick) in the CCR5 model based on 1F88 (capped sticks).

When each top-ranked ligand was visualized in Sybyl, it became apparent that the core of the ligand was flexible in the binding pocket. For the sake of clarity, the sidechain at C-8 will be referred to as the ortho sidechain as it is positioned next to the 5-membered ring on the pyridine ring; the sidechain at C-6 will be referred to as the para sidechain as it is across the pyridine ring from the 5 membered ring. Interestingly, there was enough flexibility in the pocket surrounding the core to allow for different ligands to position their sidechains differently such that not all para sidechains fell in one direction while not all ortho sidechains bound in another direction. One sidechain channel pointed down into the protein and the other sidechain binding pocket stretched to the side of the protein. Helix 6 was in between each sidechain, lending some hydrophobic properties to both with amino acids Tyr251, Phe245, and Trp248 depending on their sidechain configuration. Because all compounds share the same binding pocket, the amino acid residues will be described based on their relationship to anibamine in its current binding mode. (Figure 22) The nitrogen on the imidazolinium core is within ionic bonding distance of Glu283 on helix 7. Tyr108 and Phe182 are close enough to offer some pi-stacking interactions with the aromatic core of the molecule. The para sidechain of anibamine points out towards the side of the protein between helices 3 and 6. The long aliphatic sidechain is bordered by Val199, Phe182, and Ile198. The ortho sidechain burrows into the protein, making possible hydrophobic interactions with Phe117 on helix 1, Ile240, Val243, Tyr244, and Phe247 along helix 6. All other ligands docked in the same pocket and interacted with the same (or fewer) amino acid residues.

When looking at the shape of the 5-membered ring in each bound ligand, a direct correlation to the GOLDscore was noticed. The three lowest scoring compounds (**17b**, **17c**, and **20c**) and compound **17a**, the lowest scored of the double-sidechain compounds all had C3 in the

5-membered ring positioned towards Glu283/helix 7. In all other compounds, C3 pointed away from helix 7. The double bond configuration may play a role in the conformation of the 5 membered ring. Ligand **20c** is saturated but the angle of the bonds between carbons in the docked conformation more closely resembles a *trans* bond. All the other ligands with this shape have *trans* double bonds. The direction of the 5-membered ring might be playing a role in lowering the GOLDscore.

There did not appear to be any amino acid residue in a position to favor any double bond configuration. For each set of compounds the *trans* isomer ranked the lowest, but this may be attributed to the conformation of the 5-membered ring. The higher scores of the saturated and *cis* analogs compared to the *trans* analogs could also be a result of the simulations undertaken with anibamine as the docked ligand.

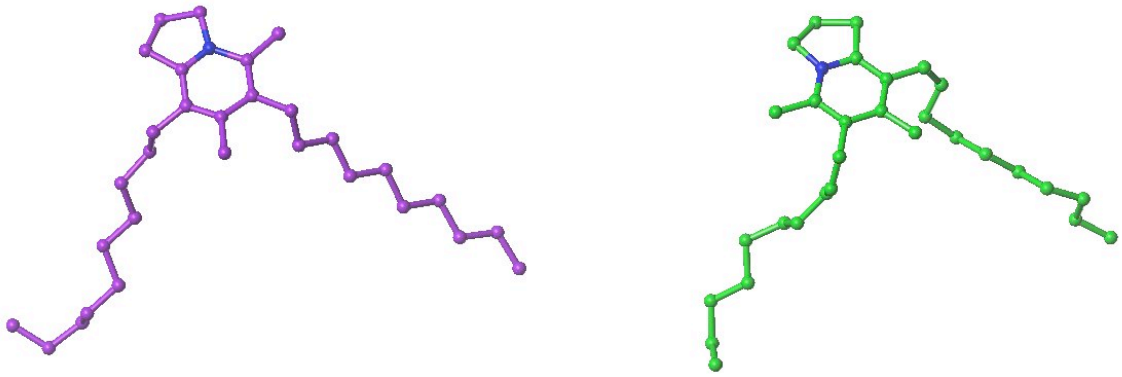

Figure 23 Binding configuration of **20a** (left) and anibamine (right) in the 1F88-based model.

The ligands with two sidechains bound the receptor in different ways. The anibamine analog **20a**, with 2 saturated sidechains, was bound in an inverted manner compared to anibamine. When superimposed, the atoms of the 5-membered rings of the compounds overlapped, but the nitrogens do not match up resulting in the para sidechain of one ligand

sharing the same binding pocket with the ortho sidechain of the other. (Figure 23) Despite this difference, these two compounds had the highest GOLDscores. The geometric isomer of anibamine (**17a**) bound in a similar manner to anibamine but had a lower GOLDscore.

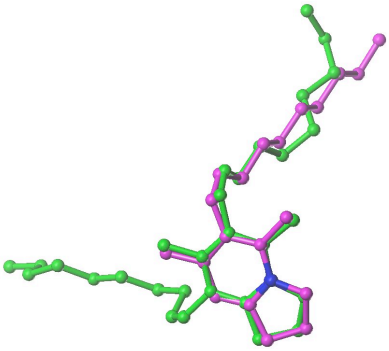

Figure 24. Overlay of Anibamine (green) and **1c** (magenta) in 1F88-based model

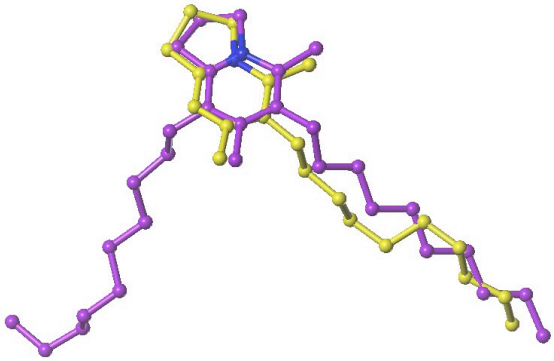

Figure 25. Overlay of **20a** (magenta) and **20c** (yellow) in 1F88-based CCR5 model.

The position of the sidechain seemed to not have much effect on the rank of the GOLDscores. All the compounds with only the ortho sidechain (**1b**, **17b**, and **20b**) as well as **1c** docked with their only sidechain directing to the side of the protein. The binding mode for ligand **1c** directly overlaps with the top ranked binding mode for anibamine (Figure 24) although their scores are very different. Compounds **17c** and **20c** were the only compounds with one sidechain to bind in such a manner that their sidechains pointed into the protein. Their structures can be overlapped with the of **20a**, which is the only other compound to have the para sidechain in that

binding channel. Figure 25 shows the overlap of **20a** and **20c** in the binding pocket of CCR5. Though the scores for **1b**, **1c**, and **20b** are higher than compounds **17c** and **20c**, ligand **17b** has the lowest GOLDscore. This may indicate that the shape of the 5-membered ring is more important in the scoring process than where the sidechain is located. In the three highest ranked compounds, a similar trend is observed. Anibamine and **20a**, although their sidechains bind in a manner opposite from the other, have higher GOLDscores than **17a** which binds in the same way as anibamine regarding the sidechains but has a different conformation in the 5-membered ring. The more sensitive part of the molecule for binding may indeed be the indazolinium core rather than the sidechains.

5. Analysis of ligand binding to CCR5 model based on 2RH1 structure

The same ligands were docked into the homology model based of the crystal structure of β_2-AR. The GOLDscores for each ligand are presented in table 8. With the exception of the score for anibamine, the value of the GOLDscores obtained for this model were close to the scores obtained for the homology model based on bovine rhodopsin. In this model, the saturated ligand **20a** ranked higher than anibamine (1a). All the *trans* isomers (**17a**, **17b**, and **17c)** ranked lower than their respective saturated analog (**20a**, **20b**, and **20c).** The *cis* ligand (1c) ranked highest in series **c**. Ligand **20b** ranked highest in the **b** series.

Table 8. GOLDscores of ligands docked into the 2RH1-based CCR5 model

ligand	Fitness	s(hb_ext)	s(vdw_ext)	S(hb_int)	s(int)	s(con)
Anibamine (1a)	61.15	0.00	53.62	0.00	-20.33	7.76
1b	52.75	0.00	39.24	0.00	-9.92	8.72
1c	53.94	0.00	39.02	0.00	-12.29	8.24
17a	55.82	0.00	52.19	0.00	-23.64	7.70
17b	53.86	0.00	41.25	0.00	-10.21	7.35
17c	52.57	0.00	39.43	0.00	-10.64	9.00
20a	63.30	0.00	60.54	0.00	-28.80	8.72
20b	55.46	0.00	40.44	0.00	-8.34	8.20
20c	53.10	0.00	53.06	0.00	-8.56	8.28

Note: S:Gold score component; hb:hydrogen bonding; vdw:Van der Waals interactions; ext:external interactions; int:internal interactions. Con:constraint.

In contrast to the binding modes adopted in the rhodopsin-based model, one sidechain from each compound docked into the same pocket in the β_2-AR based model. There was less overlap of the common cores of the molecule when compared to the previous docking study. The ligands with two sidechains displayed varied placement of the second sidechain. The binding modes of anibamine (**1a**) and **20a** are depicted in figure 26. The residues highlighted in the figure are residues found in the previously published docking study that participated in binding of anibamine. They also play a role in the binding of **20a**. The higher score of **20a** may be due to the closer proximity of one sidechain to Phe109, Tyr190, and Phe264. The second sidechain of each ligand points out toward the extracellular space. The second sidechain of ligand **17a** also pointed toward the extracellular space. The ligands with one sidechain adopted conformations that placed the sidechain in the vicinity of Phe109, Tyr190, and Phe 264 as well.

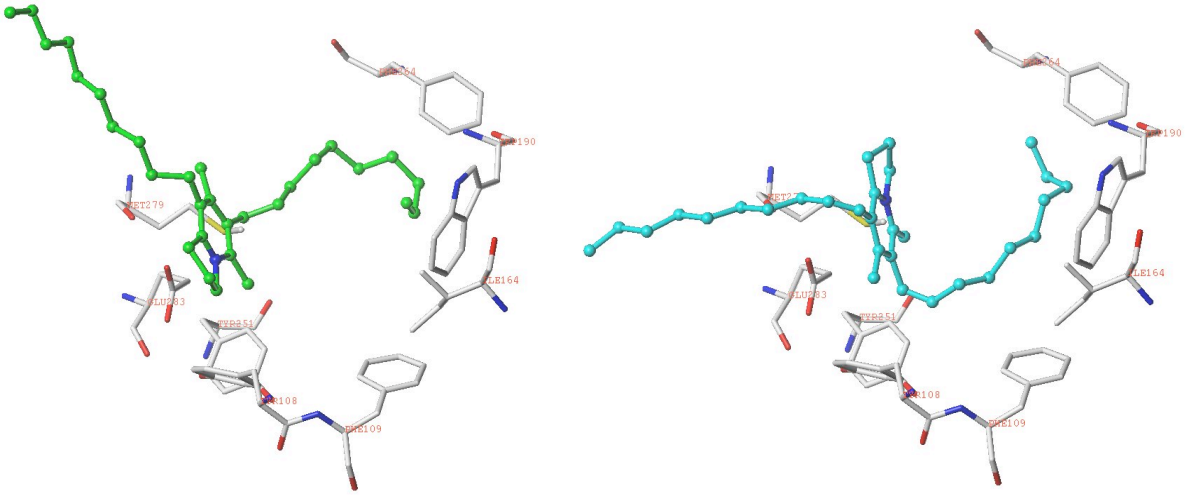

Figure 26. Binding of **1a** (left, ball and stick) and **20a** (right, ball and stick) in β_2-AR based model (capped sticks).

To adopt a conformation to place the sidechain in the pocket bordered by hydrophobic residues, the imidazolinium cores of the ligands adopted various conformations and there was no overlap. The binding modes of all series **c** ligands are shown in Figure 27. The sidechain of each ligand occupies roughly the same space in the receptor model, but it is clear that the cores are in different orientations. All ligands were within ionic bonding distance of Glu283. The GOLDscores did not seem to be effected by the shape of the core like they were in the rhodopsin based model.

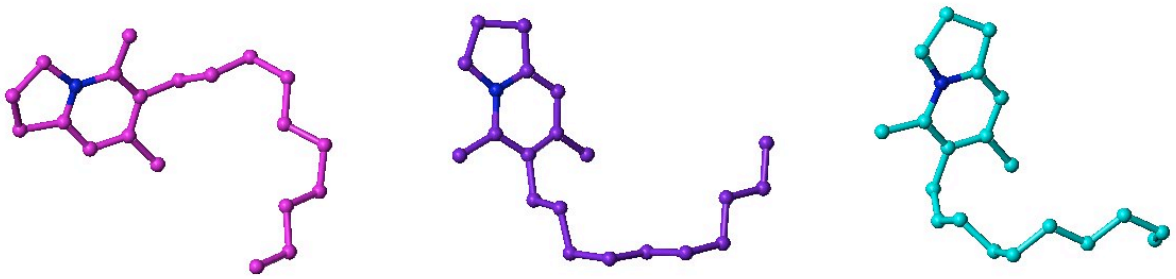

Figure 27. The binding modes of **17c** (left), **20c** (center) and **1c** (right) in β_2-AR based model.

6. Comparison of ligand docking in each receptor

Newly synthesized ligands were docked into previously constructed CCR5 homology models. The GOLDscores for ligands with two sidechains were higher in comparison to other ligands in both models. Despite using a similarity constraint for docking using the core common to all ligands, the binding modes of the pyridinium core varied in the same binding pocket. For both receptors, it seemed the interactions between the sidechains of the ligands with the amino acid residues of the receptor were more important than the position of the core. More overlap of cores among ligands was observed in the 1F88 based model. In the β_2 adrenergic receptor based model, one sidechain from each ligand docked into the same side of the binding pocket. Though the distribution of the sidechain binding mode in this receptor was more widely shared between ligands, almost no core overlap was observed. Both models present intriguing insights into the binding mode of the receptor, especially in regard to deconstruction. Because there was no defined place for the para or ortho sidechains to bind consistently in each model, it invites the question of whether the two series of deconstructed analogs might not be that different.

V. Conclusions

The high rate of prostate cancer metastasis related mortality coupled with the increase in the population of men over 50 years of age necessitates the development of novel therapeutics for the treatment of prostate cancer. Through the investigation of the inflammatory network in prostate cancer, the chemokine receptor CCR5 was found to be overexpressed in metastatic prostate cancer cell lines.[6] This was followed by the discovery that a CCR5 antagonist inhibited proliferation of PCa cell lines.[7] A novel natural product, anibamine, was isolated and found to be a micromolar inhibitor of the receptor.[10,11] Anibamine was used as a new anti-prostate cancer lead compound. The total synthesis of anibamine was completed from acetyl acetone in either ten or eleven steps. To discover the pharmacophore, analogs of anibamine were designed using the "deconstruction-reconstruction-elaboration" approach. The goal of this project to synthesize deconstructed analogs of anibamine each with a *trans* analog and a saturated analog. The establishment of a stereoselective route to only one isomer was desired as well, to increase yield and eliminate elaborate purification procedures.

Anibamine and eight analogs were successfully prepared by following the total synthesis of anibamine. Six new deconstructed analogs were synthesized from intermediates **2a** and **2b** then paralleling the synthetic route of anibamine. Separation of the isomers proved very difficult. Ultimately separation of penultimate intermediates on prep TLC was deemed the best way to separate the *cis* and *trans* isomers. Stereoselective synthesis would remove the need to separate isomers. Five different reaction conditions repeated among different aldehyde substrates were explored, resulting in *cis:trans* ratios as high as 1:1. Solubility of the long aliphatic chain

reagents appeared to be the main hindrance in successful stereoselective synthesis. Other synthetic routes are being explored to improve stereoselectivity in the hopes of making separation of isomers a non issue.

From the anti-proliferative data, however, the double bond configuration had less of an influence on activity. The compounds were tested in four different concentrations at an incubation time of 72 hours. In the DU-145 cell line, the 5-membered ring compounds had the highest activity. The 7-membered rings were the most potent in the PC-3 cell line. The majority of compounds had very strong anti-proliferative effect in the M-12 cell line, making it hard to distinguish a clear structure-activity relationship. Each cell line has a different expression level of CCR5 which can account for some of the differences in activity. Differences in signaling cascades and compensation mechanisms can also play a role in the different cell lines. The deconstructed analogs were also tested at 24 and 48 hours incubation times to both further validate the use of the 72 hours incubation time and to examine the effect of the drugs over a three day time interval. The drugs effected the cell lines at different rates but by 72 hours the overall effect of each drug had stabilized. Of the deconstructed analogs, the para sidechain drug, **20c** had the highest activity in each cell line, indicating that this sidechain may be more important for activity.

In the modeling studies, two different homology models of CCR5 were used to observe the possible binding mode of the synthesized ligands. The shared core of anibamine was used as a similarity constraint to direct the ligands to the proposed binding pocket. Interestingly, the ligands with only one sidechain frequently flipped the imidazolinium core so that the sidechain directed into the same area of the binding pocket in both models. Even the ligands with two sidechains interchanged what side of the binding pocket each sidechain occupied. Without defined binding pockets for each sidechain, the deconstructed analogs can bind in a way nearly identical to its geometric isomer, leaving little difference between analogs.

These studies are the beginning of a thorough exploration into the structure-activity relationship of anibamine. These data combined with future results will identify a next generation lead compound for anti-prostate cancer activity.

VI. Experimental

1. Chemical Synthesis

Melting points were determined on a Fisher-Scientific melting point apparatus. ^{1}H-NMR and ^{13}C-NMR spectra were obtained on a Varian Gemini 300 MHz spectrometer, Varian Mercury 300MHz NMR spectrometer or Brucker 400 MHz spectrometer and tetramethylsilane was used as an internal standard. Infrared spectra were obtained on a Nicolet 5ZDX FT-IR spectrometer. Column chromatography was performed on silica gel (grade 60 mesh; Bodman Industries, Aston, PA). Routine thin-layer chromatography (TLC) was performed on silica gel GHIF plates (250 μm, 2.5 x 10 cm; Analtech Inc., Newark, DE). Preparative TLC was performed on Partisil PK6F plates (250 μm and 500 μm, 20 x 20 cm; Whatman Int. Ltd. Maidstone, England). Preparative HPLC was performed on a Varian Dynamax Microsorb 100-5 CN column (250 x 21.5mm), using Prostar 325 UV-Vis (254, 280nm) as the detector.

A. Intermediates in synthesis of Series a:

Route 1:

3-((Dimethylamino)methylene)pentate-2,4-dione (3)

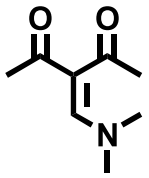

A neat mixture of *N,N*-dimethylformamide dimethyl acetal (18.77 g, 157.7 mmol) and acetylacetone (7.76 g, 77.6 mmol) was refluxed for 2 hours. The mixture was then concentrated to remove excess acetal to give a dark red oil. The crude product was recrystallized in EtOAc to give 3-((dimethylamino)methylene)pentate-2,4-dione (8.562 g, 71% yield) as light yellow crystals. M.p. 55-57°C ^{1}HNMR (300 MHz, $CDCl_3$) δ 7.45 (s, 1H), 3.00 (s, 6 H), 2.34 (s, 6H).

1-(5-Methylisoxazol-4-yl)ethanone (4)

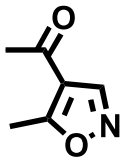

A solution of 3-((dimethylamino)methylene)pentate-2,4-dione (4.662g, 30 mmol) and hydroxylamine hydrochloride (2.885g, 30 mmol) in 50 mL MeOH was refluxed for 2 hours. The mixture was concentrated to remove MeOH then partitioned between 50 mL water and 100 mL dichloromethane. The CH_2Cl_2 layer was dried over Na_2SO_4, filtered and concentrated. The residue was purified by reduced pressure distillation to give 1-(5-methylisoxazol-4-yl)ethanone (1.922 g, 51% yield) as a colorless oil. ^{1}HNMR (300 MHz, $CDCl_3$) δ 8.49 (s, 1H), 2.73 (s, 3 H), 2.47 (s, 3H).

(*E*)-2-Methyl-4-oxo-3-(phenylamino)pent-2-enenitrile (5)

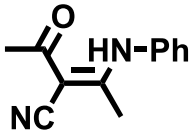

A mixture of aniline (1.295g, 13.8 mmol) and 1-(5-methylisoxazol-4-yl)ethanone (580 mg, 4.6 mmol) was refluxed for 15 minutes. After cooling the mixture was poured into ice cold 2M HCl and stirred while a precipitate formed. The precipitate was recrystallized in EtOH to give (*E*)-2-methyl-4-oxo-3-(phenylamino)pent-2-enenitrile (504 mg, 54% yield) as clear plate crystals. M.p.: 132-133°C ^{1}HNMR (300 MHz, $CDCl_3$) δ 7.47-7.35 (m, 3H), 7.14 (m, 2H), 2.43 (s, 3H), 2.27 (s, 3H).

Route 2:

2-hydroxy-4,6-dimethylnicotinonitrile (2b)

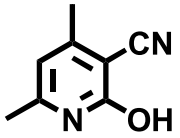

Cyanoacetamide (0.84 g, 10 mmol) was dissolved in a solution of K_2CO_3 (0.40 g, 2.89 mmol) in water (20 mL). Then acetylacetone (1.00 g, 10 mmol) was added and the reaction stirred overnight at room temperature. The precipitate was filtered and washed with hexane to give 2-hydroxy-4,6-dimethylnicotinonitrile (1.35 g, 91% yield) as a white powder. M.p.: 118-119°C ^{1}HNMR (300 MHz, $CDCl_3$) δ 12.38 (br, 1H), 6.15 (s, 1H), 2.28 (s, 3H), 2.21 (s, 3H).

5-bromo-2-hydroxy-4,6-dimethylnicotinonitrile (6)

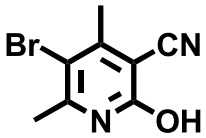

2-Hydroxy-4,6-dimethylnicotinonitrile (148 mg, 1 mmol) was dissolved in trifluoroacetic acid (0.3 mL) at 0˚C. H_2SO_4 (0.4 mL) was added followed by NBS (356 mg, 2 mmol). The reaction was kept at 0°C for 1.5 hours then poured into crushed ice. The resulting precipitate was filtered and recrystallized in a 4:1 mixture of acetone and water yielding 5-bromo-2-hydroxy-4,6-dimethylnicotinonitrile (161 mg, 71% yield) as white crystals. M.p.: 256-257°C ^{1}HNMR (300 MHz, $CDCl_3$) δ 12.84 (br, 1H), 2.43 (s, 3H), 2.37 (s, 3H).

2-hydroxy-4,6-dimethylpyridine-3,5-dicarbonitrile (2a)

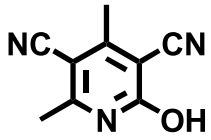

Route 1: A solution of (*E*)-2-methyl-4-oxo-3-(phenylamino)pent-2-enenitrile (500 mg, 2.5 mmol), malononitrile (165 mg, 2.5 mmol), and KOH (140 mg, 2.5 mmol) in 20 mL MeOH was refluxed overnight while a precipitate formed. The precipitate was filtered and dried to give 2-hydroxy-4,6-dimethylpyridine-3,5-dicarbonitrile (320 mg, 74% yield) as a white powder. **Route 2 (Rosemund von Braun Reaction):** CuCN (819 mg, 9.1 mmol) was dissolved in DMF (4 mL). 5-bromo-2-hydroxy-4,6-dimethylnicotinonitrile (730 mg, 7.6mmol)was added slowly then more DMF (2 mL) was added. The reaction was refluxed under N_2 protection for 50 hours. The room temperature reaction mixture was poured into an $FeCl_3$ solution (4 g $FeCl_3$, 4 mL H_2O, 1 mL HCl) and stirred at 60°C for 20 minutes. Then ice was added to 50 mL total volume. The water solution was extracted with 75 mL EtOAc three times. The combined organic layers were washed with brine, dried over Na_2SO_4, filtered and concentrated to give 200 mg crude product. The water layer was neutralized with 1M NaOH until filtration of inorganic salt was needed. The water layer was again extracted with EtOAc three times. The combined organic layers were washed with brine, dried over Na_2SO_4, filtered and concentrated to give 250 mg crude product. The inorganic salts were washed with EtOAC multiple times, the EtOAc was decanted off the brown aqueous mixture. The combined organic layers were dried over Na_2SO_4, filtered and concentrated to give 300 mg crude product. The crude products were recrystallized in AcOH to give 2-hydroxy-4,6-dimethylpyridine-3,5-dicarbonitrile (671 mg, 51% yield) as a white powder.

Route 2 (Domino Halide reaction): NaCN (47 mg, 0.96 mmol), CuI (15 mg, 0.08 mmol), KI (27 mg, 0.16 mmol), and 5-bromo-2-hydroxy-4,6-dimethylnicotinonitrile were added to a three neck flask equipped with a condenser. The flask was evacuated and filled with N_2 three times before addition of anhydrous toluene (1 mL) and *N,N*-dimethylethylenediamine (85 µl, 0.8 mmol). The reaction was heated to reflux and stirred for 24 hours. An additional 20 mL of toluene was added over the course of the reaction to dissolve more 5-bromo-2-hydroxy-4,6-dimethylnicotinonitrile. After 24 hours, TLC showed some product but mostly starting material. The reaction was stopped and the product was not isolated. M.p.: decomposed at 260°C ^{1}HNMR (300 MHz, DMSO) δ 3.33 (br, 1H), 2.49 (s, 3H), 2.22 (s, 3H).

After convergence of Routes 1 and 2:

2-Bromo-4,6-dimethylpyridine-3,5-dicarbonitrile (8a)

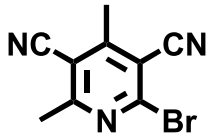

A solution of 2-hydroxy-4,6-dimethylpyridine-3,5-dicarbonitrile (420 mg, 2.4 mmol), TBAB (933 mg, 2.9 mmol) and P_2O_5 (1.45 g, 10 mmol) was heated in toluene (60 mL) under N_2 protection for 4.5 hours. Ice was added to the reaction mixture, the toluene layer was separated and kept. The water layer was neutralized with $NaHCO_3$. The water layer was then extracted with EtOAc (50 mL) three times. The combined organic layers were washed with brine, dried over Na_2SO_4, filtered and concentrated to give 1.08 g crude brown solid. The crude product was purified by column chromatography on Al_2O_3 with a Hexane:EtOAc solvent system (20:1 v/v) as

eluent to give 2-bromo-4,6-dimethylpyridine-3,5-dicarbonitrile (430 mg, 75% yield) as a white powder. M.p.: 127-129°C ^{1}HNMR (300 MHz, $CDCl_3$) δ 2.83 (s, 3H), 2.78 (s, 3H).

1-Methoxy-4-((prop-2-ynyloxy)methyl)benzene (10)

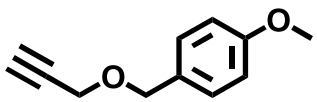

A solution of 4-methoxybenzylalcohol (1.66g, 12 mmol) in anhydrous Et_2O (12 mL) was added to a suspension of g NaH (29 m, 1.2 mmol) at room temperature and stirred for 30 minutes under N_2 protection before cooling to 0°C. Trichloroacetonitrile (1.73 g, 12 mmol) was added, and the reaction mixture was allowed to warm up slowly to room temperature over 4 hours. The solvent was evaporated, the residue was dissolved in dry hexane (14 mL) and dry MeOH (0.06 mL) and filtered through celite then concentrated to give a yellow oil (1.9 g). The crude imidate was dissolved in hexane and dichloromethane (30 mL, 2:1 v/v). Propargyl alcohol (448 mg, 0.8 mmol) was added to the reaction and the solution was cooled to 0°C and treated with a catalytic amount of 10-camphorsulfonic acid. The reaction was stirred for 20 hours under N_2 protection while a white precipitate formed. The solution was filtered through celite, washed with saturated aqueous sodium bicarbonate, dried over sodium sulfate, filtered and concentrated to give 1.4 g crude product. The crude product was purified on silica gel with hexane:EtOAc (25:1 v/v) to give 1-methoxy-4-((prop-2-ynyloxy)methyl)benzene (0.9 g, 64% yield)as a colorless oil. ^{1}HNMR (300 MHz, $CDCl_3$) δ 7.29 (m, 2H), 6.89 (m, 2H), 4.54 (s, 2H), 4.14 (d, *J=2.4 Hz*, 2H), 3.81 (s, 3H), 2.46 (t, *J=2.4 Hz*, 1H).

2-(3-((4-Methoxybenzyloxy)prop-1-ynyl)-4,6-dimethylpyridine-3,5-dicarbonitrile (11a)

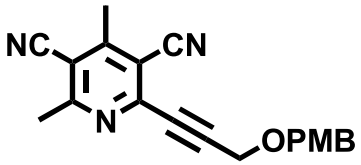

To a stirred suspension of 2-bromo-4,6-dimethylpyridine-3,5-dicarbonitrile (620 mg, 2.6 mmol), CuI, (24 mg, 0.26 mmol), $PdCl_2(PPh_3)_2$ (91 mg, 0.13 mmol), and triethylamine (18 mL) in diethyl ether (60 mL) was added 1-methoxy-4-((prop-2-ynyloxy)methyl)benzene (554 mg, 3.15 mmol) in diethyl ether (2 mL) dropwise under N_2 protection. The reaction was allowed to stir under N_2 protection for 6 hours while a precipitate formed. Then water (25 mL) was added. The organic layer was separated and the precipitate was filtered and recrystallized in EtOAc to yield 2-(3-((4-Methoxybenzyloxy)prop-1-ynyl)-4,6-dimethylpyridine-3,5-dicarbonitrile (565 mg, 66% yield) as white crystals. M.p.: 130-131°C ^{1}HNMR (300 MHz, $CDCl_3$) δ 7.35 (m, 2H), 6.90 (m, 2H), 4.68 (s, 2H), 4.48 (s, 2H), 3.8 (s, 3H), 2.83 (s, 3H), 2.77 (s, 3H).

2-(3-((4-Methoxybenzyloxy)propyl)-4,6-dimethylpyridine-3,5-dicarbonitrile (12a):

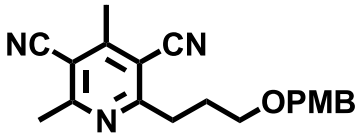

Hydrogenation was conducted on a mixture of 2-(3-((4-methoxybenzyloxy)prop-1-ynyl)-4,6-dimethylpyridine-3,5-dicarbonitrile (475 mg, 1.42mmol) and Pd/C (47 mg, 10% by weight) in MeOH (*30* mL) under 50 psi H_2 for 6 hours. The mixture was filtered through celite to remove Pd/C and concentrated to remove MeOH to give 2-(3-((4-methoxybenzyloxy)propyl)-4,6-dimethylpyridine-3,5-dicarbonitrile (450 mg, 95% yield) as a white solid without further

purification. M.p.: 90-92°C ^{1}HNMR (300 MHz, $CDCl_3$) δ 7.19 (m, 2H), 6.84 m, 2H), 4.38 (s, 2H), 3.80 (s, 3H), 3.55 (t, *J=6.0 Hz*, 2H), 3.12 (m, 2H), 2.76 (s, 3H), 2.64 (s, 3H), 2.11 (m, 2H).

2-(3-((4-Methoxybenzyloxy)propyl)-4,6-dimethylpyridine-3,5-dicarbaldehyde (13a)

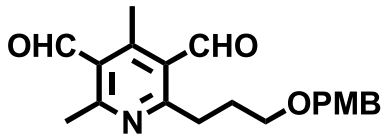

Under N_2 protection, 2-(3-((4-methoxybenzyloxy)propyl)-4,6-dimethylpyridine-3,5-dicarbonitrile (90 mg, 0.26 mmol) was dissolved in anhydrous toluene (8 mL) then cooled to -70°C. After cooling, DIBAL-H (0.56 mL of 1.0 M solution of in toluene, 0.56 mmol) was added dropwise over 15 minutes and stirred at -70°C for 2 hours. After two hours, 1 additional equivalent (0.26 mL of 1.0 M solution in toluene, 0.26 mmol) of DIBAL-H was added over 10 minutes and the reaction kept at -70°C. Over the next 2.5 hours the reaction was allowed to warm to 0°C. Then 1.0 M H_2SO_4 (3.0 mL) was added and the resulting solution was stirred overnight. The organic layer was separated; the aqueous layer was extracted with 10 mL EtOAc three times. The combined organic layers were washed with saturated aqueous $NaHCO_3$, brine, and dried over Na_2SO_4, filtered and concentrated to give 130 mg crude product as a yellow oil. The crude residue was purified by column chromatography on silica gel with a Hexane/EtOAc solvent system (5:1 v:v) to give 2-(3-((4-Methoxybenzyloxy)propyl)-4,6-dimethylpyridine-3,5-dicarbaldehyde (68 mg, 74% yield) as a colorless oil. ^{1}HNMR (300 MHz, $CDCl_3$) δ 10.61 (s, 1H), 10.59 (s, 1H), 7.24 (m, 2H), 6.87 (m, 2H), 4.41 (s, 2H), 3.80 (s, 3H), 3.51 (t, *J=6.0 Hz*, 2H), 3.15 (m, 2H), 2.77 (s, 3H), 2.75 (s, 3H), 2.05 (m, 2H).

Non-1-yl triphenylphosphonium bromide (14)

1-Bromononane (1.035g, 5 mmol) and triphenylphosphine (1.310 g, 5 mmol) were refluxed in toluene for 55 hours. After cooling, the toluene was removed by roto evaporation. The residue was washed with diethyl ether and thoroughly dried yielding non-1-yl triphenylphosphonium bromide in quantitative yield. ^{1}H NMR (DMSO, 400 mHz) δ 7.88-7.77(m, 15H), 3.56 (m, 2H), 1.47 (m, 4H), 1.19 (m, 10H), 0.82 (m, 3H).

2-(3-(4-Methoxybenzyloxy)propyl)-4,6-dimethyl-3,5-di((*Z*)-dec-1-enyl)pyridine and its three isomers: (15a and isomers)

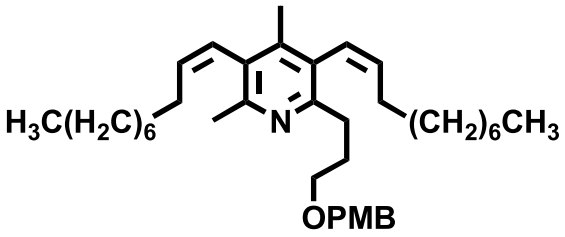

Traditional Wittig Reaction: Under N_2 protection, non-1-yl triphenylphosphonium bromide (1.100 g, 2.35 mmol) in toluene (6 mL) and LHMDS (2.1 mL of a 1.0 M solution of in THF, 2.1 mmol) were dissolved producing a bright red color. The solution was cooled to -70°C then 2-(3-((4-methoxybenzyloxy)propyl)-4,6-dimethylpyridine-3,5-dicarbaldehyde (200 mg, 0.58 mmol) in toluene (5 mL) was added dropwise over 15 minutes. The reaction was stirred at -70°C for 15 minutes then warmed to room temperature. After stirring for 45 minutes at room temperature, the reaction was quenched with saturated aqueous NH_4Cl (18 mL) producing a colorless solution. The organic layer was separated, the aqueous layer was extracted with EtOAc (50 mL) three times. The combined organic layers were washed with brine, dried over Na_2SO_4, filtered and

concentrated to give a crude oil (1.4 g). The crude product was purified by column chromatography on silica gel with hexane:EtOAc (15:1 v/v) as eluent to give 2-(3-(4-methoxybenzyloxy)propyl)-4,6-dimethyl-3,5-di((*Z*)-dec-1-enyl)pyridine and its three isomers (240 mg, 73% yield) as a colorless oil. ^{1}HNMR indicated 1:3 *E:Z* ratio. **Schlosser Modification to the Wittig Reaction:** Under N_2 protection, non-1-yl triphenylphosphonium bromide (164 mg, 0.35 mmol) and LiBr (61 mg 0.7 mmol) in anhydrous toluene/THF (5 mL, 4:1 v/v)) and PhLi (0.2 mL of a 1.8 M solution in diisopropyl ether, 0.35 mmol) were dissolved producing a dark orange solution. The resulting solution was cooled to -70°C. The crude aldehyde 2-(3-((4-Methoxybenzyloxy)propyl)-4,6-dimethylpyridine-3,5-dicarbaldehyde (20 mg, 0.06 mmol) was dissolved in toluene (1 mL) and added dropwise to the solution resulting in light orange solution. After 20 minutes, PhLi (0.2 mL of a 1.8 M solution in diisopropyl ether, 0.35 mmol) was added returning the reaction to a dark orange solution. After 20 minutes stirring at -70°C, the reaction was warmed to -25°C and 1 M ethereal HCl (0.75 mL, 1 M solution in diethyl ether, 0.75 mmol). After a few minutes, *t*-BuOK (100 mg, 0.9 mmol dissolved in a minimum amount of THF) was added to the reaction. The reaction was allowed to warm to room temperature and stirred overnight. Then water (5 mL) was added. The organic layer was separated. The aqueous layer was extracted with EtOAc (20 mL) three times. The combined organic layers were washed with saturated aqueous $NaHCO_3$, brine, and dried over Na_2SO_4, filtered and concentrated. The crude product was purified by column chromatography on silica gel with hexane:EtOAc (8:1 v/v) as eluent to give 2-(3-(4-methoxybenzyloxy)propyl)-4,6-dimethyl-3,5-di((*Z*)-dec-1-enyl)pyridine and its three isomers (20 mg, 50% yield) as a colorless oil. ^{1}HNMR indicated 1:1 *E:Z* ratio. **Grignard Reaction:** Pieces of Mg ribbon and a small amount of iodine were put in a 2 neck

flask with a condenser and degassed and filled with N_2 three times. Anhydrous THF (1 mL) was added. 1-Bromononane (0.89 mL, 4.68 mmol) was added slowly, the reaction was heated with a hot gun, then with an oil bath to maintain a slight reflux for two hours. After two hours the reaction mixture looked clear and there was no visible Mg. It was cooled to 0°C and 2-(3-((4-methoxybenzyloxy)propyl)-4,6-dimethylpyridine-3,5-dicarbaldehyde (60 mg, 0.18 mmol) in THF (0.3 mL) was added dropwise. The reaction mixture was stirred 3 hours at 0°C. TLC monitoring showed no product had formed. In the morning, reaction was quenched with 10 mL NH_4Cl then the layers were disposed. The starting material was not recovered. ^{1}HNMR (400 MHz, $CDCl_3$) δ 7.26(d, *J=8.4 Hz,* 2 H), 6.87(d, *J=8.4 Hz,* 2 H), 6.27(m, 2H), 5.78(m, 2H), 4.44(s, 2H),3.80(s, 3H), 3.50(m, 2H), 2.82(m, 2H),2.39(s, 3H), 2.22(m, 2H), 2.05(s, 3H), 1.93(m, 4H), 1.78 (m, 4 H), 1.28 (m, 20H),0.87 (m, 6 H).

3-(4,6-Dimethyl-3,5-di-((*Z*)-dec-1-enyl)pyridin-2-yl)propan-1-ol (16a) and its three isomers:

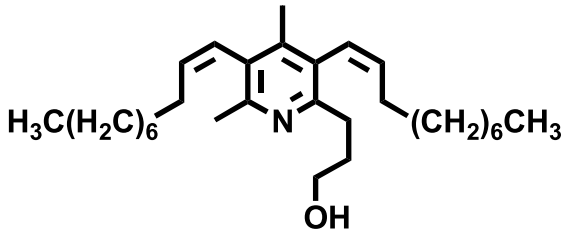

A mixture of 2-(3-(4-methoxybenzyloxy)propyl)-4,6-dimethyl-3,5-di((*Z*)-dec-1-enyl)pyridine and its three isomers (70 mg, 0.12 mmol) was refluxed in EtOH (3 mL) and 1N HCl (1.5 mL) for 5 hours. After cooling, the solution was concentrated to remove EtOH. The aqueous layer was extracted with CH_2Cl_2 (15 mL) three times. The combined organic layers were washed with brine, dried over Na_2SO_4, filtered and concentrated. The crude product (56 mg) was purified by column chromatography on silica gel with CH_2Cl_2:MeOH (40:1, v/v) as eluent to give 3-(4,6-

dimethyl-3,5-di-((*Z*)-dec-1-enyl)pyridin-2-yl)propan-1-ol (13) and its three isomers (45 mg, 87% yield) as a colorless oil. ^{1}HNMR (400 MHz, $CDCl_3$) δ 6.25 (m, 2H), 5.82 (m, 1H), 5.66 (m, 1H), 3.72 (m, 2H), 3.00 (m, 2H,), 2.92 (br, 1H), 2.39 (s, 3H), 2.23 (m, 2H), 2.06 (s, 3H), 1.92 (m, 4H), 1.76(m, 4H), 1.48 (m, 4H), 1.28 (m, 16H), 0.89 (m, 6H).

B. Final products in Series a:

Anibamine and its three isomers

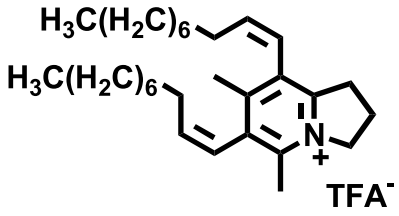

To a mixture of 3-(4,6-dimethyl-3,5-di-((*Z*)-dec-1-enyl)pyridin-2-yl)propan-1-ol (13) and its three isomers (110 mg, 0.25 mmol) and triethyl amine (75 mg, 0.75 mmol) in CH_2Cl_2 (5 mL) at 0°C was added MsCl (57 mg, 0.50 mmol) in CH_2Cl_2 (2 mL). The mixture was allowed to warm to room temperature over 60 minutes, diluted with CH_2Cl_2 (25 mL), washed with brine, dried over Na_2SO_4, filtered and concentrated. The crude product were separatedwas purified by column chromatography on silica gel with CH_2Cl_2:MeOH (15:1, v/v) as eluent to give anibamine and its three isomers (95 mg, 82% yield) as a colorless oil. The 95 mg of isomers was purified by HPLC on a Varian Dynamax Microsorb 100-5 CN column (250 x 21.5mm) eluting with a 90 min gradient CH_3CN (47.5~52.5%)/H2O (0.1% TFA) at a flow rate of 8 mL/min. (47.5% H_2O/52.5% MeCN v/v + 0.1% TFA).

Anibamine: Fractions at 55-61 minutes were collected and combined to give 50 mg crude product, which was purified by column chromatography on silica gel with CH_2Cl_2:MeOH (15:1, v/v) as eluent to give 12 mg colorless oil.

***E,E* isomer (17b):** Fractions at 77-84 minutes were collected and combined to give 40 mg crude product, which was purified by column chromatography on silica gel with CH_2Cl_2:MeOH (15:1, v/v) as eluent to give 14 mg colorless oil.

Anibamine isomers **19** and **20**: Fractions at 55-61 minutes were collected and combined to give 70 mg crude product, which was purified by column chromatography on silica gel with CH_2Cl_2:MeOH (15:1, v/v) as eluent to give 20 mg colorless oil. **1a** ^{1}HNMR (400 MHz, CD_3CN) δ 6.30 (d, *J= 11.4 Hz*, 2H), 6.09 (d t, *J= 11.4, 7.5Hz*, 1H), 6.05(d t, *J= 11.4, 7.5 Hz,*1H), 4.65 (t, *J= 7.5Hz*, 2H), 3.25 (m, 2H), 2.56 (s, 3H), 2.41 (m, 2H), 2.29 (s, 3H), 1.83 (m, 4H), 1.37 (m, 4H), 1.24 (m, 20H, 10 methylene groups), 0.89 (t, *J= 6.9Hz*, 6H); ^{13}C NMR (400 MHz, CD_3CN): δ 154.8, 154.5, 148.1, 138.7, 138.6, 135.1, 131.5, 122.4, 121.4, 57.9, 32.3, 31.8, 31.8, 29.34, 29.31, 29.31, 29.24, 29.24, 29.24, 28.98, 28.77, 28.64, 28.51, 22.6, 22.6, 20.5, 18.4, 17.5, 13.6, 13.6. **17a** ^{1}HNMR (400 MHz, CD_3CN) δ 6 6.40 (d, *J= 16.2 Hz*, 1H), 6.34 (d, *J= 16.5 Hz*, 1H), 6.03 (d t, *J= 16.2,6.9Hz*, 1H), 5.83 (d t, *J= 16.5, 6.9Hz,* 1H), 4.62 (t, *J= 7.5Hz*, 2H), 3.41 (t, *J= 7.8Hz,* 2H), 3.11 (m, 2H), 2.62 (s, 3H), 2.41 (s, 3H), 2.32 (m, 4H), 1.54 (m, 4H), 1.32 (m, 20 H), 0.91 (t, *J=6.9Hz*, 6H); 13C NMR (75MHz, CD_3CN): δ 153.6, 153.6, 147.7, 141.8, 141.6, 136.7, 132.3, 123.0, 122.4, 58.0, 33.2, 33.0, 32.8, 31.90, 31.87, 35.29, 35.29, 29.27, 29.27, 29.16, 29.07, 28.76, 28.71, 22.65, 22.65, 20.75, 18.57, 18.02, 13.66, 13.66.

6,8-Didecyl-5,7-dimethyl-2,3-dihydro-1*H*-indolizinium (20a):

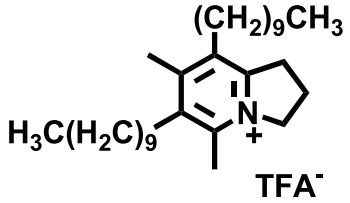

Hydrogenation was conducted on a mixture of **19a** and **18a** anibamine isomers (15 mg, 0.027 mmol) and Pd/C (2 mg, 10% by weight) in MeOH (2 mL) under 50 psi H_2 for 6 hours. The mixture was filtered through celite to remove Pd/C and concentrated to remove MeOH to give 6,8-didecyl-5,7-dimethyl-2,3-dihydro-1*H*-indolizinium (10 mg, 66% yield). ^{1}HNMR: (400 MHz, CD_3CN) δ 4.57 (m, 2H), 2.75 (m, 2H), 2.72 (m, 2H), 2,58 (s, 3H), 2.40 (s, 3H), 2.35 (m, 4H), 1.44 (m, 6H), 1.28 (m, 26 H), 0.89 (m, 6H) ^{13}CNMR: (400 MHz, CD_3CN) δ 153.81, 153.13, 146.97, 138.13, 134.76, 116.99, 57.42, 48.59, 45.53, 31.33, 29.26, 28.97, 28,94, 28.94, 28.74, 28.74, 28.68, 28.68, 28.64, 28.63, 28.07, 28.07, 27.85, 27.83, 22.09, 19.61, 16.12, 15.53, 13.08, 13.08.

C. Intermediates in synthesis of series b:

2-Bromo-4,6-dimethylnicotinonitrile (8b):

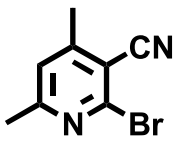

A solution of 2-hydroxy-4,6-dimethylnicotinonitrile (2.96 g, 20 mmol), TBAB (7.74 g, 24 mmol), and P_2O_5 (6.81 g, 48 mmol) in toluene (120 mL) was stirred at 90°C for 24 hours. Then ice was added to the hot reaction mixture. The organic layer was separated and the water layer was extracted with EtOAc (50 mL) twice. The combined organic layers were washed with

$NaHCO_3$ and brine, dried over Na_2SO_4, filtered and concentrated to give 3.9 g crude product. The crude product was recrystallized in EtOAc to yield 2-bromo-4,6-dimethylnicotinonitrile (3.6 g, 75% yield) as colorless needles. M.p.: 118-120°C. IR (KBr, cm^{-1}) ν_{max}: 3049, 2225, 1589. ^{1}HNMR: (300 MHz, $CDCl_3$) δ 7.12 (s, 1H), 2.60 (s, 3H), 2.57 (s, 3H). ^{13}CNMR: (300 MHz, $CDCl_3$) δ 157.46, 148.70, 137.87, 118.08, 109.91, 106.15, 19.04, 15.28.

2-(3-((4-Methoxybenzyloxy)prop-1-ynyl)-4,6-dimethylnicotinonitrile (11b):

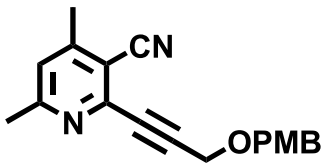

To a stirred suspension of 2-bromo-4,6-dimethylnicotinonitrile (422 mg, 2 mmol), CuI (38 mg, 0.2 mmol), $PdCl_2(PPh_3)_2$ (70 mg, 0.1 mmol), and triethylamine (12 mL) in diethyl ether (50 mL) under N_2 protection was added 1-methoxy-4-((prop-2-ynyloxy)methyl)benzene in diethyl ether (5 mL) dropwise. The reaction was allowed to stir for 40 hours. Then water (25 mL) was added. The organic layer was separated, the water layer was extracted with EtOAc (50 mL) twice. The combined organic layers were washed with brine and dried over Na_2SO_4, filtered and concentrated. The crude residue was recrystallized in EtOAc to yield 2-(3-((4-methoxybenzyloxy)prop-1-ynyl)-4,6-dimethylnicotinonitrile (485 mg, 79% yield) as colorless needles. M.p.: 80-82°C. IR (KBr, cm^{-1}) ν_{max}: 3061, 2359, 2229, 1582, 1511, 1359, 1235, 1091, 1060. ^{1}HNMR: (300 MHz, $CDCl_3$) δ 7.36 (m, 2H), 7.09 (s, 1H), 6.89 (m, 2H), 4.69 (s, 2H), 4.45 (s, 2H), 3.81 (s, 3H), 2.58 (s, 3H), 2.53 (s, 3H). ^{13}CNMR (300 MHz, $CDCl_3$) δ 156.87, 154.03,

145.80, 139.65, 124.62 (2C), 123.83, 118.29, 110.20, 108.44 (2C), 105.45, 85.84, 77.63, 65.97, 51.61, 49.88, 19.39, 14.91.

2-(3-((4-Methoxybenzyloxy)propyl)-4,6-dimethylnicotinonitrile (12b):

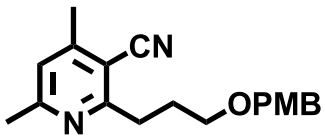

Hydrogenation was conducted on a mixture of 2-(3-((4-methoxybenzyloxy)prop-1-ynyl)-4,6-dimethylnicotinonitrile (350 mg, 1.14 mmol) and Pd/C (35 mg, 10% by weight) in MeOH (25 mL) under 46 psi H_2 for 18 hours. The mixture was filtered through celite to remove Pd/C and concentrated to remove MeOH to give 2-(3-((4-methoxybenzyloxy)propyl)-4,6-dimethylnicotinonitrile (310 mg, 87% yield) as a white powder. M.p.: 34-35°C. IR (KBr, cm^{-1}) ν_{max}: 2916, 2844, 2216, 1596, 1514, 1245, 1111, 1039. ^{1}HNMR: (300 MHz, $CDCl_3$) δ 7.27 (m, 2H), 6.94 (s, 1H), 6.87 (m, 2H), 4.45 (s, 2H), 3.80 (s, 3H), 3.55 (t, *J=6.3 Hz,* 2H), 3.06 (m, 2H), 2.53 (s, 3H), 2.47 (s, 3H), 2.09 (m, 2H) ^{13}CNMR (300 MHz, $CDCl_3$) δ 164.24, 160.93, 158.64, 150.77, 130.21, 128.80 (2C), 121.403, 116.09, 113.28 (2C), 106.35, 72.04, 68.87, 54.865, 33.58, 28.77, 24.422, 19.92.

2-(3-((4-Methoxybenzyloxy)propyl)-4,6-dimethylpyridine-3-carbaldehyde (13b):

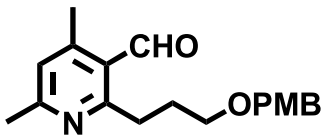

Under N_2 protection, 2-(3-((4-methoxybenzyloxy)propyl)-4,6-dimethylnicotinonitrile (250 mg, 0.80 mmol) was dissolved in anhydrous toluene (6 mL) then cooled to 0˚C. After cooling,

DIBAL-H (0.96 mL of 1.0 M solution of in toluene, 0.96 mmol) was added dropwise over 60 minutes and stirred at 0°C for 2 hours. Then 1.0 M H_2SO_4 (3.0 mL) was added and the resulting solution was allowed to warm to room temperature and stirred overnight. The organic layer was separated; the aqueous layer was extracted with EtOAc (25 mL) three times. The combined organic layers were washed with saturated aqueous $NaHCO_3$, brine, and dried over Na_2SO_4, filtered and concentrated. The crude product was purified by column chromatography on silica gel with hexane:EtOAc (3:1 v/v) as eluent to give 2-(3-((4-methoxybenzyloxy)propyl)-4,6-dimethylpyridine-3-carbaldehyde (181 mg, 71% yield) as a colorless oil. IR (KBr, cm^{-1}) ν_{max}: 2924, 2852, 1688, 1588, 1247. ^{1}HNMR: (300 MHz, $CDCl_3$) δ 10.56 (s, 1H), 7.25 (m, 2H), 6.90 (s, 1H), 6.87 (m, 2H), 4.42 (s, 3H), 3.80 (s, 3H), 3.50 (t, *J=6.3Hz,* 2H), 3.18 (m, 2H), 2.55 (s, 3H), 2.51 (s, 3H), 2.01 (m, 2H). ^{13}CNMR (300 MHz, $CDCl_3$) δ 192.65, 164.62, 162.12, 159.34, 150.12, 130.80, 129.5 (2C), 126.12, 124.86, 113.97 (2C), 72.74, 69.38, 55.45, 34.89, 29.28, 24.924, 20.92.

2-(3-((4-Methoxybenzyloxy)propyl)-4,6-dimethyl-3-(*Z*)-dec-1-enyl)pyridine (15b) and 2-(3-((4-Methoxybenzyloxy)propyl)-4,6-dimethyl-3-(*E*)-dec-1-enyl)pyridine:

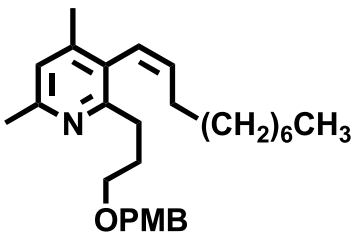

Wittig: Under N_2 protection, non-1-yl triphenylphosphonium bromide (844 mg, 1.8 mmol) in anhydrous toluene (10 mL) and LHMDS (1.6 mL of a 1.0 M solution in THF, 1.6 mmol) were dissolved producing a bright red color. The solution was cooled to -70°C then 2-(3-((4-

methoxybenzyloxy)propyl)-4,6-dimethylpyridine-3-carbaldehyde (280 mg, 0.9 mmol) in anhydrous toluene (5 mL) was added dropwise over 20 minutes diluting the dark red color of the reaction mixture to yellow. The reaction was stirred at -70°C for 15 minutes then warmed to room temperature. After 2 hours at room temperature, the reaction was quenched with saturated aqueous NH_4Cl (15 mL) producing a colorless solution. The organic layer was separated, the aqueous layer was extracted with CH_2Cl_2 (15 mL) three times. The combined organic layers were washed with saturated aqueous $NaHCO_3$, brine, dried over Na_2SO_4, filtered and concentrated. The crude product was purified by column chromatography on silica gel with hexane:EtOAc (8:1 v/v) as eluent to give a mixture of 2-(3-((4-methoxybenzyloxy)propyl)-4,6-dimethyl-3-(*Z*)-dec-1-enyl)pyridine and 2-(3-((4-methoxybenzyloxy)propyl)-4,6-dimethyl-3-(*E*)-dec-1-enyl)pyridine (300 mg, 79% yield) as a colorless oil. ^{1}HNMR indicated 1:1 *E:Z* ratio. **Schlosser Modification to the Wittig Reaction:** Under N_2 protection, non-1-yl triphenylphosphonium bromide (235 mg, 0.5 mmol) and LiBr (117 mg, 1.35 mmol) were suspended in a THF:toluene solution (10 mL, 2:3 v/v). PhLi (0.38 mL of a 1.8 M solution in diisopropyl ether, 0.675 mmol) was added dropwise producing a bright red color. The resulting solution was cooled to -70°C. 2-(3-((4-Methoxybenzyloxy)propyl)-4,6-dimethylpyridine-3-carbaldehyde (140 mg, 0.45 mmol) in toluene (1 mL) was added dropwise to the solution resulting in a lighter solution. **Batch 2:** After 30 minutes at -70°C, 4 mL of the reaction solution was removed by syringe in placed into a cold, dry flask (flask 2) while the other approximately two thirds of the reaction continued to stir at -70°C. A solution of PhLi and LiBr (0.11 mL of a 1.8 M PhLi solution in diisopropyl ether, 0.20 mmol and 17 mg of LiBr, 0.20 mmol) in THF (1.0 mL) was added to flask 2, containing the smaller portion of the reaction mixture. After 30 minutes stirring at -70°C, the reaction mixture

in flask 2 was warmed to -25°C and 1 M ethereal HCl (0.65 mL, 1 M solution in diethyl ether, 0.65 mmol) was added turning the reaction mixture to a colorless solution. After a few minutes, t-BuOK (78 mg, 0.70 mmol) was added to the reaction. The reaction was allowed to warm to room temperature and stirred for two hours. Then water (7 mL) was added. The organic layer was separated. The aqueous layer was extracted with EtOAc (20 mL) two times. The combined organic layers were washed with saturated aqueous $NaHCO_3$, brine, and dried over Na_2SO_4, filtered and concentrated. The 100 mg crude product was purified by column chromatography on silica gel with hexane:EtOAc (8:1 v/v) as eluent to give isomers **15a** (18 mg, 30% yield) as a colorless oil. ^{1}HNMR indicated 1:2 *E:Z* ratio. **Batch 1:** The first reaction flask was allowed to warm slowly to 0°C then a solution of PhLi and LiBr (0.22 mL of a 1.8 M PhLi solution in diisopropyl ether, 0.40 mmol and 38 mg of LiBr, 0.40 mmol) in THF (2.0 mL) was added, containing the smaller portion of the reaction mixture. After 30 minutes stirring at 0°C, 1 M ethereal HCl (1.3 mL, 1 M solution in diethyl ether, 1.3 mmol) was added turning the reaction mixture to a colorless solution. After a few minutes, t-BuOK (156 mg, 1.4 mmol) was added to the reaction. The reaction was allowed to warm to room temperature and stirred for two hours. Then water (14 mL) was added. The organic layer was separated. The aqueous layer was extracted with EtOAc (40 mL) two times. The combined organic layers were washed with saturated aqueous $NaHCO_3$, brine, and dried over Na_2SO_4, filtered and concentrated. The 200 mg crude product was purified by column chromatography on silica gel with hexane:EtOAc (8:1 v/v) as eluent to give isomers **15a** (30 mg, 25% yield) as a colorless oil. ^{1}HNMR indicated 1:3 *E:Z* ratio. **Grignard Reaction:** Pieces of Mg ribbon and a small amount of iodine were put in a 2 neck flask with a condenser and degassed and filled with N_2 three times. Anhydrous THF (1 mL)

was added. 1-bromononane (0.32 mL, 1.69 mmol) was added slowly, the reaction was heated with a hot gun, then with an oil bath to maintain a slight reflux. An additional 0.1 mL 1-bromononane was added and the reaction refluxed for two hours. After two hours the reaction mixture looked clear and there was no visible Mg. It was cooled to -70°C and 2-(3-((4-Methoxybenzyloxy)propyl)-4,6-dimethylpyridine-3-carbaldehyde (40 mg, **X** mmol) in THF (0.3 mL) was added dropwise. The reaction mixture was stirred for an hour at -70°C, one hour at 0°C, one hour at room temperature and overnight at reflux. TLC monitoring showed no product had formed. In the morning, the reaction was quenched with 10 mL NH_4Cl then the layers were disposed. The starting material was not recovered. **2-(3-((4-Methoxybenzyloxy)propyl)-4,6-dimethyl-3-(*Z*)-dec-1-enyl)pyridine (15b):** ^{1}HNMR (400MHz, $CDCl_3$) δ 7.25 (m, 2H), 6.86 (m, 2H), 6.82 (s, 1H), 6.24 (d, *J*= 11.1 Hz, 1H), 5.78 (d of t, *J*= 11.1 Hz, 7.3 Hz, 1H), 4.42 (s, 2H), 3.80 (s, 3H), 3.48 (t, *J*= 6.6 Hz, 2H), 2.75 (m, 2H), 2.46 (s, 3H), 2.14 (s, 3H), 1.93 (m, 2H), 1.77 (m, 2H), 1.21 (m, 12 H), 0.86 (m, 3H). ^{13}CNMR (400MHz, $CDCl_3$) δ 159.06, 158.52, 155.43, 145.64, 134.89, 130.96, 129.10 (2C), 128.74, 124.81, 121.95, 113.71 (2C), 72.27, 70.01, 55.28, 32.58, 31.85, 29.71, 29.42, 29.38, 29.22, 28.97, 28.16, 24.08, 22.65, 19.87, 14.09. **2-(3-((4-Methoxybenzyloxy)propyl)-4,6-dimethyl-3-(*E*)-dec-1-enyl)pyridine** ^{1}HNMR (400MHz, $CDCl_3$) δ 7.24 (m, 2H), 6.86 (m, 2H), 6.80 (s, 1H), 6.28 (d, *J*= 14.2 Hz, 1H), 5.65 (d of t, *J*= 14.2 Hz, 6.9 Hz, 1H), 4.42 (s, 2H), 3.80 (s, 3H), 3.49 (m, 2H), 2.84 (m, 2H), 2.44 (s, 3H), 2.22 (s, 3H), 1.98 (m, 2H), 1.77 (m, 2H), 1.45 (m, 2H), 1.21 (m, 10 H), 0.85 (m, 3H). ^{13}CNMR (400MHz, $CDCl_3$) δ 159.06, 158.51, 154.94, 145.34, 137.15, 130.95, 130.01, 129.09 (2C), 125.07, 122.42, 113.71 (2C), 72.32, 69.97, 55.28, 33.41, 32.58, 31.91, 29.60, 29.48, 29.37, 29.33, 29.28, 24.03, 22.69, 20.47, 14.11.

3-(4,6-Dimethyl-3-((*Z*)-dec-1-enyl)pyridin-2-yl)pronan-1-ol (16b) and 3-(4,6-dimethyl-3-((*E*)-dec-1-enyl)pyridin-2-yl)pronan-1-ol:

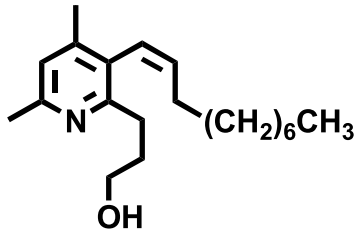

Two equal batches of and isomeric mixture of 2-(3-((4-methoxybenzyloxy)propyl)-4,6-dimethyl-3-(*Z*)-dec-1-enyl)pyridine and 2-(3-((4-methoxybenzyloxy)propyl)-4,6-dimethyl-3-(*E*)-dec-1-enyl)pyridine (175 mg, 0.41mmol) were refluxed in EtOH (9 mL) and 1N HCl (4.5 mL) for 3 hours. Each solution was concentrated to remove EtOH and extracted with CH_2Cl_2 (15 mL) three times. The combined organic layers of both reactions were washed with brine, dried over Na_2SO_4, filtered, and concentrated to give a crude oil. The combined crude product was purified by column chromatography on silica gel with CH_2Cl_2/MeOH (50:1, v/v) as eluent to give a mixture of 3-(4,6-dimethyl-3-((*Z*)-dec-1-enyl)pyridin-2-yl)pronan-1-ol and 3-(4,6-dimethyl-3-((*E*)-dec-1-enyl)pyridin-2-yl)pronan-1-ol (210 mg, 84% yield) as a yellow oil. The isomers were separated on prep arative TLC plates with Hexane/EtOAc (2:1, v/v) as eluent developed 4 times to give as the top band 3-(4,6-dimethyl-3-((*Z*)-dec-1-enyl)pyridin-2-yl)pronan-1-ol (50 mg, 100% purity) and as the lower band 3-(4,6-dimethyl-3-((*E*)-dec-1-enyl)pyridin-2-yl)pronan-1-ol (60 mg, 80% purity). **3-(4,6-Dimethyl-3-((*Z*)-dec-1-enyl)pyridin-2-yl)pronan-1-ol (16b):** ^{1}HNMR (400MHz, $CDCl_3$) δ 6.85 (s, 1H), 6.22 (d, *J=11.2 Hz*, 1H), 5.83 (d of t, *J=11.2, 7.5 Hz,* 1H), 3.69 (m, 2H), 2.95 (m, 2H), 2.51 (s, 3H), 2.18 (s, 3H) 1.88 (m, 2H), 1.77 (m, 2H), 1.20 (m, 12 H), 0.86 (m*,* 3H). ^{13}CNMR (400MHz, $CDCl_3$) δ 157.79, 154.79, 146.56, 135.28, 129.07, 124.57, 122.19, 62.79, 33.35, 32.84, 30.28, 29.40, 29.33, 29.20, 28.95, 28.81, 23.48, 22.64, 19.97, 14.08. **3-(4,6-Dimethyl-3-((*E*)-dec-1-enyl)pyridin-2-yl)pronan-1-ol:** ^{1}HNMR (400MHz,

$CDCl_3$) δ 6.83 (s, 1H), 6.26 (d, *J=16.0 Hz*, 1H), 5.65 (d of t, *J=16.0, 6.9 Hz,* 1H), 3.68 (m, 2H), 3.00 (m, 2H), 2.91 (m, 2H), 2.43 (s, 3H), 2.23 (s, 3H) 1.91 (m, 2H), 1.76 (m, 2H), 1.45 (m, 2H), 1.21 (m, 8H), 0.867(m, 3H). ^{13}CNMR (400MHz, $CDCl_3$) δ 157.76, 154.30, 146.22, 137.58, 130.43, 124.86, 122.58, 62.56, 33.39, 32.89, 30.68, 29.45, 29.32, 29.20, 28.95, 28.81, 23.48, 22.67, 20.48, 14.10.

D. Final products in series b

8-Dec-1-(*Z*)-enyl-5,7-dimethyl-2,3-dihydro-1H-indolizinium chloride (1b):

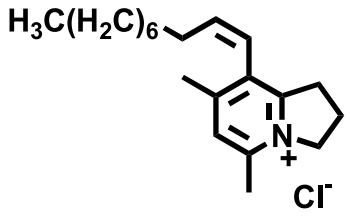

MsCl (37 mg, 0.33 mmol) in CH_2Cl_2 (1.0 mL) was added to an ice cold solution of 3-(4,6-dimethyl-3-((*Z*)-dec-1-enyl)pyridin-2-yl)pronan-1-ol (50 mg, 0.165 mmol), TEA (50 mg, 0.50 mmol) in CH_2Cl_2 (3.0 mL). The reaction was warmed to room temperature over 60 minutes. The mixture was diluted with CH_2Cl_2 (20 mL), washed with brine, dried over Na_2SO_4, filtered and concentrated to give a crude product (60 mg). The crude product was separated by column chromatography on silica gel with CH_2Cl_2/MeOH (50:3, v/v) as eluent to give 8-dec-1-(*Z*)-enyl-5,7-dimethyl-2,3-dihydro-1H-indazolinium chloride (40 mg) as a colorless oil in 70 % yield. ^{1}HNMR: (400 MHz, CD_3CN) δ 7.55 (s, 1H), 6.24 (d, *J*=10.8 Hz, 1H), 6.03 (d of t, *J*=10.8 Hz, 7.6 Hz, 1H), 4.61 (m, 2H), 3.22 (m, 2H), 2.66 (s, 3H), 2.38 (m, 2H), 2.31 (s, 3H), 1.82 (m, 2H), 1.34 (m, 2H), 1.21 (m, 10 H), 0.87 (m, 3H). *Z* ^{13}CNMR: (400 MHz, CD_3CN) δ 156.50,

156.04, 149.76, 138.56, 131.55, 127.03, 120.43, 56.53, 31.84, 31.46, 28.90, 28.81, 28.79, 28.67, 28.31, 22.24, 20.42, 19.34, 18.70, 13.25. MS m/z: 287.13.

8-dec-1-(*E)*-enyl-5,7-dimethyl-2,3-dihydro-1H-indolizinium chloride (17b) and isomer (16b):

MsCl (45 mg, 0.4 mmol) in CH_2Cl_2 (1.0 mL) was added to an ice cold solution of 3-(4,6-dimethyl-3-((*E*)-dec-1-enyl)pyridin-2-yl)pronan-1-ol (60 mg, 0.2 mmol), TEA (60 mg, 0.60 mmol) in CH_2Cl_2 (3 mL). The reaction was warmed to room temperature over 60 minutes. The mixture was diluted with CH_2Cl_2 (20 mL), washed with brine, dried over Na_2SO_4, filtered and concentrated to give a crude product (80 mg). The crude product was separated by column chromatography on silica gel with CH_2Cl_2/MeOH (50:3, v/v) as eluent to give 8-dec-1-(*E)*-enyl-5,7-dimethyl-2,3-dihydro-1H-indazolinium chloride

50 mg, 83% yield) as a colorless oil. ^{1}HNMR: (400 MHz, CD_3CN) δ 7.52 (s, 1H), 6.37 (d, *J*=16.4 Hz, 1H), 6.10 (d of t, *J*=16.4 Hz, 6.8 Hz, 1H), 4.63 (m, 2H), 3.42 (m, 2H), 2.65 (s, 3H), 2.47 (m, 3H), 2.38 (m, 2H), 2.28 (m, 2H), 1.52 (m, 2H), 1.28 (m, 10 H), 0.88 (m, 3H). ^{13}CNMR: (400 MHz, CD_3CN) δ 155.31, 155.00, 148.84, 141.19, 131.70, 127.28, 121.266, 56.25, 32.71, 32.20. 31.28, 28.76, 28.66, 28.49, 28.21, 22.05, 20.43, 19.53, 18.54, 13.06. MS m/z: 286.02.

8-Decyl-5,7-dimethyl-2,3-dihydro-1*H*-indolizinium (20b)

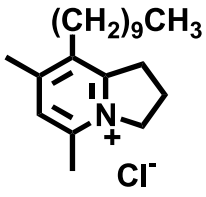

Hydrogenation was conducted on a mixture of isomers (30 mg, xx mmol) and Pd/C (3 mg, 10% by weight) in MeOH (2 mL) under 50 psi H_2 for 12 hours. The mixture was filtered through celite to remove Pd/C and concentrated to remove MeOH to give 20 mg (67% yield) 8-decyl-5,7-dimethyl-2,3-dihydro-1*H*-indolizinium. ^{1}HNMR (400MHz, CD_3CN) δ 7.43 (s, 1H), 4.54 (m, 2H), 3.39 (m, 2H), 2.69 (m, 2H), 2.60 (s, 3H), 2.48 (s, 3H), 2.41 (m 2H), 1.49 (m, 2H), 1.40 (m, 2H) 1.29 (m, 12 H) 0.89 (m, 3H). ^{13}CNMR (400MHz, CD_3CN) δ 155.96, 154.51, 149.76, 134.98, 127.40, 56.12, 31.30, 30.76, 28.97, 28.91, 28.71, 28.66, 28.50, 27.55, 22.55, 22.07, 20.03, 18.41, 18.33, 13.06. MS m/z: 289.2.

E. Intermediates in synthesis of series c:

3-Morpholinobut-2-enenitrile (7):

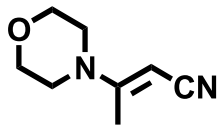

A neat mixture of morpholine (435 mg, 5 mmol), triethyl orthoacetate (810 mg, 5 mmol), and cyanoacetic acid (535 mg, 5 mmol) was refluxed for 4 hours. The solution was concentrated to remove ethanol and the crude residue was diluted with CH_2Cl_2 (3 mL), washed with saturated aqueous $NaHCO_3$ (2 mL), dried over Na_2SO_4, filtered and concentrated to give 675 mg crude red oil. The crude product was purified by column chromatography on silica gel with a hexane:ethyl acetate solvent system (2:1 v/v) to give 3-morpholinobut-2-enenitrile (300 mg, 40% yield) as a colorless solid. M.p.: 38-40°C. IR (KBr, cm^{-1}) ν_{max}: 2194, 1585, 1439, 1380, 1250, 1123, 1005. ^{1}HNMR (300MHz, $CDCl_3$) δ 3.98 (s, 1H), 3.72 (m, 4H), 3.16 (m, 4H), 2.16 (s, 3H). ^{13}CNMR (300MHz, $CDCl_3$) δ 161.62, 121.20, 65.63 (2C), 65.27, 46.02 (2C), 17.97.

6-Hydroxy-2,4-dimethylnicotinonitrile (2c)

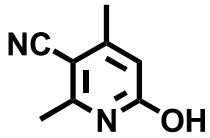

3-Morpholinobut-2-enenitrile (200 mg, 1.3 mmol) was refluxed in acetic acid (1 mL) for 7 hours. After cooling to room temperature, the reaction was concentrated to remove acetic acid. The crude residue was purified by column chromatography on silica gel with CH_2Cl_2:MeOH (30:1 v/v) as eluent to yield 6-hydroxy-2,4-dimethylnicotinonitrile (75 mg, 77% yield) as a white powder. M.p.: decomposed at 247-250°C. IR (KBr, cm^{-1}) ν_{max}: 2916, 2205, 1648. ^{1}HNMR (300MHz, DMSO) δ 12.2 (br, 1H), 6.16 (s, 1H), 2.38 (s, 3H), 2.20 (s, 3H). ^{13}CNMR (300MHz, DMSO) δ 162.75, 155.87, 151.14, 117.31, 116.79, 91.59, 20.80, 19.18.

6-Bromo-2,4-dimethylnicotinonitrile (8c):

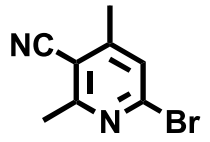

A solution of 6-hydroxy-2,4-dimethylnicotinonitrile (74 mg, 0.5 mmol), TBAB (193 mg,0.6 mmol) and P_2O_5 (177 mg, 1.25 mmol) was heated in toluene (25 mL) under N_2 protection for 1.5 hours. Ice was added to the hot reaction mixture and the organic layer was separated. The aqueous layer was extracted with EtOAc (25 mL) twice. The combined organic layers were washed with saturated aqueous $NaHCO_3$, dried over Na_2SO_4, filtered and concentrated to give 96 mg crude product. The crude product was purified by column chromatography on Al_2O_3 with hexane:ethyl acetate (20:1 v/v) solvent system to give 6-bromo-2,4-dimethylnicotinonitrile (75

mg, 71% yield) as a white solid. M.p.: 67-69°C. IR (KBr, cm^{-1}) ν_{max}: 3050, 2359, 2341, 2221, 1571. ^{1}HNMR (300MHz, DMSO) δ 7.72 (s, 1H), 2.64 (s, 3H), 2.46 (s, 3H). ^{13}CNMR (300MHz, DMSO): δ 163.02, 154.97, 144.90, 127.12, 166.36, 109.82, 23.82, 20.33.

6-(3-((4-Methoxybenzyloxy)prop-1-ynyl)-2,4-dimethylnicotinonitrile (11c):

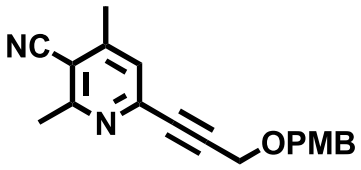

To a stirred suspension of 6-bromo-2,4-dimethylnicotinonitrile (40 mg, 0.18 mmol), CuI, (3 mg, 0.018 mmol), $PdCl_2(PPh_3)_2$ (6 mg, 0.009 mmol), and triethylamine (0.75 mL) in diethyl ether (2.5 mL) was added 1-methoxy-4-((prop-2-ynyloxy)methyl)benzene in diethyl ether (2.5 mL) dropwise under N_2 protection. The reaction was stirred under N_2 protection for 2.5 hours. Then water (5 mL) was added. The organic layer was separated, the water layer was extracted twice with EtOAc (10 mL). The combined organic layers were washed with brine and dried over Na_2SO_4, filtered and concentrated. The 50 mg of crude residue was purified by column chromotagraphy on silica gel with a Hexane/EtOAc solvent system (20:3 v:v) to give 6-(3-((4-methoxybenzyloxy)prop-1-ynyl)-2,4-dimethylnicotinonitrile (35 mg , 63% yield). M.p.: 106-107°C. IR (KBr, cm^{-1}) ν_{max}: 3051, 2999, 2906, 2215, 1606, 1575, 1249, 1179, 1029. ^{1}HNMR (300MHz, $CDCl_3$) δ 7.3 (m, 2H) 7.24 (s, 1H) 6.9 (m, 2H), 4.6 (s, 2H), 4.4 (s, 2H), 3.8 (s, 3H), 2.75 (s, 3H), 2.52 (s, 3H). ^{13}C NMR (300MHz, $CDCl_3$) δ 162.24, 159.71, 151.87, 144.59, 130.04 (2C), 129.37, 125.56, 116.146, 114.100 (2C), 109.49, 89.23, 85.05, 72.00, 57.55, 55.52, 24.09, 20.55.

6-(3-((4-Methoxybenzyloxy)propyl)-2,4-dimethylnicotinonitrile (12c)

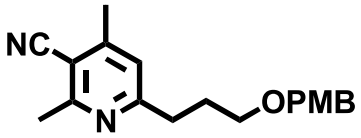

Hydrogenation was conducted on a mixture of 6-(3-((4-methoxybenzyloxy)prop-1-ynyl)-2,4-dimethylnicotinonitrile (230 mg, 0.33 mmol) and Pd/C (23 mg, 10% by weight) in MeOH (30 mL) under 50 psi H_2 for 4.5 hours. The mixture was filtered through celite to remove Pd/C and concentrated to remove MeOH to give 6-(3-((4-methoxybenzyloxy)propyl)-2,4-dimethylnicotinonitrile (200 mg, 87% yield) as a colorless oil. IR (KBr, cm^{-1}) ν_{max}: 3051, 2921, 2849, 1617, 1513, 1460, 1376, 1250. ^{1}HNMR (300MHz, $CDCl_3$) δ 7.24 (m, 2H), 6.90 (s, 1H), 6.87 (m, 2H), 4.42 (s, 2H), 3.81 (s, 3H) 3.47 (t, *J*=6.3 Hz, 2H), 2.84 (m, 2H), 2.71 (s, 3H), 2.46 (s, 3H). 2.00 (m, 2H). ^{13}C NMR (300MHz, $CDCl_3$) δ 164.91, 161.49, 159.37, 151.42, 130.71, 129.49 (2C), 121.54, 116.86, 113.95 (2C), 107.43, 72.77, 69.18, 55.48, 35.35, 29.60, 24.03, 20.56.

6-(3-((4-Methoxybenzyloxy)propyl)-2,4-dimethylpyridine-3-carbaldehyde (13c):

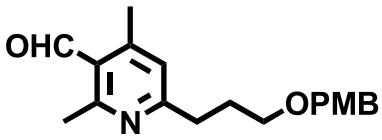

Under N_2 protection, 6-(3-((4-methoxybenzyloxy)propyl)-2,4-dimethylnicotinonitrile (180 mg, 0.58 mmol) was dissolved in anhydrous toluene (6 mL) then cooled to 0°C. After cooling, DIBAL-H (0.64 mL of 1.0 M solution of in toluene, 0.64 mmol) was added dropwise over 45 minutes and stirred at 0°C for 1.5 hours. Then 1.0 M H_2SO_4 (4 mL) was added and the resulting solution was allowed to warm to room temperature and stirred 4 hours. The organic layer was

separated; the aqueous layer was extracted with EtOAc (15 mL) three times. The combined organic layers were washed with saturated aqueous $NaHCO_3$, brine, dried over Na_2SO_4, filtered and concentrated to give 150 mg crude product. The crude product was purified by column chromatography on silica gel with hexane:EtOAc (3:1 v/v) as eluent to give 6-(3-((4-methoxybenzyloxy)propyl)-2,4-dimethylpyridine-3-carbaldehyde (135mg, 75% yield) as a colorless oil. IR (KBr, cm^{-1}) ν_{max}: 2927, 2844, 1690, 1586, 1240, 1101, 1045. ^{1}HNMR (300MHz, $CDCl_3$) δ 10.58 (s, 1H), 7.26 (m, 2H), 6.88 (s, 1H), 6.87 (m, 2H), 4.44 (s, 2H), 3.81 (s, 3H), 3.49 (t,*J*=6.3 Hz, 2H), 2.88 (m, 2H), 2.79 (s, 3H), 2.56 (s, 3H), 2.02 (m, 2H). ^{13}C NMR (300MHz, $CDCl_3$) δ 192.53, 165.49, 160.96, 159.36, 150.33, 130.77, 129.52 (2C), 126.37, 124.34, 113.96 (2C), 72.79, 69.35, 55.51, 35.27, 29.67, 23.40, 20.64.

2-(3-((4-Methoxybenzyloxy)propyl)-4,6-dimethyl-5-(*Z*)-dec-1-enyl)pyridine (15c)

and 2-(3-((4-methoxybenzyloxy)propyl)-4,6-dimethyl-5-(*E*)-dec-1-enyl)pyridine:

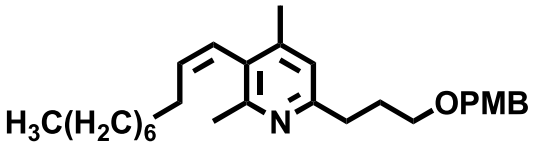

Wittig Reaction: Under N_2 protection, non-1-yl triphenylphosphonium bromide (300 mg, 0.63 mmol) in toluene (3 mL) and LHMDS (0.57 mL of a 1.0 M solution of in THF, 0.57 mmol) were dissolved producing a bright red color. The solution was cooled to -70˚C using a dry-ice/acetone bath then 6-(3-((4-methoxybenzyloxy)propyl)-2,4-dimethylpyridine-3-carbaldehyde (100 mg, 0.32 mmol) in toluene (2 mL) was added dropwise over 20 minutes. The reaction was stirred at -70°C for 15 minutes then warmed to room temperature. After stirring for an hour at room temperature, the reaction was quenched with saturated aqueous NH_4Cl (10 mL) producing a

colorless solution. The organic layer was separated, the aqueous layer was extracted with CH_2Cl_2 (15 mL) three times. The combined organic layers were washed with saturated aqueous $NaHCO_3$, brine, dried over Na_2SO_4, filtered and concentrated to give 300 mg crude product. The crude product was purified by column chromatography on silica gel with hexane:EtOAc (10:1 v/v) as eluent to give isomers 2-(3-((4-methoxybenzyloxy)propyl)-4,6-dimethyl-5-(*Z*)-dec-1-enyl)pyridine and 2-(3-((4-methoxybenzyloxy)propyl)-4,6-dimethyl-5-(*E*)-dec-1-enyl)pyridine: (90 mg, 67% yield) as a colorless oil. ^{1}HNMR indicated 3:5 *E:Z* ratio. **Schlosser Modification to the Wittig reaction:** Under N_2 protection, to a solution of non-1-yl triphenylphosphonium bromide (223 mg, 0.47 mmol) and LiBr (83 mg, 0.95 mmol) in an anhydrous toluene/THF solution (8 mL total, 3:1 v/v) was added PhLi (0.26 mL of a 1.8 M solution in diisopropyl ether, 0.47 mmol) producing an orange solution. An additional equivalent of PhLi (0.26 mL of a 1.8 M solution in diisopropyl ether, 0.47 mmol) was added, resulting in a dark red solution. The resulting solution was cooled to -70°C. 6-(3-((4-Methoxybenzyloxy)propyl)-2,4-dimethylpyridine-3-carbaldehyde (135 mg, 0.43 mmol) was dissolved in toluene (1 mL) and added dropwise to the solution resulting in an orange solution. After 1 hour, the reaction was slowly warmed to 0°C and starting material disappeared from TLC plate. Then a mixture of PhLi and LiBr (0.47 mmol) in THF (6 mL) was added returning the color to dark orange. The reaction was stirred at 0°C for an hour, then 1 M ethereal HCl (1.75 mL, 1 M solution in diethyl ether, 1.75 mmol), followed by addition of t-BuOK (192 mg, 2.15 mmol) in Et_2O (3 mL) was added to the reaction. The reaction mixture was allowed to warm to room temperature and stirred overnight. Then water (10 mL) was added. The organic layer was separated. The aqueous layer was extracted with EtOAc (30 mL) three times. The combined organic layers were washed with

saturated aqueous $NaHCO_3$, brine, dried over Na_2SO_4, filtered and concentrated. The crude product was purified by column chromatography on silica gel with hexane:EtOAc (8:1 v/v) as eluent to give isomers 2-(3-((4-methoxybenzyloxy)propyl)-4,6-dimethyl-5-(*Z*)-dec-1-enyl)pyridine and 2-(3-((4-methoxybenzyloxy)propyl)-4,6-dimethyl-5-(*E*)-dec-1-enyl)pyridine (140 mg, 77% yield) as a colorless oil. ^{1}HNMR indicated 1:2 *E:Z* ratio. **2-(3-((4-methoxybenzyloxy)propyl)-4,6-dimethyl-5-(*Z*)-dec-1-enyl)pyridine (15c):** ^{1}HNMR (400MHz, $CDCl_3$) δ 7.28 (m, 2H), 6.87 (m, 2H), 6.80 (s, 1H), 6.22 (d, *J*= 11.2 Hz, 1H), 5.78 (d of t, *J*= 11.2 Hz, 7.3 Hz, 1H), 4.45 (s, 2H), 3.80 (s, 3H), 3.51 (m, 2H), 2.77 (m, 2H), 2.39 (s, 3H), 2.13 (s, 3H), 2.01 (m, 2H), 1.77 (m, 2H), 1.21 (m, 12 H), 0.85 (m, 3H). ^{13}CNMR (400MHz, $CDCl_3$) δ 159.12, 158.70, 155.32, 145.55, 134.73, 130.82, 129.39, 129.23 (2C), 125.19, 121.25, 113.76 (2C), 72.50, 69.57, 55.28, 34.57, 31.84, 29.98, 29.71, 29.38, 29.22, 28.96, 28.74, 23.11, 22.64, 19.85, 14.09. **2-(3-((4-methoxybenzyloxy)propyl)-4,6-dimethyl-5-(*E*)-dec-1-enyl)pyridine:** ^{1}HNMR (400MHz, $CDCl_3$) δ 7.28 (m, 2H), 6.87 (m, 2H), 6.80 (s, 1H), 6.24 (d, *J*= 16.1 Hz, 1H), 5.78 (d of t, *J*= 16.1 Hz, 6.8 Hz, 1H), 4.44 (s, 2H), 3.80 (s, 3H), 3.49 (m, 2H), 2.77 (m, 2H), 2.48 (s, 3H), 2.23 (s, 3H), 2.01 (m, 2H), 1.47 (m, 2H), 1.25 (m, 12 H), 0.85 (m, 3H). *E* ^{13}CNMR (400MHz, $CDCl_3$) δ 159.11, 158.70, 155.31, 145.55, 133.12, 130.81 129.39, 129.23 (2C), 125.41, 121.87, 113.76 (2C), 72.50, 69.51, 55.28, 33.44, 31.89, 29.99, 29.71, 29.45, 29.31, 29.18, 28.96, 28.74 23.63, 20.39, 14.11.

3-(4,6-Dimethyl-5-((*Z*)-dec-1-enyl)pyridin-2-yl)pronan-1-ol (16c) and 3-(4,6-dimethyl-5-((*E*)-dec-1-enyl)pyridin-2-yl)pronan-1-ol

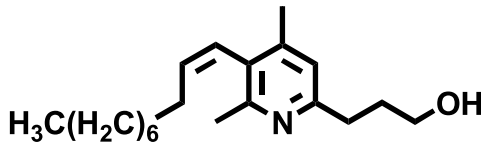

A mixture of isomers 2-(3-((4-methoxybenzyloxy)propyl)-4,6-dimethyl-5-(*Z*)-dec-1-enyl)pyridine and 2-(3-((4-methoxybenzyloxy)propyl)-4,6-dimethyl-5-(*E*)-dec-1-enyl)pyridine(140mg, 0.33 mmol) was refluxed in EtOH (6 mL) and 1N HCl (3 mL) for 3.5 hours. After cooling, the solution was concentrated to remove EtOH. The aqueous layer was extracted with CH_2Cl_2 (30 mL) three times. The combined organic layers were washed with brine, dried over Na_2SO_4, filtered and concentrated to give 180 mg crude product. The crude product was purified by column chromatography on silica gel with CH_2Cl_2:MeOH (25:1 v/v) as eluent to give isomers 3-(4,6-dimethyl-5-((*Z*)-dec-1-enyl)pyridin-2-yl)pronan-1-ol and 3-(4,6-dimethyl-5-((*E*)-dec-1-enyl)pyridin-2-yl)pronan-1-ol (76 mg, 76% yield) as a colorless oil. IR (KBr, cm^{-1}) ν_{max}: 3443, 2924, 2853, 1593, 1461, 1067. (isomeric mixture) (**16c**) *Z* ^{13}CNMR (300MHz, $CDCl_3$) δ 157.52, 154.39, 146.07, 134.67, 129.24, 124.23, 121.33, 62.46, 35.34, 33.01, 31.42, 30.64, 28.95, 28.85, 28.78, 28.51, 22.23, 19.49, 13.67 ^{13}CNMR (300MHz, $CDCl_3$) δ 156.96, 154.30, 145.57, 137.10, 130.26, 124.51, 121.40, 62.46, 35.34, 33.01, 31.42, 30.64, 29.28, 28.85, 28.34, 22.78, 22.23, 20.02, 13.67

F. Final products in series c:

6-Dec-1-(*Z*)-enyl-5,7-dimethyl-2,3-dihydro-1H-indolizinium chloride (1c) and 6-dec-1-(*E*)-enyl-5,7-dimethyl-2,3-dihydro-1H-indolizinium chloride (17c):

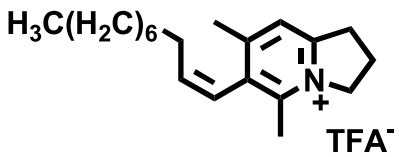

To a mixture of 3-(4,6-dimethyl-5-((*Z*)-dec-1-enyl)pyridin-2-yl)pronan-1-ol and 3-(4,6-dimethyl-5-((*E*)-dec-1-enyl)pyridin-2-yl)pronan-1-ol (75 mg, 0.25 mmol) and triethyl amine (75 mg, 0.75 mmol) in CH_2Cl_2 (4 mL) at 0°C was added MsCl (57 mg, 0.50 mmol) in CH_2Cl_2 (2.0 mL). The mixture was allowed to warm to room temperature over 1 hour, diluted with CH_2Cl_2 (20 mL), washed with brine, dried over Na_2SO_4, filtered and concentrated to give the crude product (150 mg). The crude product was purified by column chromatography on silica gel with CH_2Cl_2:MeOH (15:1 v/v) as eluent to give isomers 68-dec-1-(*Z*)-enyl-5,7-dimethyl-2,3-dihydro-1H-indolizinium chloride and 6-dec-1-(*E*)-enyl-5,7-dimethyl-2,3-dihydro-1H-indolizinium chloride (60 mg, 75% yield) as a yellow oil. Separation of isomers was attempted by both HPLC and prep TLC without success. **6-Dec-1-(*Z*)-enyl-5,7-dimethyl-2,3-dihydro-1H-indolizinium chloride/trifluroacetate (1c):** ^{1}HNMR (400MHz, CD_3CN) δ 7.61 (s, 1H), 6.26 (d, *J*=11.3, 1H), 6.07 (d of t, *J*=11.3, 7.4 1H), 4.62 (m, 2H), 3.43 (m, 2H), 2.55 (s 3H), 2.41 (m, 2H), 2.39 (s, 3H), 1.78 (m, 2H), 1.22 (m, 12H) 0.89 (m, 3H). ^{13}CNMR (400MHz, CD_3CN) δ 156.29, 155.64, 141.45, 138.22, 134.47, 121.72, 121.24, 56.82, 31.56, 31.27, 28.71, 28.62, 28.59, 28.22, 27.94, 22.01, 20.25, 17.04, 13.04. MS m/z: 286.21. **6-Dec-1-(*E*)-enyl-5,7-dimethyl-2,3-dihydro-1H-indolizinium chloride /trifluroacetate (17c):** ^{1}HNMR (400MHz, CD_3CN) δ 7.58 (s, 1H), 6.32 (d, *J*=16.3, 1H), 5.87 (d of t, *J*=16.3, 6.9 1H) 4.62 (m, 2H), 3.43 (m, 2H), 2.63 (s,

3H), 2.45 (s, 3H), 2.41 (m, 2H) 2.3 (m, 2H), 1.51 (m, 2H), 1.22 (m, 10H) 0.89 (m, 3H). ^{13}CNMR (400MHz, CD_3CN) δ 155.76, 155.02, 149.28, 138.22, 135.66, 121.92, 121.76, 56.94, 31.54, 31.27, 28.76, 28.66, 28.55, 28.14, 22.05, 20.56, 20.22, 17.37, 13.06. MS m/z: 286.21.

6-Decyl-5,7-dimethyl-2,3-dihydro-1*H*-indolizinium trifluroacetate (20c):

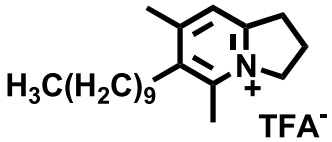

Hydrogenation was conducted on a mixture of isomers (15 mg, xx mmol) and Pd/C (2 mg, 10% by weight) in MeOH (1.5 mL) under 50 psi H_2 for 6 hours. The mixture was filtered through celite to remove Pd/C and concentrated to remove MeOH to give 6-decyl-5,7-dimethyl-2,3-dihydro-1*H*-indolizinium trifluroacetate. ^{1}HNMR (400MHz, CD_3CN) δ 7.53 (s, 1H), 4.58 (m, 2H), 3.37 (m, 2H), 2.74 (m, 2H), 2.62 (s, 3H), 2.51 (s, 3H), 2.38 (m 2H), 1.44 (m, 4 H), 1.28 (m, 12 H) 0.89 (m, 3H). ^{13}CNMR (400MHz, CD_3CN) δ 155.91, 154.51, 149.76, 137.76, 122.33, 56.94, 48.47, 38.51, 31.44, 31.31, 28.96, 28.72, 28.67, 28.12, 27.94, 22.08, 20.19, 19.72, 16.10, 13.07. MS m/z: 289.04.

2. Biological screening of CCR5 antagonists

A. Cell Culture Method

All cell lines, PC-3, DU-145 and M12, were incubated at 37 ºC in the presence of 5% CO2. RPMI 1640 serum free media (GIBCO Invitrogen) containing 1 % L-glutamine, 0.1% ITS (insulin, 5μg/ml; transferrin, 5μg/ml; and selenium, 5 μg/ml; Collaborative Research, Bedford)

and 0.1% gentamicin was used to cultivate all cells. M12 cells were first incubated in media with 5% fetal bovine serum (FBS); after 24 hours serum free media was added with 0.01% epidermal growth factor (EGF). DU-145 and PC-3 cell lines were incubated in media containing 10% FBS at all times.

B. Anti-proliferation Assay Protocol

Prostate cancer tumor cells (PC-3, M12, and DU-145) were plated into 96 well plates (BD Falcon, VWR) at a concentration of 1000 cells per well. Each cell line was plated in its respective serum containing media for a total concentration of 100 μL per well. After 24 hours, various concentrations of drugs in a 50 μL water solution were added to the cells. Control cells were given 50 μL of PBS. Seventy-two hours after incubation with drug, the serum containing media was replaced with 100 μL of serum free media, followed by addition of 10 μL of proliferative reagent WST-1 (Roche) to the wells. After 3 hours of incubation with WST-1, the absorbance of each well was measured by a EL 312e Microplate Bio-kinetics Reader (BIO-TEK Instruments). Percent inhibition of proliferation was calculated using a spreadsheet (Apple Numbers 2009). The average absorbance of the cells with drug is subtracted from the average absorbance of the cells without drug. This value is divided by the difference between the average absorbance of the cells and the average absorbance of the media giving a decimal. Multiplying this value by 100 yields the percent inhibition. The formula is as follows:

$$\text{percent inhibition} = [\ (A_{cells} - A_{drug}) / (A_{cells} - A_{media})\ ] \times 100$$

Where A_{cells} is the average absorbance of cells incubated without drug, A_{drug} is the average absorbance of cells incubated with drug and A_{media} is the average absorbance of the serum free media.

3. Molecular Dynamics Simulations and Docking of Anibamine and Analogs

Previously two homology models of CCR5 were developed in our lab. The crystal structures of bovine rhodopsin and β_2 adrenergic receptor were used to construct the homology models. The two homology models were accessed with anibamine bound. Parallel operations were performed on both receptor models. To facilitate more flexibility in ligand docking of anibamine analogs, a molecular dynamics simulation was performed to enlarge the binding pocket with anibamine bound. An aggregate was defined as all monomers greater than 10 Å away from the ligand and a distance constraint of 3 Å from the ligand nitrogen atom to O4276 on Glu283 in the receptor model was imposed. Dynamics simulations were performed for 100,000 fs, taking a snapshot every 25 fs, with Gasteiger-Hückel charges and a dielectric constant of 4.0. An average of the last 2000 fs was then minimized for 100,000 iterations with Gasteiger-Hückel and a dielectric constant of 4.0. At this point the ligand was removed and Procheck was performed on each receptor model. Amino acid residues with unfavorable sidechain angles were checked for proximity to the binding pocket. All were located away from the proposed ligand binding site.

To build the molecular library, each compound was built in Sybyl 8.1, minimized for 100,000 iterations with Gasteiger-Hückel and a dielectric constant of 4.0 and saved. The core template that was used for GOLD docking was constructed from the anibamine ligand extracted from the minimized protein models. Both aliphatic sidechains of the extracted ligand were

removed and replaced with hydrogens. The structure was saved as a template for GOLD docking.

Automated docking was performed on GOLD 3.1 Docking was performed using two constraints. The first was a distance constraint between the nitrogen on the ligand to O4276 on the receptor model of 2 to 4 Å. The second constraint was a similarity constraint by shape to the core template created from anibamine. The number of operation was increased to 300,000 to accommodate the flexible ligand sidechains. The active site was defined as a 10 Å radius from O2476. All other parameters were left in their default settings. The top ranked configurations were visualized in Sybyl.

VII. References

1. American Cancer Society. Global Cancer Facts and Figures 2007. www.cancer.org

2. Jemel, A.; Siegel, R.; Ward, E.; Hao, Y.; Xu, J.; Thun, M. J. Cancer Statistics, 2009. *CA Cancer J Clin.* **2009**, *59*, 225-249.

3. Hsing, A. W.; Tsao, L.; Devesa, S. S. International trends and patterns of prostate cancer incidence and mortality. *Int. J. Cancer (Pred. Oncol.)* **2000**, *85*, 60-67.

4. Lucia, M. S.; Torkko, K. C. Inflammation as a target for prostate cancer chemoprevention: pathological and laboratory rationale. *J. Urol*. **2004**, *171*, S30-S35.

5. Balkwill, F. and Mantavani, A. Inflammation and cancer: back to Virchow? *Lancet* **2001**, *357*, 539-545.

6. Konig, J. E.; Senge, T.; Allhoff, E. P.; Konig, W. Analysis of the inflammatory network in benign prostate hyperplasia and prostate cancer. *The Prostate* **2004**, *58*, 121-129.

7. Opperman, M. Chemokine receptor CCR5: insights into structure, function, and regulation. *Cell. Sig.* **2004**, *16*, 1201-1210.

8. Wheeler, J.; McHale, M.; Jackson, V.; Penny, M. Assessing the theoretical risk and benefit by genetic association studies of CCR5: experience in a drug development programme for Maraviroc. *Clin. Ther.* **2007**, *12*, 233-235.

9. Wu, X.; Lee, V. C.; Chevalier, E.; Hwang, S. T. Chemokine receptors as targets for cancer therapy. *Curr. Pharm. Des.* **2009***, 15,* 742-757.

10. Vaday, G. G.; Peehl, D. M.; Kadam, P. A.; Lawrence, D. M. Expression of CCL5 (RANTES) and CCR5 in prostate cancer. *The Prostate* **2006***, 66*, 124-134.

11. Jayasuriya, H.; Herath, K. B.; Ondeyka, J. G.; Polishook, J. D.; Bills, G. F.; Dombrowski, A. W.; Springer, M. S.; Siciliano, S.; Malkowitz, L.; Sanchez, M.; Guan, Z. Q.; Tiwari, S.; Stevenson, D. W.; Borris, R. P.; Singh, S. B. Isolation and structure of antagonists of chemokine receptor (CCR5). *J. Nat. Prod.* **2004**, *67*, 1036-1038.

12. Klausmeyer, P.; Chmurny, G. N.; McCloud, T. G.; Tucker, K. D.; Shoemaker, R. H. A novel antimicrobial indolizinium alkaloid from *Aniba panurensis*. *J. Nat. Prod*. **2004**, *67*, 1732-1735.

13. Adams, J. Synthesis and biological evaluation of CCR5 antagonists as novel anti-prostate cancer agents. Master's Thesis, Virginia Commonwealth University, August 2007.

14. Li, G.; Watson, K.; Buckheit, R. W.; Zhang, Y. Total synthesis of anibamine, a novel natural product as a chemokine receptor CCR5 antagonist. *Org. Lett.* **2007**, *9*, 2043-2046.

15. Nelson, W. G. and De Marzo, A. M.; Isaacs, W.B. Mechanisms of disease: prostate cancer. *N. Engl. J. Med.* **2003**, *349*, 366-381.

16. Hart, C.A.; Brown, M.; Bagley, S.; Sharrard, M.; Clarke, N.W. Invasive characteristics of human prostatic epithelial cells: understanding the metastatic process. *Br. J. Cancer,* **2005***, 92,* 503-512.

17. Trojan, L.; Schaaf, A.; Steidler, A.; Haak, M.; Thalmass, G.; Knoll, T.; Gretz, N.; Alken, P.; Michel, M. S. Identification of metastasis-associated genes in prostate cancer by genetic profiling of human prostate cancer cell lines. *Anticancer Res.* **2005**, *25*, 183-191.

18. Maitland, N. J. and Collins, A. T. Inflammation as the primary aetiological agent of human prostate cancer: a stem cell connection? *J. Cell. Biochem.* **2008**, *105*, 931-939.

19. Bonkhoff, H. and Remberger, K. Differentiation pathways and histogenic aspects of normal and abnormal prostatic growth: a stem cell model. *The Prostate* **1996**, *28,* 98-106.

20. Webber, M. M.; Bello, D.; Quadar, S. Immortalized and tumorigenic adult human prostatic epithelial cell lines: characteristics and applications. Part 3. Oncogenes, suppressor genes, and applications. *The Prostate* **1997**, *30*, 136-142.

21. Webber, M. M.; Bello, D.; Quadar, S. Immortalized and tumorigenic adult human prostatic epithelial cell lines: characteristics and applications. Part 1. Cell markers and immortalized nontumorigenic. *The Prostate* **1996**, *29*, 386-394.

22. Doll, J. A.; Zhu, X.; Furman, J.; Kaleem, Z.; Torres, C.; Humphrey, P. A.; Donis-Keller, H. Genetic analysis of prostatic atypical adenomatous hyperplasia (adenosis). *Am. J. Pathol.* **1999**, *155*, 967-971.

23. De Marzo, A. M.; Marchi, V. L.; Epstein, J. I.; Nelson, W. G. Proliferative inflammatory atrophy of the prostate. Implications for prostatic carcinogenesis. *Am. J. Pathol.* **1999**, *155,* 1985-1992.

24. Webber, M. M.; Bello, D.; Quadar, S. Immortalized and tumorigenic adult human prostatic epithelial cell lines: characteristics and applications. Part 2. Tumorigenic cell lines. *The Prostate* **1997**, *30*, 58-64.

25. Bae, V. L.; Jackson-Cook, C. K.; Maygarden, S. J.; Plymate, S. R.; Chen, J.; Ware, J. L. Metastatic sSublines of an SV40 large T antigen immortalized human prostate epithelial cell line. *The Prostate* **1998***, 34,* 275-282.

26. Bae, V. L.; Jackson-Cook, C. K.; Brothman, A. R.; Maygarden, S. J.; Ware, J. L. Tumorigenicity of SV40 T antigen immortalized human prostate epithelial cells: Association with decreased epidermal growth factor receptor (EGFR) expression. *Int J Cancer* **1994**, *58*, 721–729.

27. Nelson, W. G.; De Marzo, A. M.; DeWeese, T. L.; Isaacs, W.B. The role of inflammation in the pathogenesis of prostate cancer. *J. Urol*. **2004**, *172*, S6-S12.

28. Sáenz-López, P.; Carretero, R.; Cózar, J. M.; Romero, J. M.; Canton, J.; Vilchez, J. R.; Tallada, M.; Garrido, F.; Ruiz-Cabello, F. Genetic polymorphisms of *RANTES, IL1-A, MCP-1* and *TNF-A* genes in patients with prostate cancer. *BMC Cancer* **2008**, *8*, 382-??

29. Balistreri, C. R.; Carruba, G.; Calabrò, M.; Campisis, I.; Di Carlo, D.; Lio, D.; Romano, G.C.; Candore, G.; Caruse, C. CCR5 proinflammatory allele in prostate cancer risk *Ann*. *NY Acad*. *Sci*. **2009**, *1155,* 289-292.

30. Petersen D. C.; Severi, G.; Hoang, H. N.; Padilla, E. J. D.; Southey, M. C.; English, D. R.; Hopper, J. L.; Giles, G. G.; Hayes, V. M. No association between common chemokine and chemokine receptor gene variants and prostate cancer risk. *Cancer Epidemiol. Biomarkers Prev.* **2008***, 17*, 3615-3617.

31. Nelson, W. G.; De Marzo, A. M.; DeWeese, T. L. The molecular pathogenesis of prostate cancer: Implications for prostate cancer prevention. *Urology* **2001**, *57*, 39-45.

32. O'Hayre, M.; Salanga, C. L.; Handel, C. L.; Allen, S. J. Chemokines and cancer: migration, intracellular signalling and intercellular communication in the microenvironment. *Biochem. J.* **2008**, *409*, 635-649.

33. Allen, S. J.; Crown, S. E.; Handel, T. M. Chemokine: receptor structure, interactions, and antagonism. *Annu. Rev. Immunol.* **2007**, *25*, 787-820.

34. Mellado, M.; Rodriguez-Frade, J. M.; Manes, S.; Martinez, A. C. Chemokine signaling and functional responses: the role of receptor dimerization and TK pathway activation. *Annu. Rev. Immunol.* **2001**, *19*, 397-421.

35. Leach, K.; Charlton, S.J.; Strange, P.G. Analysis of second messenger pathways stimulated by different chemokines acting at the chemokine receptor CCR5. *Biochem Pharmacol.* **2007** *74*, 881-890.

36. Thelen, M. Dancing to the tune of chemokines. *Nat. Immunol.* **2001**, *2*, 129-134.

37. Tanaka, T.; Bai, Z.; Srinoulprasert, Y.; Yang, B.; Hayasaka, H.; Miyasaka, M. Chemokines in tumor progression and metastasis. *Cancer Sci.* **2005**, *96*, 317-322.

38. Slettenaar, V. I. F. and Wilson, J. L. The chemokine network: A target in cancer biology? *Adv. Drug. Del. Rev.* **2006**, *58*, 962-974.

39. Ruffini, P. A.; Morandi, P.; Cabioglu, N.; Altundag, K.; Cristofanilli, M. Manipulating the chemokine-chemokine receptor to treat cancer. *Cancer* **2007**, *109*, 2392-2404.

40.Mantovani, A.; Bottazzi, B.; Colotta, F.; Sozzani, S.; Ruco, L. The origin and function of tumor-associated macrophages. *Immunol Today* **1992**, *13*, 265-270.

41. Vicari, A. P.; Treilleux, I.; Lebecque, S. Regulation of the trafficking of tumour-infiltrating dendritic cells by chemokines. *Sem. Cancer Biol.* **2004**, *14*, 161-169.

42. Hanahan, D. and Weinburg, A. Hallmarks of Cancer Review. *Cell* **2000**, *100*, 57-70.

43. Homey, B.; Muller, A.; Zlotnik, A. Chemokines: agents for the immunotherapy of cancer? *Nat. Rev. Immunol.* **2002**, *2*, 175-84.

44. Bogenrieder, T. and Herlyn, M. Axis of evil: molecular mechanisms of cancer metastasis. *Oncogene* **2003**, *22*, 6524-6536

45. Opdenakker, G. and Van Damme, J. Chemotactic factors, passive invasion and metastasis of cancer cells. *Immunol. Today* **1992**, *13*, 463-464.

46. Vicari, A.P. and Caux, C. Survey: Chemokines in cancer. *Cytokine & Growth Factor Rev.* **2002**, *13*, 143-154.

47. Muller, A.; Homey, B.; Soto, H.; Ge, N.; Catron, D.; Buchanan, M. E.; McClanahan, T.; Murphy, E.; Yuan, W.; Wagner, S. N.; Barrerak, J. L.; Mohark, A.; Verásteguik, E.; Zlotnik, A. Involvement of chemokine receptors in metastasis. *Nature* **2001**, *410*, 50-56.

48. Singh, S.; Sadanandam, A.; Singh, R. K. Chemokines in tumor angiogenesis and metastatis. *Cancer Metastasis Rev.* **2007**, *26*, 453-467.

49. Koizumi, K.; Hojo, S.; Akashi, T.; Yasumoto, K.; Saiki, I. Chemokine receptors in cancer metastasis and cancer cell derived chemokines in host immune response. *Cancer Sci.* **2007**, *98*, 1652-1658.

50. Viola, A. and Luster, A. D. Chemokines and their receptors: drug targets in immunity and inflammation. *Annu. Rev. Pharmacol. Toxicol.* **2008**, *48*, 171-197.

51. Cardaba, C. M.; Kerr, J. S.; Mueller, A. CCR5 internalisation and signalling have different dependence on membrane lipid raft integrity. *Cell. Signal.* **2008**, *20*, 1687-1694.

52. Oberlies, N. H. and Kroll, D. J. Camptothecin and Taxol: Historic achievements in natural products research. *J. Nat. Prod.* **2004**, *67,* 129-135.

53. Newman, D. J.; Cragg, G. M.; Snader, K. M. Natural products as sources of new drugs over the period 1981-2002. *J. Nat. Prod.* **2003**, *66,* 1022-1037.

54. Dixon, R. A. Natural Products and plant disease resistance. *Nature* **2001**, *411,* 843-847.

55. Dixon, N.; Wong, L. S.; Geerlings, T. H.; Micklefield, J. Cellular targets of natural products. *J. Nat. Prod. Rep.* **2007**, *24,* 1288-1310.

56. Breinbauer, R.; Vetter, I. R.; Waldmann, H. From Protein Domains to Drug Candidates-Natural Products as Guiding Principles in the Design and Synthesis of Compound Libraries. *Angew. Chem. Int. Ed.* **2002**, *41,* 2878-2890.

57. Clardy, J. and Walsh, C. Lessons from natural molecules. *Nature* **2004**, *432*, 829-837.

58. Evans, B. E.; Rittle, K. E.; Bock, M. G.; DiPardo, R. M.; Freidinger, R. M.; Whitter, W. L.; Lundell, G. F. ; Veber, D. F.; Anderson, P. S.; Chang, R. S. L.; Lotti, V. J.; Cerino, D. J.; Chen, T. B.; Kling, P. J.; Kunkel, K. A.; Springer, J. P.; Hirschfield, J. Methods for drug discovery: development of potent, selective, orally effective cholecystokinin antagonists. *J. Med. Chem.* **1988,** *31,* 2235-2246.

59. Mann, J. Natural Products in cancer chemotherapy: past, present, and future. *Nat. Rev. Cancer* **2002**, *2,* 143-148.

60. Dholwani, K. K.; Saluja, A. K.; Gupta, A. R.; Shah, D. R.; A review on plant-derived natural products and their analogs with anti-tumour activity. *Indian J. Pharm.* **2008**, *40*, 49-58.

61. Itokawa, H.; Morris-Natschke, S. L.; Akiyama, T.; Lee, K. Plant-derived natural product research aimed at new drug discovery. *J. Nat. Med.* **2008***, 62,* 263-280.

62.Guéritte-Voegelein, F.; Guénard, D.; Lavelle, F. Le Goff, M.; Mangatal, L.; Potier, P. Relationships between the structure of Taxol analogues and their antimitotic activity. *J. Med. Chem.* **1991**, *34*, 992–998.

63. Nicolaou, K. C.; Vourloumis, D.; Winssinger, N.; Baran, P. S. The art and science of total synthesis at the dawn of the twenty-first century *Angew. Chem. Int. Ed.* **2000**, *39,* 44-122.

64. Njardarson, J. T.; Gaul, C.; Shan, D.; Huang, X.; Danishefsky, S. J. Discovery of potent cell migration inhibitors through total synthesis: Lessons from structure−activity studies of (+)-migrastatin *J. Am. Chem. Soc.* **2004**, *126,* 1038-1040.

65. Paterson, I. and Anderson, E. A. The renaissance of natural products as dug candidates. *Science* **2005**, *310*, 451-453.

66. Schenone, P.; Mosti, L.; Menozzi, G. Reaction of 2-Dimethylaminomethylene-1,3-diones with dinucleophiles. I.Synthesis of 1,5-disubstituted 4-acylpyrazoles. *J. Heterocycl. Chem*. **1982**, *19*, 1355-1361.

67. Menozzi, G.; Schenone, P.; Mosti, L. Reaction of 2-Dimethyaminomethylene-1,3-diones with dinucleophiles. II. Synthesis of 5-(alkyl)(phenyl)-4-acylsoxazoles and 6,7-dihydro-1,2-benisoxazol-4(5*H*)-ones. *J. Heterocycl. Chem*. **1983**, *20*, 645-648.

68. Alberola, A.; Antolin, L. F.; Gonzalez, M. A.; Laguna, M. A.; Pulido, F. J. Base-induced cleavage of 4-functionalized-3-unsubstituted isoxazoles. Synthesis of 5-aminoazoles and 4-cyanoazoles. *J. Heterocycl. Chem*. **1987**, *25*, 393-397.

69. Alberola, A.; Antolin, L. F.; Gonzalez, M. A.; Pulido, F. J. Base-induced cleavage of 4-functionalized-3-unsubstituted isoxazoles. Synthesis of 2-aminopyrimidines and pyrimidine-2-(3*H*)-thiones. *J. Heterocycl. Chem.* **1986**, *23*, 1035-1038.

70. Haley, C. A. C. and Maitland, M. Organic reactions in aqueous solution at room temperature. Part I. The influence of pH on condensations involving the linking of carbon to nitrogen and of carbon to carbon. *J. Chem. Soc*. **1951**, 3155-3174.

71. Mal, P.; Lourderaj, U.; Parveen; Venugopalan, P.; Moorthy, N. J.;Sathyamurthy, N. Conformational control and photoenolization of pyridine-3-carboxaldehydes in the solid state: Stabilization of photoenols via hydrogen bonding and electronic control. *J. Org. Chem.* **2003**, *68*, 3446-3453.

72. Friedman, L. and Shechter, H. Dimethylformamide as a useful solvent in preparing nitriles from aryl halides and cuprous cyanide; improved isolation techniques. *J. Org. Chem.* **1961**, *26*, 2522-2524.

73. Zanon, J.; Klapars, A.; Buchwald, S.L. Copper-Catalyzed Domino Halide Exchange-Cyanation of Aryl Bromides. *J. Am. Chem. Soc.* **2003**, *125*, 2890-2891.

74. Rene, L.; Poncet, J.; Auzou, G. A one pot synthesis of b-cyanoenamines. *Synthesis*, **1986**, *5,* 419-420.

75. Sibgatulin, D. A.; Volochnyuk, D. M.; Kostyuk, A. N. Reaction of unsymmetric trifluoromethyl-containing 1,3-dicarbonyl compound with 'push-pull' enamines. *Tetrahedron Lett.* **2007**, *48*, 2775-2779.

76. Kato, Y.; Okada, S.; Tomimoto, K.; Mase, T. A facile bromination of hydroxyheteroarenes. *Tetrahedron Lett.* **2001**, *42*, 4849-4851.

77. Dahan, A. and Portnoy, M. Synthesis of homo- and heteroprotected furcated units for modular chemistry. *J. Org. Chem.* **2001**, *66,* 6480-6482.

78. Lautens, M. and Yoshida, M. Rhodium-catalyzed addition of arylboronic acids to alkynyl aza-heteraromatic compounds in water. *J. Org. Chem.* **2003**, *68*, 762-769.

79. Sonogashira, K.; Tohda, Y. Hagihara, N. A convenient synthesis of acetylenes: catalytic substitutions of acetylenic hydrogen with bromoalkenes, iodoarenes, and bromopyridines.*Tetrahedron Lett.* **1975**, *50*, 4467-4470.

80. Song, Z. J.; Zhao, M.; Desmond, R.; Devine, P.; Tschaen, D. M.; Tillyer, R.; Frey, L.; Heid, R.; Xu, F.; Foster, B.; Li, J.; Reamer, R.; Volante, R.; Grabowski, E. J. J.; Dolling, E. H.; Reider, P. J.; Okade, S.; Kato, Y.; Mano, E. Practical asymmetric synthesis of an endothelin receptor antagonist *J. Org. Chem.* **1999**, *64*, 9658-9667.

81. Sarkar, T. K.; Panda, N.; Basak, S. A sequential Pummerer-Diels-Alder route for the generation and trapping of Furo[3,4-*c*]pyridines: Synthesis of heterocyclic analogues of 1-Arylnapthalene lignans. *J. Org. Chem.* **2003** *68*, 6919-1927.

82. Schlosser, M.; Tuong, H. B.; Schaub, B. The betaine-ylide route to trans-alkenols. *Tetrahedron Lett.* **1985**, *26*, 311-314.

83. Schlosser, M.; Stereochemistry of the Wittig reaction. *Top. Stereochem.* **1970**, *5*, 1-30.

84. Wang, Q.; Deredas, D.; Huynh, C.; Schlosser, M. Sequestered alkyllithiums: Why phenyllithium alone is suitable of betaine-ylid generation. *Chem. Eur. J.* **2003**, *9*, 570-574.

85. Jenkins, D. J.; Riley, A. M.; Potter, B. V. L. Chiral cyclopentane-based mimics of D-Myo-Inositol 1,4,5-triphosphate from D-glusoce.

86. Bates, R. W. and Boonsombat, J. The pyridinium reduction route to alkaloids: a synthesis of (±)-tashiromine. *J. Chem. Soc.*, *Perkin Trans.* **2001**, *1*, 654-656.

87. Cell proliferation reagent WST-1. **2007** accessed from www.roche-applied-science.com.

88. Li, G.; Haney, K. M.; Kellog, G. E.; Zhang, Y. Comparative docking study of anibamine as the first natural product CCR5 antagonist in CCR5 homology models. *J. Chem. Inf. Model.* **2009**, *49*, 120-132.

Vita

Kendra May Haney was born January 21, 1984 in Laguna Beach, California to John and Margery Haney, joining two older siblings, Blythe and Brett. She graduated from Dana Hills High School, Dana Point, California in 2002 as a Valedictorian. She received her Bachelor of Science in Biochemistry from Washington and Lee University, Lexington, Virginia in 2006. In the fall of 2006 she enrolled at Virginia Commonwealth University as a graduate student in the Department of Medicinal Chemistry. She has one publication entitled “Comparative docking study of anibamine as the first natural product CCR5 antagonist in CCR5 homology models” published in the Journal of Chemical Information and Modeling in 2009 under the direction of her advisor, Yan Zhang.